## Acknowledgements

II

**Abstract**

Nitrification, the microbial oxidation of ammonia to nitrate, is a key step in the biological cycling of nitrogen, and is often used in wastewater treatment for removal of ammonium. Fish-farming in flow-through systems such as open net pens is the largest contributor to human discharge of inorganic nutrients along the Norwegian coast. It is important to limit these emissions by converting to recirculating systems for nitrogen removal. However, the nitrification process is known to be sensitive to high concentrations of salts, a factor of importance when establishing technology for treatment of saline wastewaters.

The aim of this thesis was to investigate and compare the microbial communities of nitrifying biofilms adapted to different salinities. Two continuous biofilm reactor systems were operated, one supplied with seawater-based cultivation medium, while the other was supplied with tapwater-based cultivation medium. The microbial communities in the two reactors were investigated by denaturing gradient gel electrophoresis (DGGE) and fluorescence *in situ* hybridization (FISH). A batch culture salinity response test was carried out to investigate the acute effect of different salinities on the nitrification activity in the seawater-adapted culture.

DGGE analysis based on 16S rRNA and *amoA* sequences showed that the seawater-based reactor had lower microbial diversity than the tapwater-based reactor, and that different nitrifiers seemed to dominate in the two reactors. Ammonia- and nitrite-oxidizers affiliated with the nitrosomonads and with *Nitrospira* were identified in both reactors. Ammonia-oxidizers related to *Nitrosomonas oligotropha* seemed to dominate in the tapwater-based reactor, while *Nitrosomonas halophila* seemed to dominate in the seawater-based reactor. The batch culture salinity respons test, compared to a similar experiment by (Kristoffersen 2004), indicated that the nitrifying culture adapted to high salinity was more halotolerant than a culture adapted to low salinity.

IV

## Sammendrag

Nitrifikasjon er en mikrobiell prosess der ammonium oksideres til nitrat. Nitrifikasjon er en viktig prosess i den biologiske nitrogensyklus, og er ofte brukt innen vannrensing for å fjerne ammonium. Fiskeoppdrett i åpne merder er den største bidragsyteren til menneskaskapte utslipp av uorganiske næringssalter langs norskekysten, og det er viktig begrense disse utslippene ved å gå over til resirkulerte systemer for nitrogenfjerning. Nitrifikasjonsprosessen er kjent for å være følsom for høye saltkonsentrasjoner, og det er viktig å ta hensyn til dette når teknologi for rensing av avløpsvann med høyt saltinnhold etableres.

Målet med denne oppgaven var å undersøke og sammenlikne mikrobielle samfunn i nitrifiserende biofilmer adaptert til ulike saliniteter. To kontinuerlige reaktorsystemer ble drevet, én ble forsynt med sjøvannsbasert kultiveringsmedium, den andre ble forsynt med springvannsbasert kultiveringsmedium. De mikrobielle samfunnene i de to reaktorene ble undersøkt ved hjelp av denaturerende gradient gelelektroforese (DGGE) og fluorescens *in situ* hybridisering (FISH). En salinitetsresponstest ble utført for å undersøke den akutte effekten av ulike saliniteter på nitrifikasjonsaktiviteten i den sjøvanns-adapterte kulturen.

DGGE-analyse basert på sekvenser av 16S rRNA og *amoA* indikerte at den sjøvannsbaserte reaktoren hadde lavere mikrobiell diversitet enn den springvannsbaserte reaktoren, og at ulike nitrifiserende bakterier dominerte i de to reaktorene. Ammonium- og nitrittoksiderende bakterier beslektet med *Nitrosomonas* og *Nitrospira* ble funnet i begge reaktorene. Ammonium-oksiderende bakterier beslektet med *Nitrosomonas oligotropha* så ut til å dominere i den springvannsbaserte reaktoren, mens *Nitrosomonas halophila* var mer dominerende i den sjøvannsbaserte reaktoren. Salinitetsresponstesten, sammenliknet med et liknende eksperiment utført av Kristoffersen (2004), indikerte at den nitrifiserende kulturen adaptert til høy salinitet var mer halotolerant enn en kultur adaptert til lav salinitet.

# Contents

x

# List of Abbreviations

$\beta$-AOB  Ammonia-oxidizing bacteria within the $\beta$-proteobacteria

$pMMO$  Particulate methane monooxygenase

AMO  Ammonia monooxygenase

Annamox  Anaerobic ammonia-oxidation

AOA  Ammonia-oxidizing archaea

AOB  ammonia-oxidizing bacteria

bp  Basepair(s)

BSA  Bovine Serum Albumin

cfu  Colony-forming units

CLSM  Confocal laser scanning microscopy

Cy  Cyanine

DAPI  4',6-diamidino-2-phenylindole

DGGE  Denaturing Gradient Gel Electrophoresis

FISH  Fluorescence *in situ* hybridization

FITC  Fluorescein isothiocyanate

g  Gravity

HAO  Hydroxylamine oxidoreductase

HeNe  Helium-neon laser

IUB  International Union of Biochemistry

MBBR  Moving bed biofilm reactor

MOB  Methane-oxidizing bacteria

NCIMB  The National Collection of Industrial, Marine and Food Bacteria

NOR   Nitrite oxidoreductase

NXR   Nitrite oxidoreductase

PCR   Polymerase Chain Reaction

pmoA  Particulate methane monooxygenase gene A

RDP   Ribosomal Database Project

rpm   Revolutions per minute

SDS   Sodium dodecyl sulfate

SIV   Sterile Ion Free Water

UV    Ultraviolet light

VBNC  Viable-but-nonculturable

# Chapter 1

# Introduction

## 1.1 Nitrification

Nitrification is a microbial process where ammonia ($NH_3$) (Suzuki et al. 1974) is oxidized to nitrate ($NO_3^-$). This is a key step in the biogeochemical cycling of nitrogen. The redox cylce for nitrogen is shown in Figure 1.1. Ammonia is released mainly by ammonificaton; break-down of organic, nitrogen-containing molecules, such as proteins. Some ammonia is incorporated into biomass, while some is used as an energy source by nitrifying microorganisms. Nitrifying organisms oxidize ammionia to nitrate, which can be assimilated into biomass, or reduced to dinitrogen gas by denitrification. The loop is closed when nitrogen-fixing bacteria reduce the dinitrogen gas to ammonia (Fiencke et al. 2005, Bock & Wagner 2006).
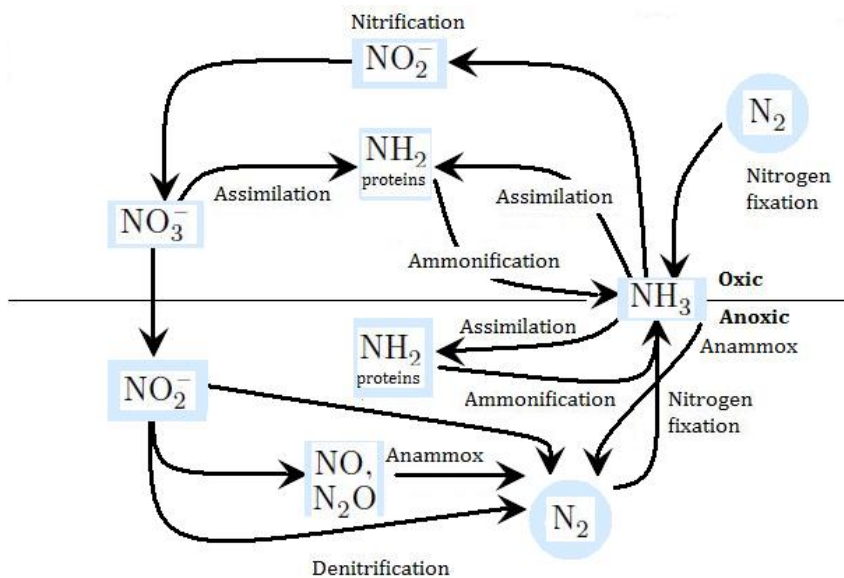


Figure 1.1: The redox cycle for nitrogen. The Figure is adapted from Madigan & Martinko (2006).

Nitrification is a two-step process. Ammonia is first oxidized to nitrite by ammonia-oxidizing microorganisms, then further to nitrate by nitrite oxidizing microorganisms. Chemolithoautotrophic bacteria have traditionally been thought of as the key nitrifiers. The ammonia-oxidizing bacteria (AOB) catalyze the oxidation of ammonia to nitrite in two steps, using two enzymes. The initial oxidation of ammonia to hydroxylamine, according to equation 1.1, is catalyzed by the enzyme ammonia monooxygenase (AMO). The oxidation of hydroxylamine to nitrite (as nitrous acid), shown in equation 1.2, is catalyzed by the enzyme hydroxylamine oxidoreductase (HAO) (Fiencke et al. 2005, Bock & Wagner 2006).

$$\mathrm{NH_3 + O_2 + 2H_2^+ + 2e^- \rightarrow NH_2OH + H_2O} \quad \Delta G_0' = -137 kJ \cdot mol^{-1} \quad (1.1)$$

$$\mathrm{NH_2OH + \frac{1}{2}O_2 \rightarrow HNO_2 + 2H^+ + 2e^-} \quad \Delta G_0' = -114 kJ \cdot mol^{-1} \quad (1.2)$$
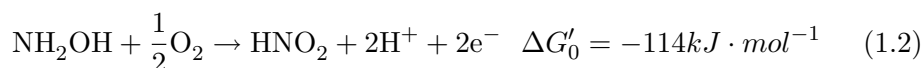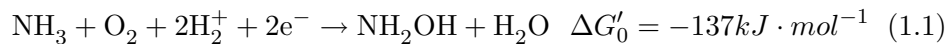
The oxidation of nitrite to nitrate is shown in equation 1.3. The nitrite-oxidizing bacteria (NOB) catalyze this reaction by using the enzyme nitrite oxidoreductase (NOR or NXR) (Fiencke et al. 2005, Bock & Wagner 2006).

$$\mathrm{NO_2^- + \frac{1}{2}O_2 \rightarrow NO_3^-} \quad \Delta G_0' = -54 kJ \cdot mol^{-1} \quad (1.3)$$
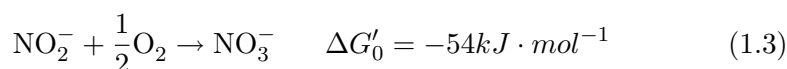
The energy yield from nitrification is poor. This results in low growth rates of nitrifying bacteria, and it can take several months to obtain pure cultures (Koops & Pommerening-Röser 2005, Spieck & Bock 2005).

## 1.2 The microbiology of nitrification

The nitrifying bacteria have for a long time been recognized as the microbes that mediate nitrification. During the last years, new players in the cycling of nitrogen have been discovered. Evidence suggest that anaerobic ammonia-oxidation (annamox) and ammonia-oxidation by *Archaea* are essential processes for the global cycling of nitrogen. The following sections will deal with the different nitrifying microorganisms.

### 1.2.1 Ammonia-oxidizing bacteria

Former classification of litho autotrophic ammonia-oxidizing bacteria based on cell morphology (e.g. Watson (1971)), led to the distinction of five different groups of bacteria; *Nitrosomonas*, *Nitrosococcus*, *Nitrosospira*, *Nitrosolobus* and *"Nitrosovibrio"*. Later phylogenetic analysis of AOB showed that these genera belong to two distinct classes, the $\beta$-proteobacteria and the $\gamma$-proteobacteria. Figure 1.2 is a phylogenetic tree showing different AOB and NOB (Koops & Pommerening-Röser 2005).

Most AOB belong to the $\beta$-proteobacteria. There are two different clusters within the $\beta$-AOB; the *Nitrosomonas* cluster and the *Nitrosospira* cluster. The *Nitrosomonas* cluster comprise the species of the genus Nitrosomonas, and *"Nitrosococcus mobilis"*. *"Nitrosococcus mobilis"* was formerly classified within the *Nitrosococcus* genus, but phylogenetic analysis showed that it actually clustered within the *Nitrosomonas*. The *Nitrosospira* cluster comprise the genera *Nitrosospira*, *Nitrosolobus* and *"Nitrosovibrio"*. Even though these genera have quite different morphologies, they have very high 16S rRNA sequence similarities, and can be classified as a single genus

3
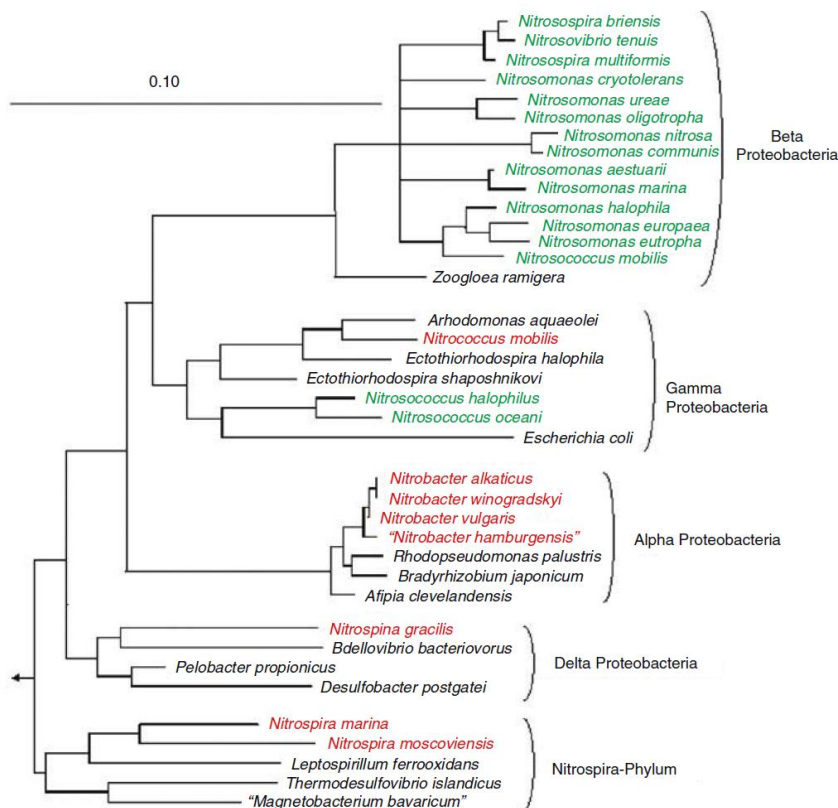
Figure 1.2: The 16S rRNA-based phylogenetic relationship of nitrifying bacteria. Ammonia-oxidizing bacteria are indicated in green, nitrite-oxidizing bacteria are indicated in red. The bar indicates 10 % sequence divergence. The Figure is from Bock & Wagner (2006).

(Head et al. 1993). However, the 16S rRNA gene does not give sufficient resolution to clearly distinguish between closely related species (Koops & Pommerening-Röser 2005).

Only a few AOB belong to the γ-proteobacteria. Two species are known; *Nitrosococcus oceani* and *Nitrosococcus halophilus*, belonging to the *Nitrosococcus* genus (Koops & Pommerening-Röser 2005).

### 1.2.2   Nitrite-oxidizing bacteria

Based on morphological characteristics, four genera of nitrite-oxidizing bacteria have been described; *Nitrobacter, Nitrococcus, Nitrospina* and *Nitrospira* (Watson & Waterbury 1971, Spieck & Bock 2005). These are more widely phylogenetically distributed than the ammonia-oxidizing bacteria (Figure 1.2). The *Nitrobacter* genus belongs to the α-proteobacteria and

4

comprise four described species. The *Nitrococcus* genus belongs to the $\gamma$-proteobacteria, and is related to the ammonia-oxidizing *Nitrosococcus* genus. The *Nitrospina* genus is affiliated with the $\delta$-proteobacteria, but it has been shown that it is not closely related to other members of the delta subdivision of the proteobacteria (Teske et al. 1994). The *Nitrospira* genus is not affiliated with the proteobacteria, but belongs to a separate phylum (Ehrich et al. 1995).

### 1.2.3 Nitrifying archaea

Cultivation-independent techniques (see section 1.4) made the discovery of ammonia-oxidizing archaea possible. Shotgun sequencing of environmental genomes in the Sargasso Sea by Venter et al. (2004) resulted in findings of archaeal genes for the ammonia monooxygenase enzyme (*amoA*, *amoB* and *amoC*, see section 1.4.2), indicating the ability of archaea to oxidize ammonia to nitrite. Treusch et al. (2005) found crenarchaeotal homologues to the bacterial *amoA* gene in soil, and demonstrated the expression of these genes. Könneke et al. (2005) managed to isolate the first ammonia-oxidizing crenarchaeon, *Nitrosopumilus maritimus*, and could report that this crenarchaeon converts ammonia to nitrite with bicarbonate as the only carbon source. Genes for hydroxylamine oxidoreductase, the enzyme that calalyze the oxidation of hydroxylamine to nitrite, have not been found in archaea (Francis et al. 2007, Prosser & Nicol 2008).

Leininger et al. (2006) showed that ammonia-oxidizing archaea were actually more abundant than ammonia-oxidizing bacteria in soil. *amoA* gene copies from *Archaea* were up to 3000 times more abundant than bacterial *amoA* genes. Furthermore, Wuchter et al. (2006) showed that the copy number of crenarchaeotal *amoA* was 1-3 orders of magnitude higher than bacterial *amoA*, and that the abundance of ammonia-oxidizing *Crenarchaeota* correlated with the level of ammonia oxidation in the sea. This indicates a major role for *Archaea* in the nitrogen cycle, both in the sea and in soil. Park et al. (2006) showed the occurrence of ammonia-oxidizing *Archaea* in activated sludge bioreactors for wastewater treatment (Francis et al. 2007, Prosser & Nicol 2008).

## 1.3 Natural and engineered nitrifying habitats

Nitrifying organisms are widely distributed in different environments such as soil, lakes and oceans. Different groups of nitrifiers are specialized in different habitats, and have different requirements for temperature, substrate concentration, oxygen level and concentration of salts. Figure 1.3 shows some ecophysiological characteristics of ammonia-oxidizing bacteria (Koops & Pommerening-Röser 2005, Fiencke et al. 2005).
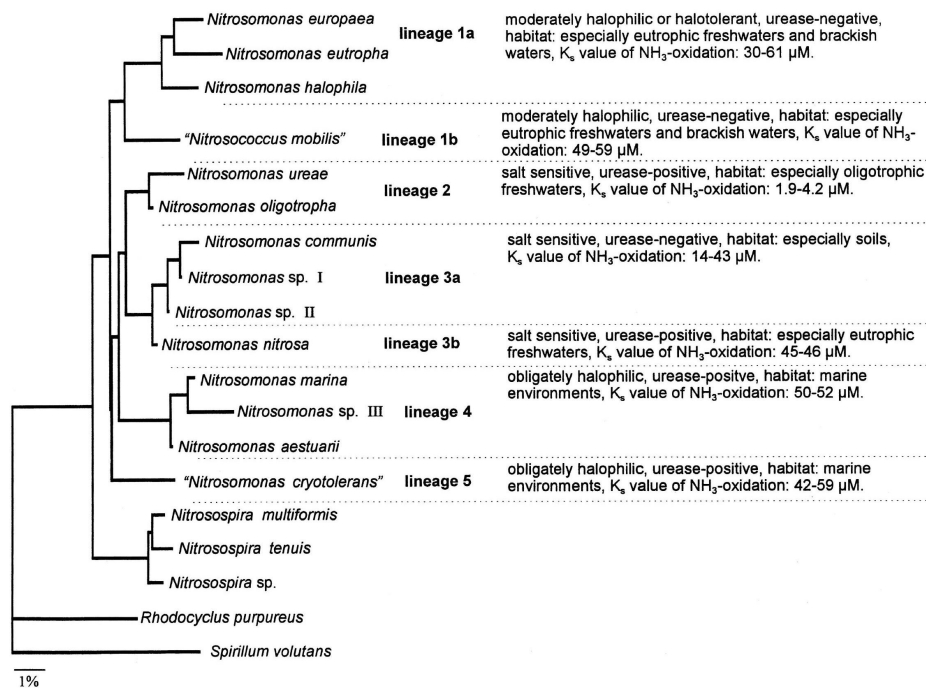
Figure 1.3: Phylogenetic tree of different $\beta$-AOB, and some of their ecophysiological characteristics. The Figure is adapted from Koops & Pommerening-Röser (2005).

### 1.3.1 Nitrification in wastewater treatment

Release of effluents with high concentrations of ammonia/urea, such as municipal wastewater, can lead eutrophication of the recipient, oxygen depletion and serious toxic effects on aquatic organisms (Manahan 2005). It is therefore important to limit the discharge of ammonia into the environment. The biological nitrification process is used in combination with denitrification in wastewater treatment to remove inorganic nitrogen.

The ability of nitrifying bacteria to grow in biofilms can be utilized in wastewater treatment. Bacteria that grow on surfaces can easily be retained in the reactor, preventing wash-out of the nitrifiers. This is necessary because nitrifying bacteria have low growth rates. There are also several other advantages with biofilm reactors, biofilms are for example more resistant to toxic substances. Several biofilm reactor types have been developed. The fundamental principle for biofilm reactors is to have a high surface area for biofilm growth (Hem et al. 1994, Wijffels & Tramper 1995).

Much of the research conducted on nitrifying organisms is aimed at improving the nitrification process in wastewater treatment plants. Many wastewater treatment plants experience problems with the nitrification process; the nitrification is often unstable, and nitrite has a tendency to accu-

mulate in the system due to incomplete nitrification. The nitrification is, according to Graham et al. (2007) particularly vulnerable because of chaotic behaviour and a fragile AOB-NOB mutualism. New methods make it possible to investigate the microbes behind the process. According to Moussa et al. (2006), "there is an urgent need for interdisciplinary research at the interface between molecular microbial ecology and process engineering to understand the link between microbial diversity, process efficiency and process stability".

Several research projects have aimed at investigating the microbial communities in wastewater treatment plants. The nitrosomonads (*Nitrosomonas* and *Nitrosococcus mobilis*) are generally found to be the dominating ammonia-oxidizing bacteria in wastewater treatment plants. Traditionally, *Nitrobacter* was considered to be the most important nitrite-oxidizer, but later *Nitrospira* was found to be dominating in many wastewater treatment plants (Wagner et al. 2002). Ammonia-oxidizing archaea have also been found in wastewater treatment plants (Park et al. 2006, Haseborg et al. 2009).

### 1.3.2 Nitrification in saline environments; employment in aquaculture

Fish-farming in flow-through systems such as open net pens is, according to the Norwegian Climate and Pollution Agency (Selvik et al. 2007, The Climate and Pollution Agency 2009), the largest contributor to human discharge of inorganic nutrients (nitrogen and phosphorus) along the Norwegian coast. It is important to limit these emissions. When converting to recirculating systems for fish production, the water has to be treated according to the requirements of the fish, which means that the concentration of ammonium, a potent fish toxin, has to be reduced to low levels (<10 $\mu$g/L $NH_3$).

Many plants for treatment of high salinity wastewater (>10 g $Cl^-$/L) have experienced serious operational problems because the nitrification process seems sensitive to high concentrations of salts. Both long start-up periods and incomplete nitrification have been reported (Nijhof & Bovendeur 1990, Dincer & Kargi 1999, Kim et al. 2000, Yu et al. 2002, Campos et al. 2002, Uygur & Kargi 2004).

Several studies have aimed at investigating the long-term adaptation of nitrifying bacteria to high salinity. Campos et al. (2002) reported that adapted biomass was less sensitive to high salinity. Moussa et al. (2006), on the other hand, could not detect differences in nitrification activity between adapted and non-adapted cultures.

Changes in the microbial community composition after gradually increasing the salinity in non-adapted cultures have been observed. Chen et al. (2003) reported a microbial community shift occurring between 10

and 18 g $Cl^-$/L, where non-saline-resistant species such as *Nitrosomonas europaea* and *Nitrosomonas eutropha* were replaced by *Nitrosococcus mobilis*, while the only detected nitrite-oxidizer, *Nitrobacter*, disappeared above 10 g $Cl^-$/L. Moussa et al. (2006) detected ammonia-oxidizing species of *Nitrosomonas europaea*, *Nitrosomonas oligotropha*, *Nitrosococcus mobilis* and *Nitrosospira* at chloride concentrations below 10 g/L. At chloride concentrations between 20 and 30 g/L, *Nitrosomonas europaea* and *Nitrosococcus mobilis* were the dominant ammonia-oxidizers, while only *Nitrosomonas europaea* could be detected at higher concentrations. No nitrite-oxidizers were detected at chloride concentrations above 10 g/L, but after recovery experiments, *Nitrobacter* could be detected.

Ammonia-oxidizing archaea have also been detected in environments with high salinity. Moin et al. (2009) detected higher numbers of archaeal *amoA* genes than bacterial *amoA* genes in salt marsh sediments, and suggested that the salinity may be an important environmental factor for ammonia-oxidizing *Archaea*. Bernhard et al. (2010) investigated nitrifying communities along an estuarine salinity gradient, and found that the abundance of ammonia-oxidizing archaea was always greater than ammonia-oxidizing bacteria. The abundance of ammonia-oxidizing *Archaea* was greatest at intermediate salinity (approximately 20 g $Cl^-$/L).

## 1.4 The methodological challenge

### 1.4.1 The limitations of cultivation-dependent techniques

Traditionally, methods to investigate microbial communities were based on techniques such as microscopic identification of different morphological characteristics, or investigation of metabolic traits such as the ability to grow on different media. These traditional techniques are inadequate to evaluate the diversity of microorganisms in a sample. In contrast to animals and plants, morphologically similar microorganisms can be totally different species. The investigation of metabolic traits of microorganisms is dependent upon cultivation of pure cultures of the microorganisms. The problem is that many bacterial species do not have the ability to grow on the cultivation media available today. In addition, some organisms may enter a dormant state due to unfavorable environmental conditions, often referred to as viable-but-nonculturable, VBNC (Barer et al. 1993). With cultivation-based techniques, only a small portion of the microbial community can be detected (Madigan & Martinko 2006). This is frequently referred to as "The Great Plate Count Anomaly", a term coined by Staley & Konopka (1985). The problem is well illustrated when comparing plate counts (cfu) with direct microscopic counts for the quantification of microorganisms. It has repeatedly been shown that the cell number measured by plate count techniques is much lower than the cell number measured by direct microscopic

counts. Amann et al. (1995) reviewed results from cfu counts and direct microscopic counts from different habitats as shown in Table 1.1.

Table 1.1: The culturability of bacteria in different habitats, given as the percentage of culturable bacteria (cfu) in comparison with total cell counts. The table is adapted from Amann et al. (1995).

| Habitat | Culturability (%) |
| --- | --- |
| Seawater | 0.001-0.1 |
| Freshwater | 0.25 |
| Mesotrophic lake | 0.1-1 |
| Unpolluted estuarine waters | 0.1-3 |
| Activated sludge | 1-15 |
| Sediments | 0.25 |
| Soil | 0.3 |

The microorganisms that are obtained by standard cultivation techniques are able to grow rapidly. They thrive in growth media with higher nutrient concentrations than usually found in nature, and typically at aerobic and mesophilic conditions. These organisms have been referred to as the "weeds" of the microbial world (Madigan & Martinko 2006, Hugenholtz 2002). Our knowledge of prokaryotic diversity from cultivation-based techniques is therefore restricted to a few bacterial phyla.

To improve the bias of cultivation-based techniques, molecular approaches have been developed. These techniques make it possible to analyze microbial communities qualitatively and quantitatively. The direct retrieval of DNA sequences from microbial communities, and classification of microbial species from the sequence information is essential (Amann et al. 1995, Madigan & Martinko 2006, Hugenholtz 2002).

### 1.4.2  Evolutionary chronometers

Evolutionary chronometers are used to measure the evolutionary distance between organisms. This enables us to classify organisms according to their phylogeny. Commonly used as evolutionary chronometers are the genes coding for ribosomal rRNA, and genes for proteins that are widely distributed throughout different groups of organisms. By comparing the gene sequence of the unknown species with the sequence of already classified species, the phylogenetic affiliation can be estimated (Madigan & Martinko 2006).

The fundamental assumption or approximation is that the sequence of the molecular chronometer changes randomly in time. The amount of mutations a gene has, compared to the ancestral gene is then the product of the mutation rate and the time over which the mutations has occurred.

We cannot compare the sequence from an unknown species with the sequence from some original ancestor. Instead, we compare the sequence of the unknown species with sequences from classified species. The sequence divergence between two different species will be approximately twice as high as the sequence divergence to their common ancestor (Woese 1987).

A molecular chronometer has to change at a rate that is appropriate for the phylogenetic change to be measured. A high rate of change makes it possible to measure small phylogenetic distances. To measure large phylogenetic distances, the rate of change should be low. The chronometer must have some regions of conservation for the alignment of homologous sequences from different species (Madigan & Martinko 2006).

It is unfortunately hard to find a DNA or protein sequence that change randomly in time. The genes that are suitable as chronometers are usually conserved due to the high phylogenetic distances to be measured. Mutations in such genes are usually not accumulated completely randomly. Mutations that have a functional effect will be influenced by selection. When the function of proteins changes during evolution, nonrandom mutations will accumulate, and the phylogenetic distance might be overestimated (Woese 1987).

**16S rRNA as a molecular chronometer**

The prokaryotic 16S rRNA gene is widely used as an evolutionary chronometer. The function of the 16S rRNA has remained constant. This constancy gives the 16S rRNA a good clock-like behaviour, i.e. the rate of sequence change has been quite constant. 16S rRNA (or 18S rRNA in eukaryotes) are present in all organisms, and all organisms can therefore be compared by using the 16S rRNA as a chronometer. 16S rRNA have several functional domains that have evolved at different rates. This makes the 16S rRNA gene suitable for phylogenetic analysis over different evolutionary ranges. PCR primers for different microbial groups can be designed, e.g. the domain bacteria or specific microbial phyla. The highly conserved domains permit accurate alignment of different sequences (Stahl 1997, Röling & Head 2005). The widespread use of the 16S rRNA for phylogenetic analysis has made large amounts of 16S rRNA sequence data available. This makes it possible to classify unknown species more accurately. More than 1,000,000 16S rRNA sequences have been deposited into the ribosomal database project (RDP) (Cole et al. 2003).

**The *amoCAB* operon as a molecular chronometer**

In addition to 16S rRNA genes, genes encoding functional proteins can also be used as phylogenetic markers. There are several advantages to using protein-coding genes instead of 16S rRNA. 16S rRNA based phylogeny is

| amoC (813-825 bp) | IS | amoA (825-831 bp) | amoB (1248-1263 bp) |
|---|---|---|---|

Figure 1.4: The structure of the *amoCAB* operon with the *amoC*, *amoA* and *amoB* genes, and an intergenic space (IS). The Figure is adapted from Junier et al. (2009).The structure of the *amoCAB* operon varies slightly between different ammonia-oxidizers, especially between $\beta$- and $\gamma$-AOB. Multiple copies of the genes have been found in many ammonia-oxidizers (McTavish et al. 1993, Norton et al. 1996, 2002).

not necessarily related to the physiology of organisms. Organisms that are phylogenetically unrelated may have similar functional characteristics. Primers for protein-coding genes can amplify genes from microbes that have the same functional characteristics, e.g. metabolic capability, whether they are phylogenetically related or not. This can make it easier to study microorganisms with similar functions in a microbial community.

Nitrifying bacteria are closely phylogenetically related. It is therefore possible to design 16S rRNA primers that are more or less specific for the functional groups of AOB or NOB. But when there is a slight lack of specificity of the PCR primers targeting 16S rRNA genes, the genes from non-target microbial species will be amplified (Stephen et al. 1996, Norton et al. 1996, Rotthauwe et al. 1997). This will make the detection of the target group more difficult. It can therefore be advantageous to use genes involved in the nitrifying process for classification of unknown species.

The *amoA* gene has frequently been used for the analysis of ammonia-oxidizing bacteria (Sinigalliano et al. 1995, Rotthauwe et al. 1997, Alzerreca et al. 1999). The *amoA* gene is located in an operon together with the *amoC* and *amoB* genes, depicted in Figure 1.4 (McTavish et al. 1993, Bergmann & Hooper 1994, Klotz & Norton 1995, Klotz et al. 1997, Sayavedra-Soto et al. 1998). These genes code for the different subunits in the ammonia monooxygenase (AMO) enzyme, catalyzing the oxidation of ammonia to hydroxylamine in the nitrification process (Hollocher et al. 1981).

The *amoA* gene encodes the active, membrane-bound subunit of the AMO enzyme (McTavish et al. 1993). Rotthauwe et al. (1997) were the first to use the *amoA* gene as a functional marker for analysis of $\beta$-AOB. Widespread use of the *amoA* gene as a phylogenetic marker (Purkhold et al. 2000, Nicolaisen & Ramsing 2002, Ebie et al. 2004, Hornek et al. 2006) for the analysis of nitrifying microbial communities has made many *amoA* sequences available for phylogenetic classification of unknown species.

The *amoA* gene is very conserved. This gives less resolution for phylogenetic analysis than what the 16S rRNA gene can provide (Purkhold et al. 2003). The other genes in the *amoCAB* operon have also been investigated for their potential as phylogenetic markers (Junier et al. 2008, 2009). It has recently been shown that the *amoB* gene has the highest sequence vari-

ability, suggesting that *amoB* can give higher resolution for phylogenetic analysis (Junier et al. 2009) than the *amoA* gene.

Archaeal genes analogous to bacterial *amoA, amoB* and *amoC* genes have also been found (Venter et al. 2004, Treusch et al. 2005). The archaeal variants of these genes are not closely related to the bacterial genes. The archaeal *amoA* gene has been used to investigate the abundance and diversity of AOA in different habitats (Coolen et al. 2006, Wuchter et al. 2006, Park et al. 2008, Tourna et al. 2008, Nicol et al. 2008). Phylogenetic analysis of several hundred variants of the archaeal *amoA* gene has revealed a large AOA diversity (Francis et al. 2005), and archaeal *amoA* genes seem to be ubiquitous in soils, sediments, aquatic environments and wastewater bioreactors (Venter et al. 2004, Francis et al. 2005, Leininger et al. 2006, Wuchter et al. 2006, Park et al. 2006).

## 1.5 Molecular methods to analyze microbial communities

During the last two decades, several molecular techniques to analyze microbial communities have been developed. Fluorescence *in situ* hybridization (FISH) and Denaturing Gradient Gel Electrophoresis (DGGE) are two techniques that have become especially important in microbial ecology. They are often used in combination, as in this thesis.

### 1.5.1 PCR-DGGE

Denaturing gradient gel electrophoresis (DGGE) is a DNA fingerprinting technique which enables us to get rapid and simplified information about microbial communities. Prior to DGGE, DNA from the environmental sample has to be extracted. Polymerase chain reaction (PCR) is then used to amplify specific DNA fragments from the microbes that are present. Universal primers, or primers that are specific for certain functional or phylogenetic groups are normally used, resulting in amplification of equal-length sequences from different organisms (Muyzer et al. 1993).

The principle for DGGE (Figure 1.5) is the electrophoretic separation of equal-length DNA fragments in a polymer gel with an increasing denaturing gradient. The DNA fragments are separated according to their melting behaviour, dependent upon the base composition. When the DNA fragments reach the point in the gel where the amount of denaturing substances, i.e. formamide and urea, cause the DNA fragments to partially denature, the DNA fragments will stop in the gel. Single stranded DNA is more retarded in the gel than double stranded DNA because the free nucleotides of single stranded DNA gets more entangled in the gel network (Muyzer et al. 1993, Felske & Osborn 2005). To prevent the DNA strands from denaturing com-
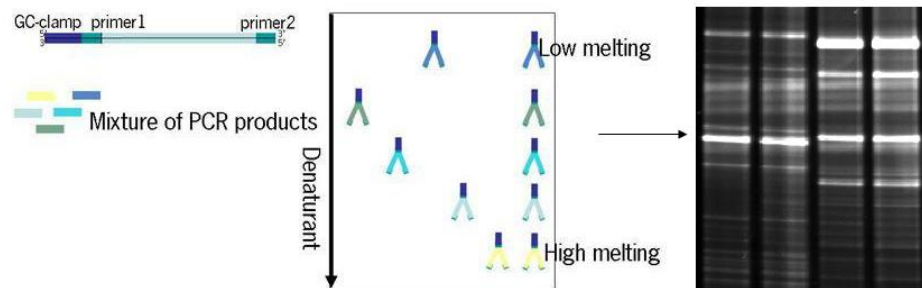
Figure 1.5: The principle for separation of DNA fragments by DGGE (left). When DNA fragments denature in the denaturing gradient of the gel, the migration stops. A GC rich sequence at the end of the DNA fragments (the GC-clamp) keeps the DNA fragments from denaturing completely. The Figure is adapted from Plant Research International (2010). The picture to the right shows an actual DGGE gel after staining of DNA with SYBRGold. The four lanes are four different samples. Each band should ideally represent one DNA sequence from one microbial species.

pletely, a GC rich sequence, denoted GC-clamp, is added to one end of the DNA fragments. The GC-clamp is added during PCR by using a primer with the GC-rich sequence in the 5'-end. Single stranded DNA kept together by the GC-clamp will practically stop in the gel (Muyzer et al. 1993, Felske & Osborn 2005). The resulting pattern of different bands in the gel can give information about the diversity and organization of the microbial community. Bands in the gel can also be excised and sequenced.

### PCR primers for the detection of nitrifiers

Table 1.2 shows some primers that have been developed for the detection of AOB, NOB and archaeal 16S rRNA and functional genes.

Since nitrifying bacteria are phylogenetically related, it is possible to design 16S rRNA primers that are more or less specific for groups of nitrifiers. NOB are more widely phylogenetically distributed than AOB, and 16S rRNA primers must be designed to target smaller groups within the NOB, e.g. the *Nitrospira* genus or the *Nitrobacter* genus. Primers targeting all NOB would lack specificity. Primers targeting archaeal 16S rRNA have also been developed, mostly general primers for the domain *Archaea*.

The 16S rRNA primers for AOB do not have optimal specificities, and many nitrifiers can be excluded due to mismatches with the primers. A different strategy is to use the *amoA* gene for detection of AOB. Rotthauwe et al. (1997) was the first to use the *amoA* gene to study populations of β-AOB in microbial communities. Rotthauwe et al. (1997) developed the fre-

Table 1.2: Primers targeting 16S rRNA and functional genes of AOB and NOB.

| Primer | Target organism | Sequence (5'-3') | Reference |
|---|---|---|---|
| 16S rRNA | | | |
| $\beta$AMOF | $\beta$-AOB | TGGGGRATAACGCAYCGAAAG | McCaig et al. 1994 |
| $\beta$AMOR | $\beta$-AOB | AGACTCCGATCCGGACTA CG | McCaig et al. 1994 |
| CTO189F | $\beta$-AOB | GGAGRAAAGCAGGGGATCG | Kowalchuk et al. 1997 |
| CTO654R | $\beta$-AOB | CTAGCYTTGTAGTTTCAAACG C | Kowalchuk et al. 1997 |
| NitA | $\beta$-AOB | CTTAAGTGGGGAATAACGCATCG | Voytek & Ward 1995 |
| NitB | $\beta$-AOB | TTACGTGTGAAGCCCTACCCA | Voytek & Ward 1995 |
| NOC1 | $\gamma$-AOB | CGTGGGAATCTGGCCTCTAGA | Voytek 1996 |
| NOC2 | $\gamma$-AOB | AGATTAGCTCCGCATCAGCT | Voytek 1996 |
| GAOB16S-F | $\gamma$-AOB | GCGTGGGAATCTGGCCTCTA | Moin et al. 2009 |
| GAOB16S-R | $\gamma$-AOB | CATCGCTGCTTGGCCACCT | Moin et al. 2009 |
| Nbacter-1050R | Nitrobacter | CACCTGTGCTCCATGCTCCG | Freitag et al. 2005 |
| Nspira-705R | Nitrospira | GGCCTTCYTCCCGAT | Freitag et al. 2005 |
| Arch-20F | Domain Archaea | TTCCGGTTGATCCYGCCRG | DeLong, 1992 |
| Arch-958R | Domain Archaea | TCCGGCGTTGAMTCCAATT | DeLong, 1992 |
| PARCH-340F | Domain Archaea | CCCTACGGGGYGCASCAG | Øvreås et al. 1997 |
| PARCH-519R | Domain Archaea | TTACCGCGGCKGCTG | Øvreås et al. 1997 |
| amoA/pmoA | | | |
| amoA-1F | $\beta$-AOB | GGGGHTTYTACTGGTGGT | Rotthauwe et al. 1997 |
| amoA-2R | $\beta$-AOB | CCCCTCKGSAAAGCCTTCTTC | Rotthauwe at al. 1997 |
| A189F | AOB and MOB | GGNGACTGGGACTTCTGG | Holmes et al. 1995 |
| A682R | AOB and MOB | GAASGCNGAGAAGAASGC | Holmes et al. 1995 |
| amoAF-i | $\beta$-AOB | GGGGITTITACTGGTGGT | Hornek et al. 2006 |
| amoAR NEW | $\beta$-AOB | CCCCTCBGSAAAVCCTTCTTC | Hornek et al. 2006 |
| amoAR-i | $\beta$-AOB | CCCCTCIGIAAAICCTTCTTC | Hornek et al. 2006 |
| amoA121F | $\beta$-AOB | ACCTACCACATGCACTT | Webster et al. 2002, Junier et al. 2008 |
| amoA359RC | $\beta$-AOB | GGGTAGTGCGACCACCAGTA | Webster et al. 2002, Junier et al. 2008 |
| amoA-3F | $\gamma$-AOB | GGTGAGTGGGYTAACMG | Purkhold et al. 2000 |
| Arch-amoA26F | Archaea | GACTACATMTTCTAYACWGAYTGGGC | Park et al. 2008 |
| Arch-amoA417R | Archaea | GGKGTCATRTATGGWGGYAAYGTTGG | Park et al. 2008 |
| Arch-amoAF | Archaea | GCTCTAATTATGACAGTATAC | Park et al. 2008 |
| Arch-amoAR | Archaea | AYCATGTTGAAYAATGGTAATGAC | Park et al. 2008 |
| Arch-amoA-for | Archaea | CTGAYTGGGCYTGGACAT | Wuchter et al. 2006 |
| Arch-amoA-rev | Archaea | TTCTTCTTTGTTGCCCAGTA | Wuchter et al. 2006 |
| amoB | | | |
| amoB-4R | $\gamma$-AOB | GCTAGCCACTTTCTGG | Purkhold et al. 2000 |
| amoBMF | AOB | TGGTAYGACATKAWATGG | Calvó & Garcia-Gil 2004 |
| amoBMR | AOB | RCGSGGCARGAACATSGG | Calvó & Garcia-Gil 2004 |
| nrxA | | | |
| F1norA | NOB | CAGACCGACGTGTGCGAAAG | Poly et al. 2008 |
| R1norA | NOB | TCYACAAGGAACGGAAGGTC | Poly et al. 2008 |

14

quently used *amoA* primers *amoA*-1F and *amoA*-2R. Since then, the pool of *amoA* sequence data in the databases have increased, and new primers have been made, although the *amoA*-1F and *amoA*-2R primers are still frequently used. The *amoA*-1F and *amoA*-2R primers are degenerated. Hornek et al. (2006) developed the primers *amoA*f-i, *amoA*r NEW and *amoA*r-i which amplify the same sequence as the traditional *amoA* primers, but with inosine bases instead of degenerations to reduce multiple band patterns from the degenerated primers. Another, newer primer pair amplifying a slightly shorter segment of the *amoA* gene in β-AOB was designed by Webster et al. (2002), and re-evaluated and updated by Junier et al. (2008). This primer pair was designed especially for DGGE analysis.

It is difficult to design primers that target both β- and γ-AOB *amoA* without targeting the closely related *pmoA* gene. The *pmoA* gene encodes the membrane-bound particulate methane monooxygenase (pMMO) in methanotrophs (McDonald & Murrell 2006). The A189f/A682r primer pair targets both AOB *amoA* genes and MOB *pmoA* genes. Primers targeting the archaeal amoA gene have been developed to investigate ammonia-oxidizing archaea.

The *amoB* and *amoC* genes have also been used as phylogenetic marker genes, and primers targeting AOB and AOA have been developed (Könneke et al. 2005).

The functional gene *nxrA*, which encodes the catalytic subunit of the nitrite oxidoreductase in NOB, has recently been used to investigate nitrite-oxidizing communities by PCR-DGGE. Poly et al. (2008) developed primers for PCR-based investigation of nitrite-oxidizing communities. These were later modified for DGGE by Wertz et al. (2008).

**Sequence analysis**

After separation of equal-length DNA fragments from different organisms in an environmental sample by DGGE, it is possible to cut out DNA material from the DGGE gel, re-amplify the DNA fragments, and sequence them. This gives the possibility to determine the microbial origin of the different bands in the DGGE gel. The identity of the DGGE bands can be assessed by comparing the DNA sequence with sequences deposited in databases, e.g. GenBank (Benson et al. 2008). An operational species definition based on DNA similarity can be applied. Generally, if two organisms have 16S rRNA sequence similarity below 97 %, they can be regarded as different species (Stackebrandt & Goebel 1994, Amann et al. 1995, Röling & Head 2005, Staley 2006).

The first step in detailed phylogenetic sequence analysis is usually alignment of the different sequences. Sequences from databases can be included in the alignment to increase the quality of the alignment. Bases that are conserved between different organisms are aligned, and gap characters are

introduced at places where deletions or insertions have occurred. The result is a set of sequences that are equally long, and where conserved bases are identified and aligned (Röling & Head 2005).

Several methods have been developed to calculate phylogenetic relationships from molecular sequences, e.g. maximum likelihood methods, parismony methods and distance methods. The phylogenetic distances between sequences can be visualized in phylogenetic trees. Such trees can be constructed by using several methods. The statistical validity of the calculated phylogenetic groupings is often tested by using bootstrap analysis. The bootstrap analysis gives a measure of the robustness of the phylogenetic trees (Röling & Head 2005, Holmes 2003).

### 1.5.2   Methodological biases

DGGE is dependent upon extraction of nucleic acids from the environmental samples and PCR amplification of marker sequences. Both DNA extraction and PCR can introduce biases, giving a wrong impression of the microbial diversity.

**PCR artefacts**

Artefacts can be produced during PCR, and may lead to an overestimation of the microbial diversity. The polymerase enzyme is not entirely accurate, and incorrect nucleotides can be incorporated. This is especially true for the frequently used Taq polymerase, which lacks proofreading exonuclease activity (Röling & Head 2005).

A sometimes encountered PCR problem is the formation of chimeric DNA molecules. Chimeras are DNA molecules that originate from more than one parent DNA strand. They can be produced after incomplete synthesis of target DNA fragments. The incomplete products can anneal to homologous DNA molecules from other organisms in the sample and form heteroduplexes. These heteroduplexes will then be amplified during the next PCR cycles, resulting in DNA fragment that consist of DNA originating from different organisms. To avoid formation of chimeras, the elongation step should be long to reduce the extent of incomplete synthesis from premature elongation termination. PCR artefacts tend to be more dominating after many PCR cycles. It is therefore best to limit the number of PCR cycles (Amann et al. 1995, Röling & Head 2005).

**Differential amplification**

The distribution of different sequences in a PCR product, e.g. as visualized by the intensity of different bands in a DGGE gel, does not necessarily reflect the true diversity and distribution of microorganisms in an environmental

sample. The efficiency of amplification may vary considerably between different target sequences. This can lead to wrong impression of abundances of microorganisms. Differential amplification during PCR can be caused by different accessibility of primers to different templates, different primer-template annealing efficiencies, and different elongation efficiencies (Röling & Head 2005).

### 1.5.3   FISH

Fluorescence *in situ* hybridization (FISH) is a technique that is used to analyze organisms or genes directly in their environment. FISH is frequently used in microbial ecology to detect specific phylogenetic groups in environmental samples. Cells are detected by using short oligonucleotide probes that are labelled with a fluorescent molecule. After fixation and permeabilization of the microbial cells, probes may enter and hybridize to nucleic acids with a nucleotide sequence that corresponds to that of the probe. One sample may be hybridized with several probes simultaneously, if the different probes are labelled with fluorochromes of different colour. (Giovannoni et al. 1988, DeLong et al. 1989, Amann et al. 1990).

Normally the probe targets 16S rRNA because the high ribosomal copy number facilitates sufficient signal for detection. 16S rRNA is also established as a phylogenetic marker (see section 1.4.2), and a large pool of sequence data is available for probe design. The different levels of sequence conservation within the 16S rRNA molecule allows design of probes that target different phylogenetic levels, e.g. the domain *Bacteria* or the genus *Nitrospira*. The rRNA is usually to conserved to design probes that are specific for single species (Amann et al. 1990, Wagner et al. 2003). Figure 1.6 shows the basic methodological steps in FISH.

After hybridization, stained cells can be detected and quantified. Quantification can be done by direct counting of single cells with an epifluorescence microscope. However, microbes in environmental samples are often in dense aggregates or biofilms, and in such samples it can be difficult to count cells directly. When using confocal laser scanning microscopy (CLSM), thicker samples can be analyzed quantitatively by measuring the area (in pixels) of stained biomass. The spatial organization of intact cell aggregates or biofilms can also be analyzed be scanning different optical sections in the samples (Daims et al. 2001, 2005).

The FISH technique suffers from some limitations. Target cells may not be detected due to a number of factors such as insufficient permeabilization of cells, low rRNA levels giving insufficient signal, secondary folding of the rRNA making some regions inaccessible to probes and background fluorescence. Several modifications of the FISH technique have been developed to overcome such methodological limitations (Wagner et al. 2003, Amann & Fuchs 2008).
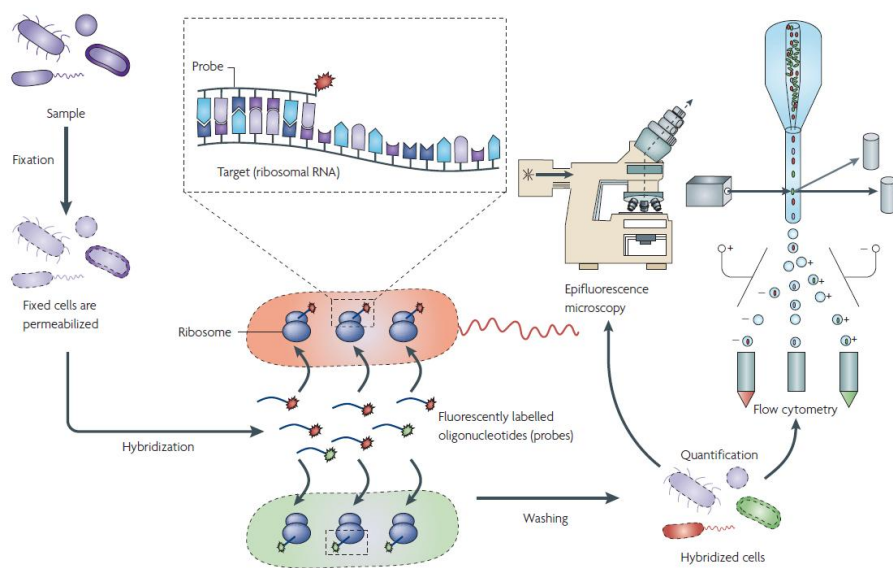
Figure 1.6: The basic steps in FISH. The microbial cells are fixated to stabilize cell components, and to permeabilize the cell membrane. Oligonucleotide probes are added, and hybridization conditions are optimized for specific hybridization. The stringency of hybridization is adjusted by adding formamide to the hybridization buffer. After washing off excess probe, the sample is analyzed by fluorescence microscopy or flow cytometry. The Figure is from Amann & Fuchs (2008).

### 1.5.4 The rRNA approach

DGGE gives information about the DNA sequences that are present in an environment. Unfortunately, the biases that can be introduced from the methodological limitations make it difficult to prove whether the sequences present were from organisms that are important players in the habitat. FISH can be used to verify the quantitative significance of different organisms in the sample. The combination of 16S rRNA sequence analysis and FISH is referred to as the rRNA approach, shown in Figure 1.7. Sequence information from the microbial community under investigation can be used to design oligonucleotide probes for FISH, which brings us back to the starting material, making a closed loop (Amann et al. 1995, Hugenholtz 2002).
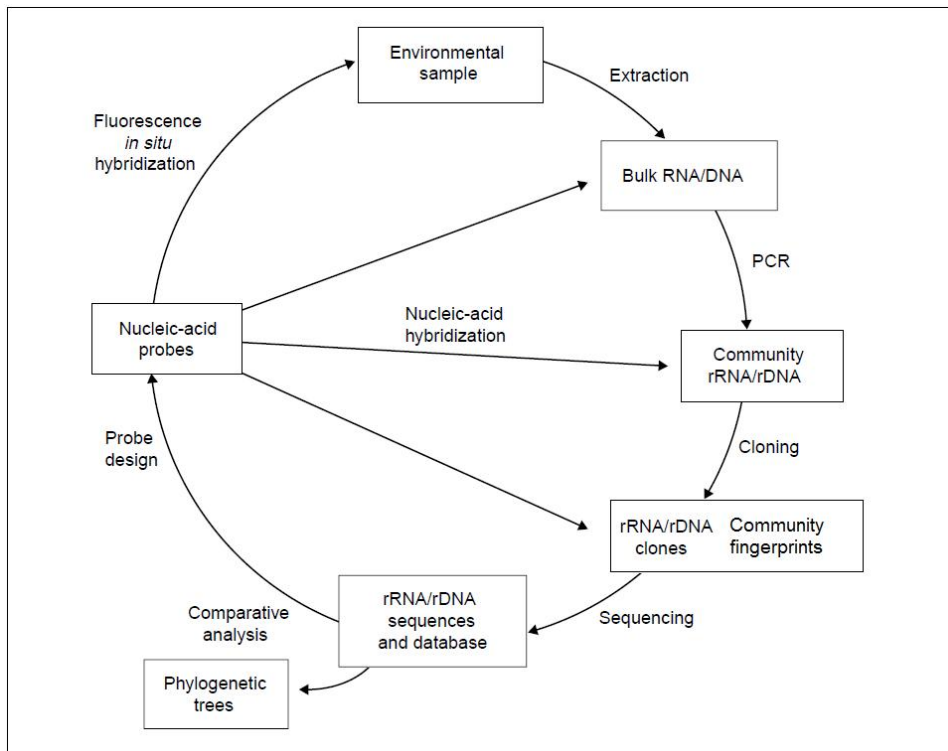


Figure 1.7: The full-cycle rRNA approach. Adapted from Hugenholtz (2002)

## 1.6 Previous research at the Department of Biotechnology

Kristoffersen (2004) tested the acute effect of different salinities on the activities in two different nitrifying biofilm cultures. These biofilm cultures grew on the same type of biofilm carriers, and were of the same origin as the biofilm inoculations used in this thesis. Two batch reactors, one with a biofilm culture adapted to tapwater-based cultivation medium, one with a culture adapted to 2/3 seawater, were supplied sequentially with cultivation media with different contents of seawater. The biofilm adapted to low salinity was supplied with cultivation media of increasing seawater content, while the biofilm adapted to high salinity was supplied with cultivation media of decreasing seawater content.

The nitrifying activity in the biofilm adapted to low salinity decreased with increasing seawater content (Figure 1.8), while the nitrifying activity in the biofilm adapted to high salinity did not seem to be affected much by the seawater content (Figure 1.9). In the culture adapted to 2/3 seawater, the activity was slightly lower at high salinities, but this effect was smaller than in the culture adapted to low salinity.
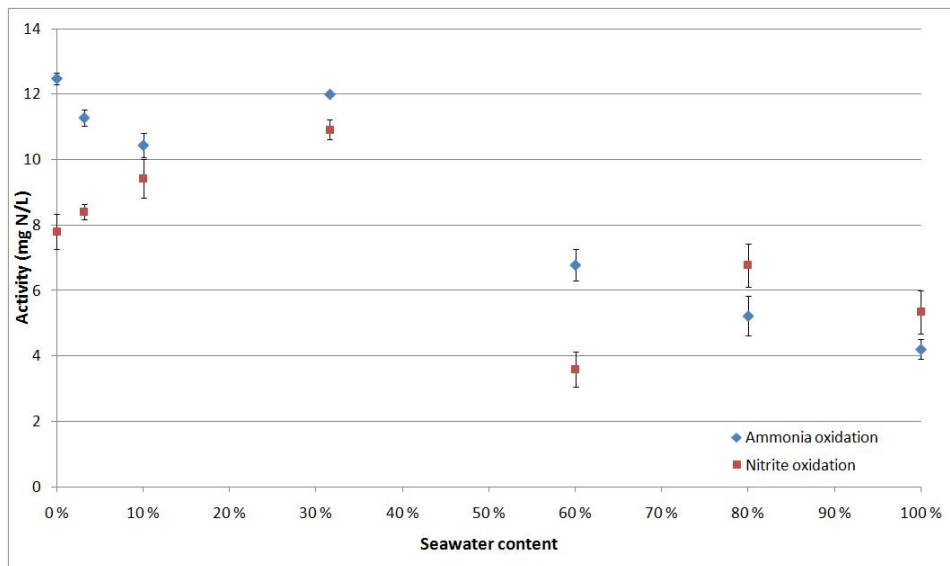


Figure 1.8: Nitrification activities in a culture adapted to low salinity, at different salinities. The ammonia oxidation activity is given as mg $NH_4^+$-N removed/Lh, the nitrite oxidation activity is given as $NO_3$-N produced/Lh. The error bars indicate the standard error.
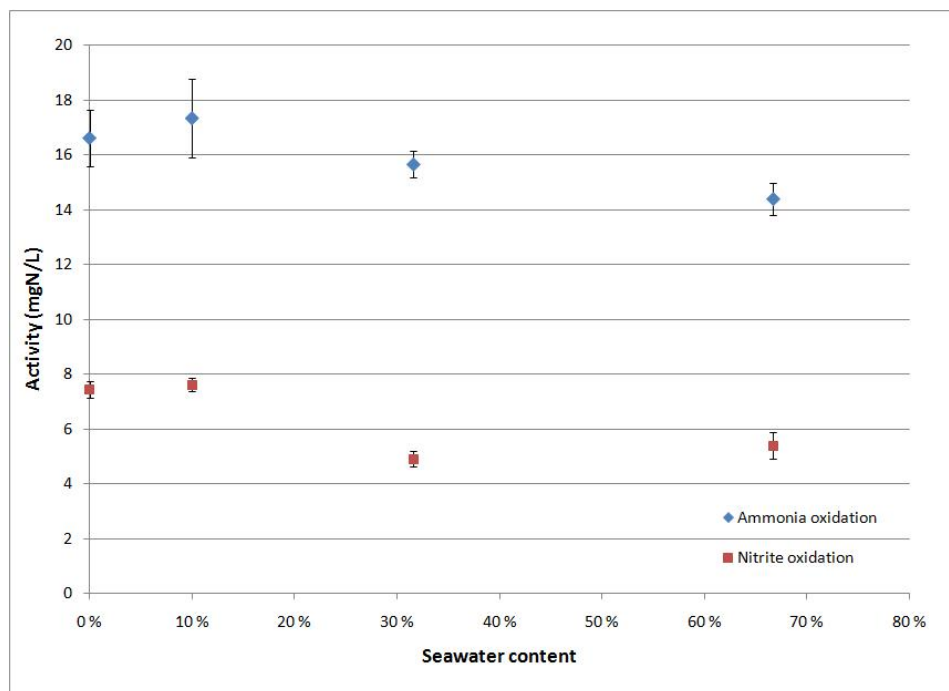
Figure 1.9: Nitrification activities in a culture adapted to 2/3 seawater, at different salinities. The ammonia oxidation activity is given as mg $NH_4^+$-N removed/Lh, the nitrite oxidation activity is given as $NO_3$-N produced/Lh. The error bars indicate the standard error.

Pedersen (2007) re-inoculated the nitrifying cultures from Kristoffersen (2004), and continued the operation of nitrifying reactors supplied with tapwater-based and seawater-based cultivation media for enrichment of nitrifying bacteria adapted to different salinities. Preliminary experiments to analyze the nitrifying communities with PCR-DGGE were started.

## 1.7 Scope

The nitrifying cultures from Kristoffersen (2004) and Pedersen (2007) were available for further investigation. The aim of this thesis was to investigate and compare the microbial communities in these cultures, adapted to seawater-based and tapwater-based cultivation media. This included further operation of continuous, lab-scale nitrifying reactors, measurements of nitrification activities and characterization of the microbial communities by DGGE and FISH. The molecular techniques had to be tested and optimized with regard to choice of PCR primers for detection of nitrifiers, PCR reagents and temperature regime, denaturing gradients for separation of sequences and preposition for and testing of the FISH technique.

# Chapter 2

# Materials and Methods

## 2.1 Biofilm cultivation systems

Two continuous biofilm reactor systems were operated in order to cultivate nitrifying bacteria. The reactors were moving bed biofilm reactors (MBBR) with AnoxKaldnes™K1 biofilm carriers, shown in Figure 2.1. One of the reactors was supplied with a tap water-based medium, while the other was supplied with seawater-based medium.

### 2.1.1 Inoculation

#### Inoculation of the tap water-based reactor

The reactor for enrichment of nitrifying bacteria adapted to low salinity was inoculated in connection with a student course in Environmental Biotechnology (TBT4130) at NTNU, by instructions from me. The inoculum was enriched nitrifying sludge that originated from a nitrification pilot plant at the Department of Hydraulic and Environmental Engineering at NTNU. The pilot plant was supplied with fresh domestic wastewater. The nitrifying sludge had been enriched over several years in previous lab courses, and had been frozen and re-inoculated multiple times. In addition, the reactor was inoculated with some material from Ladehammeren wastewater treatment plant in Trondheim. This material was biofilm scrapings from the inlet to the flocculation and sedimentation chambers, after pre-treatment steps. The reactor was filled with 300 mL of unused AnoxKaldnes K1 biofilm carriers. This gave a hydraulic filling degree of approximately 40 %.

#### Inoculation of the seawater-based reactor

The seawater-based reactor was inoculated with 180 mL of AnoxKaldnes biofilm carriers, that already had an established nitrifying biofilm. The inoculum originated from Statoil's aerated lagoon at Mongstad, treating wastewater from the oil refinery. The lagoon has a salinity of approximately 20 ‰. The inoculum was first enriched for nitrifiers by Norevik
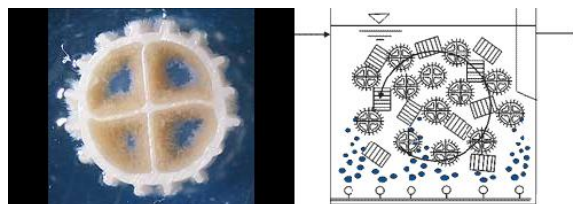


Figure 2.1: The biofilm principle for the nitrifying reactors. An AnoxKaldnes K1 biofilm carrier is shown to the left. The picture to the right shows how the biofilm carriers were distributed in the reactors (AnoxKaldnes n.d).

(2004), and later by Kristoffersen (2004) and Pedersen (2007). Approximately 1/3 of the biofilm carriers used in the seawater-based reactor came from a similar reactor operated by Pedersen (2007), that had been supplied with a seawater-based medium made from 2/3 of seawater and 1/3 of tap-water, corresponding to a salinity of approximately 21 ‰. The rest of the biofilm carriers came from another, but similar reactor that had been fed with a medium made from up to 100 % seawater (Kristoffersen 2004), with a salinity of approximately 32 ‰ (Granum & Myklestad 2002). All biofilm carriers had been stored at -20 °C prior to inoculation. No additional, unused biofilm carriers were added after inoculation. This gave a hydraulic filling degree of approximately 13 %.

### 2.1.2 Cultivation media

The two reactors were continuously fed with cultivation media made from the compounds listed in tables 2.1 and 2.2 (Østgaard et al. 1994). The medium for the reactor with low salinity was made by dissolving the compounds in tables 2.1 and 2.2 in tap water. The medium for the seawater-based reactor was made from 2/3 of seawater and 1/3 of tap water, which gave a salinity of approximately 21 ‰(Granum & Myklestad 2002). The seawater was collected from approximately 700 meters of depth in Trondheimsfjorden, outside the biological station in Trolla, and stored in a large plastic container in the dark at room temperature. The seawater was filtered through a Whatman GF/F filter prior to use in the medium. The pH in both media was adjusted to 7.5 by adding NaOH or HCl.

### 2.1.3 Continuous reactor set-up and regulation

**Reactor layout**

The layouts of the tap water-based and the seawater-based reactors were similar. Figure 2.2 shows the experimental set-up for the reactors.

Table 2.1: Composition of the medium fed to the nitrifying reactors. $(NH_4)_2SO_4$ was supplied as the sole energy source in the medium. $K_2HPO_4$ or $NaH_2PO_4$ was the source of phosphorus (in the fresh-water and saline reactors, respectively[1]), while $NaHCO_3$ was a carbon source as well as a pH-buffer. The composition of the trace metal stock solution is listed in Figure 2.2.

| Compound | Amount per 10 L medium | |
| --- | --- | --- |
| | Tapwater-based medium | Seawater-based medium |
| $(NH_4)_2SO_4$ | Varying | Varying |
| $K_2HPO_4$ | 4 g | |
| $NaH_2PO_4$-$H_2O$ | | 0.05 g |
| $NaHCO_3$ | 10 g | 10 g |
| Trace metal stock solution | 100 mL | 100 mL |
| Tap water | 10 L | 3.3 L |
| Sea water | | 6.6 L |

[1] In the seawater-based reactor, $NaH_2PO_4$ was used as a phosphorus source instead of $K_2HPO_4$, because of previous experience with precipitation of $K_2HPO_4$ at high salinity (Kristoffersen 2004).

Table 2.2: Composition of the trace metal stock solution added to the media.

| Compound | Amount (g) per L stock solution |
| --- | --- |
| $MgSO_4$-$7H_2O$ | 2.5 |
| $MnCl_2$-$4H_2O$ | 0.55 |
| $CaCl_2$-$2H_2O$ | 1.5 |
| $ZnCl_2$ | 0.068 |
| $CoCl_2$-$6H_2O$ | 0.12 |
| $NiCl_2$-$6H_2O$ | 0.12 |

Both reactors were small, bench scale reactors; the tapwater-based reactor had a hydraulic volume of 1 L, while the seawater-based reactor had a hydraulic volume of 1.4 L. The reactors were simple glass containers with silicone lids with holes for inlet, pH control and aeration equipment. The glass containers had outer heating jackets for temperature control. Metal grids were in front of the reactor outlets to keep the biofilm carriers inside. The reactors were mixed using magnetic stirrers to evenly distribute air, medium and biofilm carriers in the reactor. The reactors were covered with black fabric or plastic bags to avoid growth of phototrophes. Figure 2.3 is a photograph that shows the seawater-based reactor.
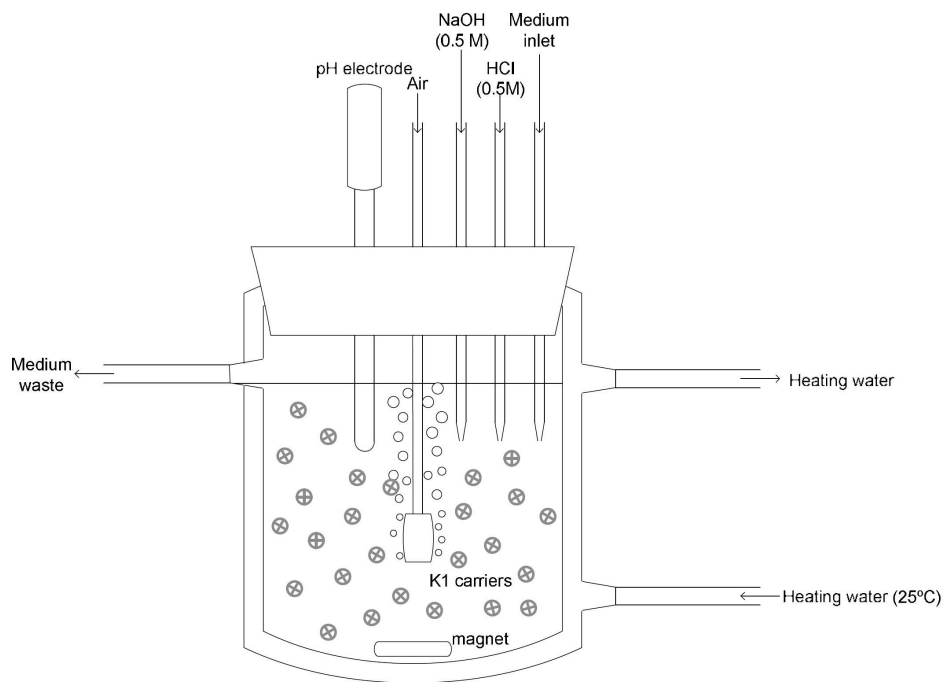
Figure 2.2: The experimental set-up for the nitrification reactors. The Figure is from Colaço (2009).
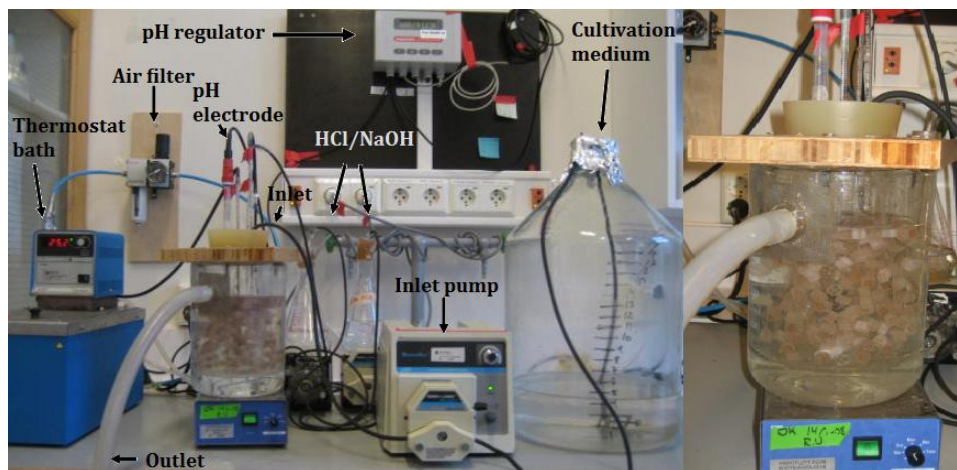


Figure 2.3: The seawater-based nitrifying reactor with aeration, pH control, stirring, temperature control and continuous medium supply (left). Close-up on the reactor with biofilm carriers (right).

**Inlet flow regulation**

The cultivation media were fed to the reactors by adjustable Masterflex pumps (Cole-Parmer L/S® variable-speed console drive with Easy-Load® pump head). The inlet flows were monitored by measuring the medium consumption and occasionally by measuring the flow from the inlet tube.

**Aeration**

The reactors were supplied with air via a submerged aquarium air stone. Due to problems with contamination of the compressed air by compression oil, the air was cleansed by bubbling it through a water bottle, before entering the reactors. Later in the experiment, the air to the seawater-based reactor was cleansed by an active carbon filter (Bosch Rexroth). Dissolved oxygen concentration in the reactors was never measured, but the aeration was kept quite constant, except for in a few occasions where problems with the air supply was experienced.

**pH regulation**

The pH in the reactors was kept between 7.2 and 7.8 (tapwater-based reactor) and 7.4 and 7.6 (seawater-based reactor) by automatic pH controllers (Consort pH controller R301) that by signals from a pH electrode (Mettler-Toldeo) in the reactors, supplied the reactors with 0.5 M HCl or 0.5 M NaOH. Four Masterflex pumps (Cole-Parmer L/S® economy fixed-speed drive) pumped NaOH or HCl into the reactors when necessary.

**Temperature regulation**

The temperature in the reactors was kept at 25 °C by a circulating bath (Cole-Parmer® polystat®) pumping water into outer heating jacket compartments of the reactors. The temperature in the seawater-based reactor was regulated by a circulating bath without a cooling function. The temperature in the reactor could therefore exceed 25 °C if the room temperature was high. The temperature in the tapwater-based reactor was regulated to 25 °C by a refrigerated circulating bath.

### 2.1.4 Analytical procedures for monitoring the nitrification activities in the reactors

Concentrations of ammonium, nitrite and nitrate were measured from five to seven days a week to monitor the nitrifying activity in the reactors. Appendix A and Appendix B show the results from all measurements in the tapwater-based and the seawater-based reactors, respectively. Samples for measurement of these concentrations were obtained by taking out approximately 5 mL of medium from the reactors. All samples were filtered

through 0.45 $\mu$m syringe filters (Sarstedt). Ammonium, nitrite and nitrate concentrations were measured photometrically by the use of Dr. Lange cuvette-tests LCK 303, LCK 341 and LCK 339 (Hach Lange). Samples from the seawater-based reactor were treated with Dr. Lange chloride elimination syringes LCK 341 prior to the photometric assays to avoid interference from chloride ions, as previously experienced (Kristoffersen 2004). The concentrations of ammonium, nitrite and nitrate were also measured in the incoming medium when new medium had been made.

Nitrification activities were calculated using data from the concentration measurements. Nitrification activities, given as the rate of ammonium consumption and nitrate production, were calculated using equations 2.1 and 2.2.

$$\text{Rate of ammonium consumption} = \frac{(\text{NH}_3\text{-N in}) - (\text{NH}_3\text{-N out})}{\text{Reactor hydraulic volume}} \times \text{flow}$$
$$(2.1)$$

$$\text{Rate of nitrate production} = \frac{(\text{NO}_3\text{-N out}) - (\text{NO}_3\text{-N in})}{\text{Reactor hydraulic volume}} \times \text{flow} \quad (2.2)$$

### 2.1.5 Operation and sampling

The tap water-based reactor was started during a student course in environmental biotechnology (TBT4130), by instructions from me. After the student course, the reactor was operated by Colaço (2009). The saline nitrifying reactor was operated for 137 days. During operation, the feeding rates to the reactors were regulated to achieve high nitrification rates.

Biofilm carriers were sampled from the reactors and fixated for FISH or frozen at -20 °C for subsequent DNA isolation and PCR-DGGE. Figure 2.4 and 2.5 are timelines for the tapwater-based and the seawater-based reactors, showing times for inoculation and sampling. At each sampling for FISH, 4-5 biofilm carriers were taken out from each reactor. 4 biofilm carriers from each reactor were sampled for DGGE. Due to shorter equivalent operation time of the tap water-based reactor (from day 122 after inoculation, the tap water-based reactor was used for toxicity testing of amines (Colaço 2009)), less samples were taken from this reactor.
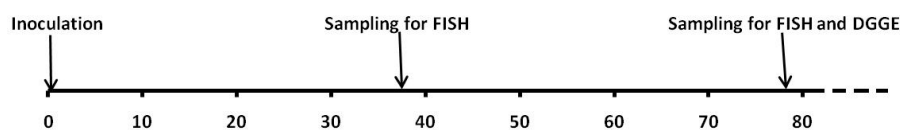
Figure 2.4: Events during the operation of the tap water-based reactor. The time is given in days after inoculation. Operation of the reactor was continued after the last sampling by Colaço (2009).
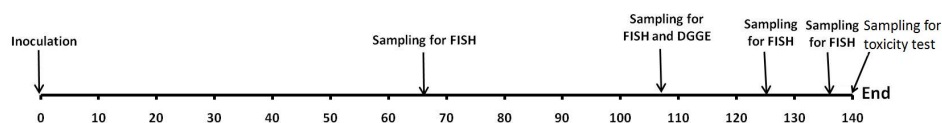


Figure 2.5: Events during the operation of the seawater-based reactor. The time is given in days after inoculation.

### 2.1.6 Batch culture salinity response test

The acute effect of changes in salinity on the nitrification activity was tested on the culture from the seawater-based reactor only. The experiment was carried out as previously described by Kristoffersen (2004), in a batch reactor. The batch reactor was aerated and mixed as the continuous reactors and the pH and temperature was controlled in the same manner. Nitrification media with 0 %, 10 %, 66.7 % and 100 % seawater were made as described in section 2.1.2. The different cultivation media were tested sequentially on the same culture, in descending order of seawater content. First, 100 mL of biofilm carriers from the continuous culture were inoculated with 0.5 L of the cultivation medium with 100 % seawater. The concentrations of ammonium, nitrite and nitrate were measured every 30 minutes for three hours. After three hours, the cultivation medium was changed to the medium with 66.7 % seawater, and the concentrations of ammonium, nitrite and nitrate were once again measured every 30 minutes for three hours. The media with 10 % and 0 % seawater were tested similarly.

The concentrations of ammonium, nitrite and nitrate over time were plotted for each salinity. The nitrification activity was calculated from the slopes of linear regression curves on the linear parts of the concentration data. Regression and calculation of standard errors were performed in SYSTAT (Wilkinson 2010).

30

## 2.2 PCR-DGGE

The samples for PCR-DGGE were four biofilm carriers from the tap water-based reactor, and four biofilm carriers from the seawater-based reactor. The biofilm carriers from each reactor had been sampled simultaneously, as described in section 2.1.5. The DNA from the biofilm on the biofilm carriers were isolated, DNA sequences were amplified, separated by DGGE and sequenced, as described in the following sections.

### 2.2.1 DNA extraction from biofilm carriers

DNA was isolated from the biofilm on the biofilm carriers with the Qiagen® DNeasy blood and tissue kit, using the protocol for Gram-negative bacteria (*DNeasy® Blood and Tissue Handbook* 2006), but with some adjustments (Pedersen 2007) as described below. The biofilm carriers were cut into smaller pieces by using a sterile scalpel, and the pieces were put into sterile 1.5 mL eppendorf tubes. To lyse the cells, the pieces were suspended in 180 $\mu$L of Buffer ATL and 20 $\mu$L of proteinase K, and incubated at 54 °C for approximately two hours. After incubation, the lysates were transferred to new tubes, to get rid of the plastic pieces from the biofilm carriers. 200 $\mu$L of Buffer AL and 200 $\mu$L of ethanol (96 %) were added, and mixed by careful vortexing. The mixtures were transferred to DNeasy Mini spin columns placed in 2 mL collection tubes, and centrifuged at 8500 rpm for 1 minute. The DNeasy membranes were washed with 500 $\mu$L of Buffer AW1, and centrifuged at 8500 rpm for 1 minute. The membranes were then washed with 500 $\mu$L of Buffer AW2, and centrifuged at 14000 rpm for 3 minutes, according to the DNeasy protocol. The DNA was eluted into a sterile 1.5 mL eppendorf tube with 2x50 $\mu$L of Buffer AE by centrifugation at 8500 rpm for 1 minute.

The DNA purity and concentration in the eluates were measured by using a NanoDrop® ND-1000 spectrophotometer.

### 2.2.2 Cultivation and DNA extraction from *amoA* controls

Various clones of the *amoA* gene were used as positive controls. These clones were supplied as *Escherichia coli* stab cultures with AOB *amoA* plasmids or AOA *amoA* fosmid by Sven Leininger at the University of Bergen, Department of Biology. The clones were AOB *amoA* genes from *Nitrosomonas europaea* ATCC 19718, *Nitrosospira multiformis* ATCC25196 and *Nitrosovibrio tenuis* NV-12 (Leininger et al. 2006), and the AOA *amoA* gene from the crenarchaeotal clone 54d9 (Treusch et al. 2005).

The transformed *E. coli* cultures with AOB *amoA* plasmids or AOA *amoA* fosmid were cultivated over night in 10 mL standard LB medium (5 g yeast extract, 10 g peptone, 5 g NaCl per litre) in a shaking incubator

at 37 °C and 70 rpm. *E. coli* cultures with AOB *amoA* plasmids were grown with 100 µg/mL sterile filtered ampicillin, while *E. coli* cultures with AOA *amoA* fosmid were grown with 12.5 µg/mL sterile filtered chloramphenicol.

Total DNA was isolated from the *E. coli* cultures by using the Qiagen® DNeasy blood and tissue kit, protocol for Gram-negative bacteria (*DNeasy® Blood and Tissue Handbook* 2006). Cells from 1.5 mL of each culture were harvested by centrifugation according to the protocol. The cells were lysed with proteinase K for two hours, and DNA was eluted with 2x50 mL of elution buffer. The DNA purity and concentration in the eluates were measured by using a NanoDrop® ND-1000 spectrophotometer.

### 2.2.3 PCR

**PCR primers**

Table 2.3 shows the different primers used for PCR. PCR primers targeting both *rRNA* genes and *amoA* genes were used. The specificity of som primers was evaluated by querying the primer sequence in NCBI primer-BLAST available from http://blast.ncbi.nlm.nih.gov/Blast.cgi.

Table 2.3: PCR primers utilized, their target organisms and length of amplified product.

| Forward primer | Reverse primer | Target organisms and gene | Amplified product (bp) | Reference |
|---|---|---|---|---|
| 338f-GC[1] | 517r | Bacterial 16S rRNA | 237 | Amann et al. 1990, Muyzer et al. 1993 |
| 20Archf | 958Archr | Archaeal 16S rRNA | 1037 | DeLong 1992 |
| *amoA*-1F-GC[1] | *amoA*-2R | $\beta$-AOB *amoA* gene | 531 | Rotthauwe et al. 1997 |
| A189f | A682r-GC[1] | AOB *amoA* and MOB *pmoA* | 571 | Holmes et al. 1995 |
| amoA121f-GC[1] | amoA359rC | $\beta$-AOB *amoA* | | Junier et al. 2008 |
| Arch-amoA-for | Arch-amoA-rev | Archaeal *amoA* | 296 | Wuchter at al. 2006 |

[1] A 40 bp GC-clamp with sequence 5'-CGC CCG CCG CGC GCG GCG GGC GGG GCG GGG GCA CGG GGG G-3' was used (Muyzer et al. 1993).

**PCR reagents and buffers**

Table 2.4 shows the reagents and buffers used in each PCR reaction. The PCR reactions were prepared by first adding the DNA template to PCR tubes, placed in a PCR cooler rack. Then, a mastermix consisting of the components listed in Table 2.4 was made, and added to the PCR tubes with the template. The PCR reaction mixtures were put directly into a thermocyler (UnoCycler Thermal Cycler chassis with 96 well gradient block, VWR Collection) at 95 °C.

Table 2.4: PCR reagents and buffers. The concentrations used were slightly different depending on the $MgCl_2$ concentration. The amount of the reagents in each 50 $\mu$L reaction are shown. For reaction volumes of 25 $\mu$L, all amounts were halved.

| Reagent | Low $MgCl_2$ concentration | | High $MgCl_2$ concentration | |
|---|---|---|---|---|
| | Amount ($\mu$L) | Concentration | Amount ($\mu$L) | Concentration |
| 10x PCR buffer | 5 | 1x | 5 | 1x |
| dNTPs (10 mM) | 1 | 0.2 mM | 1 | 0.2 mM |
| $MgCl_2$ (25 mM) | 1 | 2 mM[1] | 0 | 1.5 mM[1] |
| BSA (10 mg/mL) | 1.5 | 0.3 mg/mL | 2 | 0.4 mg/mL |
| Forward primer (2 $\mu$M) | 10 | 0.4 $\mu$M | 7.5 | 0.3 $\mu$M |
| Reverse primer (2 $\mu$M) | 10 | 0.4 $\mu$M | 7.5 | 0.3 $\mu$M |
| $Taq$ polymerase (5 units/$\mu$L) | 0.4 | 2 units/reaction | 0.25 | 1.25 units/reaction |
| Sterile ion free water | 18.6 | | 25 | |
| Template | 2.5 | 10-200 ng/reaction | 1-2 | 10-200 ng/reaction |

[1] The 10x buffer contained 15 mM of $MgCl_2$. The $MgCl_2$ concentration shown is the total concentration from the buffer and the additional $MgCl_2$ added.

Reagents and buffer from the Qiagen $Taq$ PCR Core Kit were used. The bovine serum albumin (BSA) was supplied from New England Biolabs® Inc. Sterile ion free water (SIV) was supplied from 5 PRIME, and stored in aliquots of approximately 1 mL.

Different $MgCl_2$ concentrations were used with different primers. A higher $MgCl_2$ concentration was used for PCR with the primer set 338f-GC/517r, according to a PCR-DGGE protocol developed by Ole-Kristian

Hess-Erga at the Department of Biotechnology at NTNU. The reagent concentrations were in accordance with the specifications from Qiagen (*Taq PCR Handbook* 2008).

The amount of template in each PCR reaction was adjusted according to the primer set that was used. The amount of template per PCR reaction varied between 10 ng and 200 ng. The DNA samples were diluted to give the proper amount of template. The template volume added to the PCR mix was in some cases adjusted as well, to give the optimal amount of template. In addition to the DNA samples, a non-template control was always included.

**PCR temperature regime**

Two different temperature regimes were used for the different primer pairs. These temperature regimes are outlined in Table 2.5.

The annealing temperature for all primers had to be optimized, except for the general 16S rRNA primer pair 338f-GC/517r, where a 55 °C annealing temperature was used according to a PCR-DGGE protocol developed by Ole-Kristian Hess-Erga at the Department of Biotechnology at NTNU (described in section 2.2.4). Optimization of annealing temperatures was done by performing temperature gradient PCR. The PCR products were evaluated by agarose gel electrophoresis (see below) to determine the optimal annealing temperature.

The temperature cycle (denaturation, annealing and elongation) was repeated from 30-40 times, depending on the primer pair and purpose of the PCR.

Table 2.5: PCR regime

| Step | Temperature (°C) | Time long cycle | Time short cycle |
|------|------------------|-----------------|------------------|
| Initial denaturation | 95 | 4 min | 3 min |
| Denaturation | 95 | 30 sec | 30 sec |
| Annealing | Varying | 60 sec | 30 sec |
| Elongation | 72 | 90 sec | 60 sec |
| Final elongation | 72 | 30 min | 30 min |
| Stop | 4 | $\infty$ | $\infty$ |

**Evaluation of PCR products**

The PCR products were verified by agarose gel electrophoresis in an Owl EasyCast™Mini Gel System (Thermo Scientific). The agarose gel consisted of 1-1.5 % agarose (Electran, mol.bio grade) in 1xTAE buffer (per litre: tris base 5.04 g, concentrated acetic acid 1.14 mL, 0.5 M EDTA (pH 8.0) 2 mL).

1 $\mu$L of 6x loading dye (Fermentas) was added to 5 $\mu$L of PCR product and run at 100 V for approximately 45 minutes. A 100 bp DNA ladder (GeneRuler™, Fermentas) was used to verify the correct length of the PCR products.

DNA in the agarose gels were stained in an ethidium bromide solution for 5-10 minutes, and washed in MilliQ water for approxomately 15 minutes. The gels were photographed in UV light in a gel documentation system (G:BOX, Syngene).

### 2.2.4 DGGE

Denaturing gradient gel electrophoresis was carried out according to the PCR-DGGE protocol developed by Ole-Kristian Hess-Erga at the Department of Biotechnology at NTNU. This procedure is described in detail in Appendix D. The procedure was performed with an Ingeny PhorU system, where an acrylamide gel with a denaturing gradient was cast between two glass plates.

The DGGE gels had acrylamide concentrations of 6 % or 8 %, depending on the length of the DNA fragments. The short fragments from PCR with the primer pair 338f-GC/517r were separated in 8 % acrylamide gels, while longer fragments from PCR with the *amoA* primers were usually separated in 6 % acrylamide gels.

The DNA fragments were separated in different denaturing gradients, e.g. 30 % to 60 %, where a denaturing percentage of 80 corresponds to 7 M of urea and 40 % formamide. See appendix D for a detailed description of the gel casting.

After gel casting, the gel was transferred to the Ingeny phorU buffer system filled with 0.5x TAE at 60 °C. The gel was pre-run and conditioned at 100-120 V and 40-50 mA for 10-15 minutes before sample application. 15 $\mu$L of each DNA sample was mixed with 3 $\mu$L of a 6x loading dye, prior to application on the gel. The gel was run for 5-10 minutes at 100-120 V without circulation of the buffer, to avoid disturbing the samples. The gel was then run with circulation for 17-23 hours.

After electrophoresis, the gel was transferred to a transparent plastic sheet, and nucleic acids were stained with SYBR Gold (Invitrogen). The staining solution was made by mixing 3 $\mu$L of SYBR Gold and 600 $\mu$L of 50xTAE buffer, and adjusting the volume to 30 mL with MilliQ water. The staining solution was spread over the gel, and the gel was incubated for 1-2 hours in the dark. After staining, the gel was rinsed in MilliQ water, and viewed in UV light in a gel documentation system (G:BOX, Syngene).

### 2.2.5 DGGE band pattern analysis

The band patterns in the DGGE gels were analyzed by using the GEL2k program developed by Norland (2004). GEL2k was used for band identification, generation of grey level histograms for each lane in the gel, and quantification based on peak areas in the histograms. The histogram peak area for each band was normalized by dividing on the total peak area for all bands in the lane, giving fractional peak areas.

The range-weighted richness, the Shannon index, the evenness and Bray-Curtis dissimilarities were calculated from the normalized peak areas (Bray & Curtis 1957, Peet 1975, Marzorati et al. 2008). The Bray-Curtis dissimilarities were calculated in SYSTAT (Wilkinson 2010). The range-weighted richness was calculated according to Equation 2.3, and is the band richness (N) of the gel multiplied by the denaturing gradient needed to describe the total diversity of the sample ($D_g$) (Marzorati et al. 2008).

$$Rr = N \times D_g \qquad (2.3)$$

The Shannon diversity index (H') was calculated according to Equation 2.4, where p is the normalized fractional area of a band's histogram peak, and S is the number of bands. The Shannon diversity will be largest when all bands have equal peak areas. The Shannon index will in such a case be defined by equation 2.5 (Peet 1975).

$$H' = -\sum_{i=1}^{s} p_i \ln p_i \qquad (2.4)$$

$$H_{max} = \ln S \qquad (2.5)$$

The evenness (J') was calculated according to equation 2.6 (Peet 1975).

$$J = \frac{H'}{H_{max}} \qquad (2.6)$$

Pareto-Lorenz evenness curves were plotted to give an impression of the distribution of bands in the sample (Marzorati et al. 2008). The fractional histogram peak areas were ranked from the highest to the lowest, and the cumulative peak areas were calculated. The cumulative areas were plotted towards the cumulative proportion of bands. The resulting curves represented the degree of evenness in the molecular composition of the PCR product, and could indicate the degree of evenness in the microbial community. A 45 ° diagonal "perfect evenness curve" was also plotted. The perfect evenness curve represented the scenario where all bands in the DGGE gel had similar histogram peak areas.

The Gini coefficient, defined as the fraction of the area above the perfect evenness curve that is covered by the Pareto-Lorenz curve (Wittebolle et al.

2009), was calculated by measuring the total area under the Pareto-Lorenz curves, and subtracting with the area under the perfect evenness curve, which is 0.5, and dividing on the area above the perfect evenness curve (0.5). The areas under the Pareto-Lorenz curves were calculated by summarizing the areas under the curves at each data point. The partial areas were calculated by multiplying the average cumulative peak area between two data points with the change in cumulative proportion of bands, i.e. $\overline{y} \times \delta x$.

### 2.2.6 Collection, re-amplification and sequencing of DGGE bands

DGGE bands were cut out of the gel by pressing pipette tips (1000 $\mu$L) into the bands in the gel. The pipette tips with gel and DNA material were incubated over night in 20 $\mu$L of sterile filtered (0.2 $\mu$m) MilliQ water in 1.5 mL microsentrifuge tubes at 4 °C. After incubation, the pipette tips were removed, after making sure that no gel remained in the pipette tips.

DNA was re-amplifed in a similar PCR reaction as prior to DGGE. The 16S rRNA sequences were re-amplified with modified M13 primers (Eurofins MWG Operon) to obtain longer reads during sequencing. After PCR, the PCR products were verified by agarose gel electrophoresis as described in section 2.2.3.

The PCR products were purified by using the QIAquick® PCR Purification Kit according to the specifications from the manufacturer. The PCR Purification Spin Protocol was used (*QIAquick Spin Handbook* 2008). Elution was done with 30 $\mu$L 0.2 $\mu$m sterile filtered MilliQ water. The DNA concentration and purity after elution was measured with a NanoDrop® ND-1000 spectrophotometer.

The purified PCR products were shipped to Eurofins MWG Operon for sequencing by the "Value Read Tube" service.

### 2.2.7 16S rRNA sequence analysis

The sequence chromatograms had already been base-called and quality checked by Eurofins MWG Operon, so no programs (e.g. Phred/Phrap) were used to analyze the raw chromatograms. The sequences had been quality-clipped so that only regions with an average quality score below 20 (where the probability that a predicted base is wrong is 1/100) remained. Sequences with lengths below 100 nucleotides after quality-clipping were not subjected to further sequence analyses. This was according to the quality standards recommended by Eurofins-DNA.

The sequences that fulfilled initial quality checks were manually inspected by investigating their chromatograms for double peaks and ambiguous bases. Primer sequences were deleted from the dataset.

All sequences were aligned towards database sequences using the NAST tool available from greengenes.lbl.gov (DeSantis et al. 2006). The default settings for alignment were used, except for the minimal length requirement which was reduced to 80 nucleotides.

The aligned sequences were checked for chimeras by using the CHIMERA_CHECK program version 2.7 available through the ribosomal database project II (Cole et al. 2003). The sequence length requirement was adjusted to 100 nucleotides.

The NAST aligned sequences were classified according to NCBI taxonomies by using the Greengenes classification tool Simrank. Some sequences were also submitted to NCBI nucletotide-BLAST, available from http://blast.ncbi.nlm.nih.gov/Blast.cgi.

Phylogenetic trees were constructed using the MEGA4 software, version 4.1 (Tamura et al. 2007). The DGGE sequences and reference sequences were aligned in MEGA4 by the CLUSTAL W algorithm prior to tree construction. The reference sequences were 16S rRNA sequences from different nitrifying bacteria, added directly to MEGA by the GenBank application in the MEGA alignment explorer. Some sequences delivered from the NAST alignment program were also used as reference sequences. These sequences were, according to NAST, the nearest isolated neighbours to the DGGE sequences.

### 2.2.8  *amoA* sequence analysis

The quality of the *amoA* sequences was evaluated as described in section 2.2.7. The sequences were manually inspected by investigating the sequence chromatograms. Primers and regions of bad quality were deleted from the dataset. Ambiguous bases remaining in the dataset were replaced with IUB codes (Cornish-Bowden 1985). For sequence comparison at protein-level, the nucleotide sequences were translated by using the ExPASy translate tool available from http://au.expasy.org/tools/dna.html (Gasteiger et al. 2003). The phylogeny of the sequences were evaluated in nucleotide-BLAST and translated nucleotide-BLAST available from http://blast.ncbi.nlm.nih.gov/Blast.cgi. The sequences were manually aligned towards sequences from GenBank in the MEGA4 software, and Neighbour-Joining phylogenetic trees were constructed.

## 2.3 FISH

Fluorescence *in situ* hybridization was performed according to Daims et al. (2005). Only specifications and modifications of the protocol are described in the following sections.

### 2.3.1 Sampling and fixation

Biofilm carriers for FISH were collected from the tap water-based and the seawater-based reactors at the times indicated in section 2.1.5. Each biofilm carrier constituted one sample. The samples were fixated for FISH immediately after sampling. The biofilm on the biofilm carriers were scraped off on a piece of aluminium foil by using sterile plastic inoculation loops or other suitable tools. The biofilm was washed from the aluminium foil into 1.5 mL microsentrifuge tubes with 0.5-1.5 mL 1xPBS. The tubes were centrifuged (15,000xg, 4 °C) for 5 minutes, and the pellet was re-suspended in 1.5-0.5 mL 1xPBS. The rest of the fixation procedure was done according to Daims et al. (2005). Both Gram-negative and Gram-positive cells were fixated.

On day 77 after inoculation of the tap water-based reactor and 107 after inoculation of the seawater-based reactor, whole biofilm carriers were also fixated. Four biofilm carriers from each reactor were fixated. The biofilm carriers were cut into two pieces using a sterile scalpel, so that they could fit into 1.5 mL microsentrifuge tubes. The biofilm carriers were carefully washed by adding 1 mL of 1xPBS. The biofilm carrier pieces were then transferred to new 1.5 mL microsentrifuge tubes, and fixated by adding 1 mL of either 96 % ethanol or 4 % PFA solution (for fixation of Gram-positive and Gram-negative cells, respectively). The PFA fixated biofilm carrier samples were incubated according to the protocol (Daims et al. 2005), and then carefully washed three times in 1 mL 1xPBS. 700 $\mu$L of 1xPBS and 700 $\mu$L of 96 % ethanol were added to the tubes, and then stored at -20 °C.

### 2.3.2 Cultivation of *Nitrosomonas europaea* NCIMB 11850

A culture of *N. europaea* NCIMB 11850 (MacDonald & Spokes 1980) was used as a positive control during FISH. The culture was delivered in a lyophilized state by NCIMB, The National Collection of Industrial, Marine and Food Bacteria. The culture was revived and cultivated according to the instructions from the manufacturer, in a medium for ammonia-oxidizing bacteria (NCIMB growth medium number 181). Table 2.6 shows the composition of the cultivation medium.

The medium was autoclaved at 121 °C for 15 minutes. After autoclaving, sterile 5 % $Na_2CO_3$ was added until the medium had a pale pink colour. The *N. europaea* culture was incubated at 30 °C and 70 rpm in the

Table 2.6: The composition of the cultivation medium for ammonium-oxidizing bacteria.

| Compound | Amount per L |
| --- | --- |
| $(NH_4)_2SO_4$ | 235 mg |
| $KH_2PO_4$ | 200 mg |
| $CaCl_2$-$2H_2O$ | 40 mg |
| $MgSO_4$-$7H_2O$ | 40 mg |
| $FeSO_4$-$7H_2O$ | 0.5 mg |
| NaEDTA | 0.5 mg |
| Phenol red | 0.5 mg |

dark. Additional $Na_2CO_3$ was added during incubation to restore the pink colouration.

After approximately two months of cultivation, cells from the culture was fixated according to Daims et al. (2005).

### 2.3.3 *in situ* hybridization

**Sample application and dehydration**

The fixated biofilm scrapings and the *N. europaea* conrol were applied to teflon-coated microscopic slides with 10 wells (Menzel-Gläser Diagnostika, 10 well, 6.7 mm). Some of the slides were coated with poly-L-lysine according to Daims et al. (2005), to prevent detachment of cells. Samples that were intended for epifluorescence microscopy were sonicated for 3-4 minutes to dissolve cell aggregates in the biofilm. In these cases, 10-15 $\mu$L of sample was applied to each well on the slide. Samples that were intended for confocal laser scanning microscopy were not sonicated, and 30-50 $\mu$L of sample was applied to each well. In some cases, the slides were covered with 0.5-1 % agarose after sample application, according to Daims et al. (2005).

The samples of intact biofilm fixated on the biofilm carriers were covered in 0.5-1 % agarose. The thick biofilm could then be removed from the biofilm carriers in intact order. The pieces of biofilm were put on microscopic slides, and covered once more in agarose.

After sample application on the microscopic slides, the samples were dehydrated in a series of different ethanol concentrations, according to Daims et al. (2005)

**Hybridization with oligonucleotide probes**

The hybridization was done according to Daims et al. (2005). Table 2.7 shows the oligonucleotide probes that were used for *in situ* hybridization and their 5'-end fluorescent dye molecule. The database probeBase (Loy et al. 2003, 2007) was used to find information about the different probes.

Table 2.7: Fluorescent oligonucleotide probes that were used, their fluorescent label and specificity.

| Probe | Label | Specificity | Reference |
|-------|-------|-------------|-----------|
| EUB338 I, II, III | FITC | Domain Bacteria | Amann et al. 1990, Daims et al. 1999 |
| Nso190 | Cy3 | Betaproteobacterial ammonia-oxidizing bacteria | Mobarry at al. 1996 |
| NIT3 + CNIT3 | Cy3/none | Nitrobacter ssp. | Wagner et al. 1996 |

Probes were delivered from Eurofins MWG Operon. Stock solutions of probes were made by dissolving the lyophilised probes in sterile MilliQ water to concentrations of 500 or 330 ng/$\mu$L. Probes labelled with FITC were diluted to 500 ng/$\mu$L, and probes labelled with Cy3 were diluted to 330 ng/$\mu$L. The stock solutions were stored at -20 °C in aliquots of 5 $\mu$L. Before use, the aliquots were diluted to 50 $\mu$L with sterile MilliQ water. This gave concentrations of 50 ng/$\mu$L for probes labeled with FITC, and 33 ng/$\mu$L for probes labelled with Cy3. The probes EUB338I, EUB338II and EUB338III, were aliqouted together with a total volume of 15 $\mu$L.

Samples were hybridized to the general probes for bacteria EUBI, EUBII and EUBIII, and one of the more specific probes. Hybridization with the EUB-mix and the specific probe was done simultaneously when possible. If the hybridization conditions (formamide concentration) for the EUB-mix and the specific probe were not congruent, the probes were hybridized sequentially, the probe demanding the most stringent hybridization condition first. As a background or autofluorescence reference standard, one well with biofilm sample was always left unhybridized. No probes were applied to this well.

After hybridization, drops of an antifadent solution (Citifluor™ Glycerol/PBS solution AF1) were applied between the wells, and cover slips were put on top of the slides so that the antifadent became evenly distributed over the whole slide.

### 2.3.4  Microscopy and quantification

The FISH samples were investigated by epifluorescence microscopy and confocal laser scanning microscopy (CLSM). Two different epifluorescence microscopes were used; Zeiss Axioplan with Zeiss filtersets 49 488049-9901, 38 HE 489038-9901 and 43 HE 489043-9901, connected to a Qimaging QICAM Fast1394 documentation system and Zeiss Axio Scope.A1 with filter sets 09 488009-0000, 15 488015-0000 and 01 488001-0000. Quantification after epifluorescence microscopy was done by counting single cells.

Two different CLSM microscopes were used; Leica TCS SP5 with argon 488 and helium-neon (HeNe) 541 lasers, and Zeiss LSM 510 Meta with argon 488 and HeNe 543 lasers. Quantification was done by thresholding pictures in ImageJ and measuring the signal as area in pixels (Collins 2007).

# Chapter 3

# Results and discussion

## 3.1 Operation of the nitrifying reactors

In the following sections, the operational conditions and nitrification activities in the tap water-based and the seawater-based reactors are presented. All operational changes and measurements of ammonium, nitrite and nitrate are documented in appendices A and B.

### 3.1.1 The tapwater-based reactor

Figure 3.1 shows how the flow and the concentration of ammonium in the cultivation medium, constituting the loadingrate, was regulated during the experimental period.



Figure 3.1: Flowrate and the concentration of ammonium in the cultivation medium, constituting the loadingrate to the reactor.

Figure 3.2 shows the concentrations of ammonium, nitrite and nitrate in the reactor, with the corresponding calculated activities in figure 3.3. The ammonium concentration in the reactor decreased from day 5 (Figure 3.2), indicating ammonia oxidation activity, also shown in Figure 3.3. From day 8, the nitrite concentration in the reactor started to increase, and reached very high levels during the following days. It seemed like the nitrite-oxidizers could not keep up with the rate of ammonia oxidation. As a countermeasure to avoid possible nitrite inhibition (Henze et al. n.d.), the flow rate was increased on day 9 with the intention to wash out the accumulated nitrite. These countermeasures did not seem to reduce the nitrite

Figure 3.2: The concentration of ammonium in the cultivation medium, and the concentrations of ammonium, nitrite and nitrate in the reactor. No nitrite measurements were taken from day 42 to 56.

concentration, instead the loading rate was decreased on day 11 by reducing the flow rate, and on day 17 by reducing the concentration of ammonium in the cultivation medium. These adjustments are evident on the activity graph for ammonia oxidation (Figure 3.3), as a clear reduction of the ammonia oxidation rate. Starvation of the ammonia-oxidizing bacteria would decrease the conversion to nitrite, giving the nitrite-oxidizers a chance to keep up. By day 26, all nitrite was removed, and the feeding rate was gradually increased accordingly, to increase the ammonia substrate feeding, and thereby the nitrification activity showed in Figure 3.3. The nitrifying culture adapted to higher loading rates, removing all available ammonium. The nitrite oxidation rate slowly increased after removal of the high nitrite levels. Figure 3.4 shows the nitrification activities as percentage of available ammonium and nitrite, and it is evident that the ammonia and nitrite oxidation was near 100 % from day 26. The concentrations of ammonium and nitrite in the reactor only increased transiently a couple of times when the loading rate was increased, but no more than a few days were needed to adapt to the increased ammonia availability.

Towards the end of the operation period, it seemed like the nitrite oxidation capacity had reached a maximum. As shown in figure 3.4, the nitrite oxidation was below 100 % from day 56. Increasing the loading rate further led to accumulation of ammonium and nitrite. Further operation of the

reactor by Colaço (2009) did not result in higher nitrification activities.
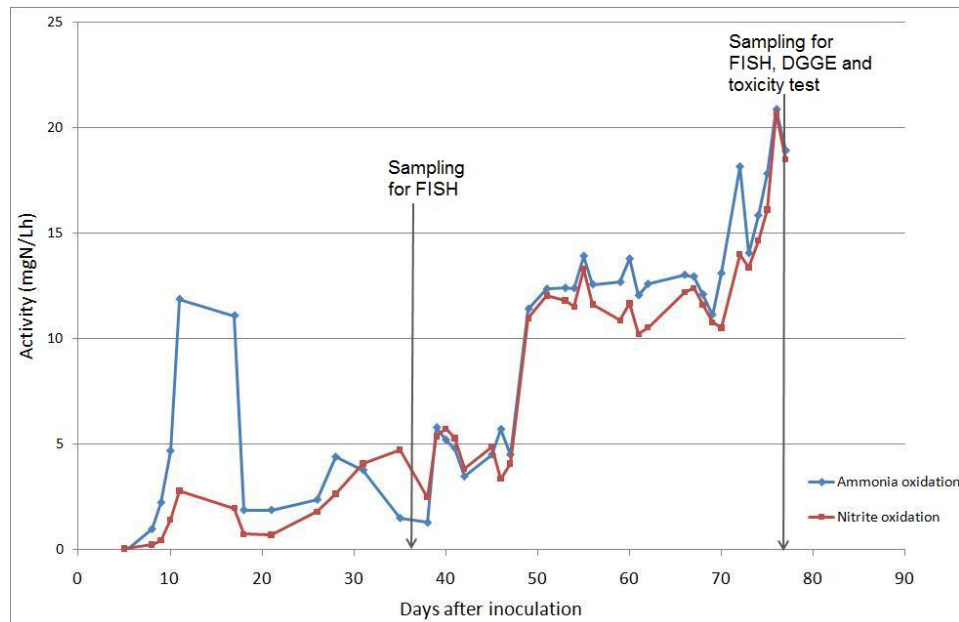


Figure 3.3: The nitrifying activity in the tap water-based reactor. The activities are given as rate of ammonium removal and rate of nitrate production.
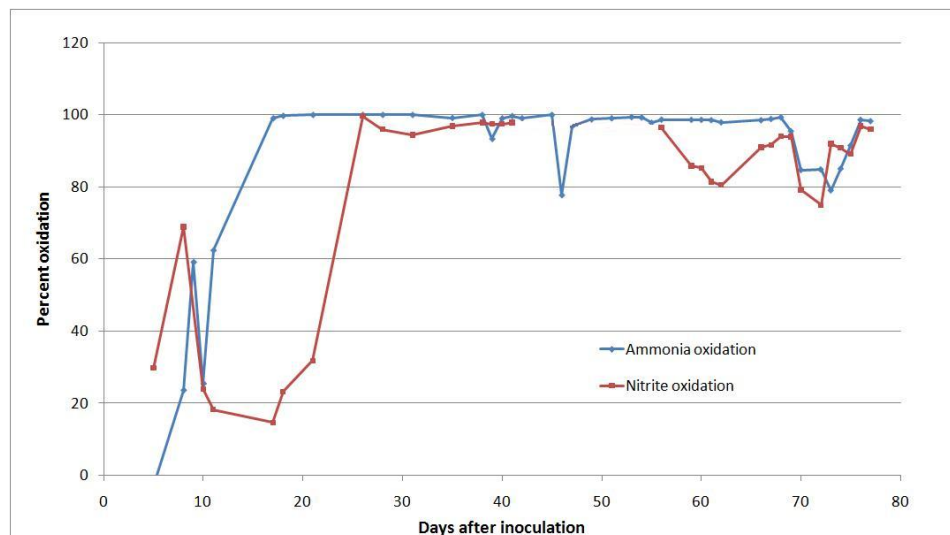


Figure 3.4: The percentage of available ammonium-N and nitrite-N that was oxidized. No nitrite measurements were taken from day 42 to 56.

**Data quality**

Figure 3.5 shows the mass balance for nitrogen, i.e. $N_{in}$-$N_{out}$, during the operation period.
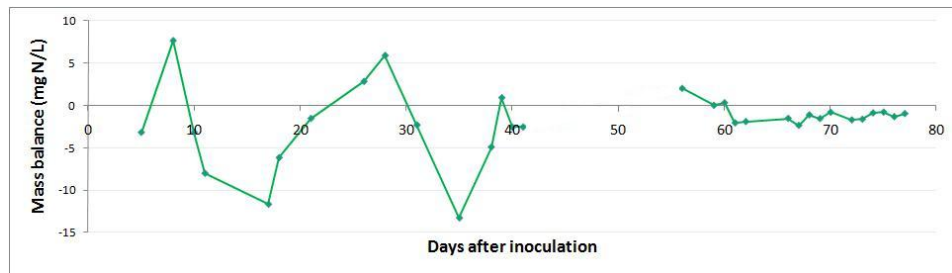


Figure 3.5: The mass balance of nitrogen during the operation of the tapwater-based reactor. No nitrite measurements were taken from day 42 to 56.

The average mass balance during the experimental period was $-1.9 \pm 0.7$ mg N/L, with a standard deviation of 4 mg N/L, and these deviations can be considered insignificant for the purpose of this investigation. It should be stressed that every time the nitrogen loading is changed (Figure 3.1), transients will temporarily invalidate the steady state assumption of mass balance. Some correlations could be found between such changes and the major deviations in Figure 3.5.

### 3.1.2 The seawater-based reactor

Figure 3.6 shows how the flow and the concentration of ammonium in the cultivation medium, constituting the loadingrate, was regulated during the experimental period.
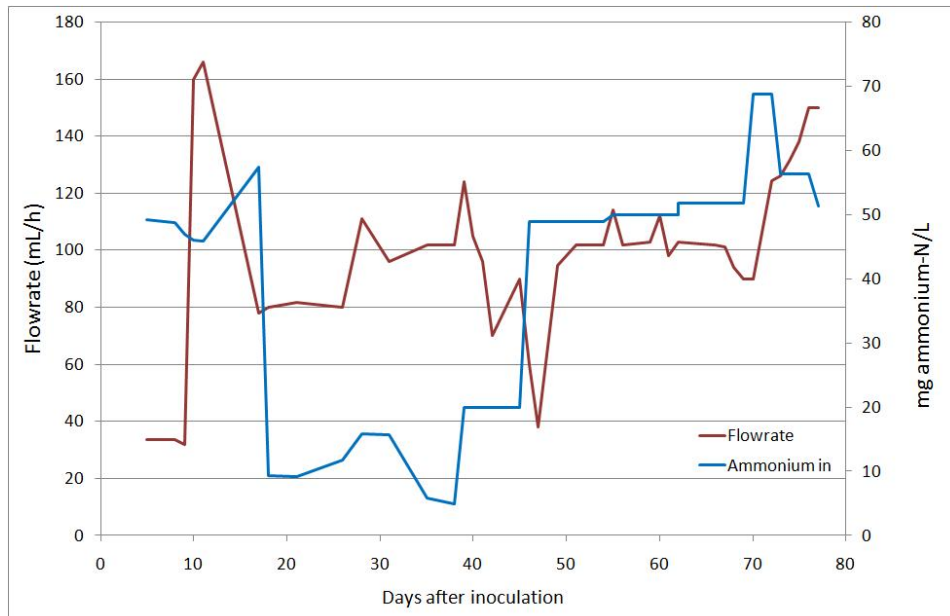
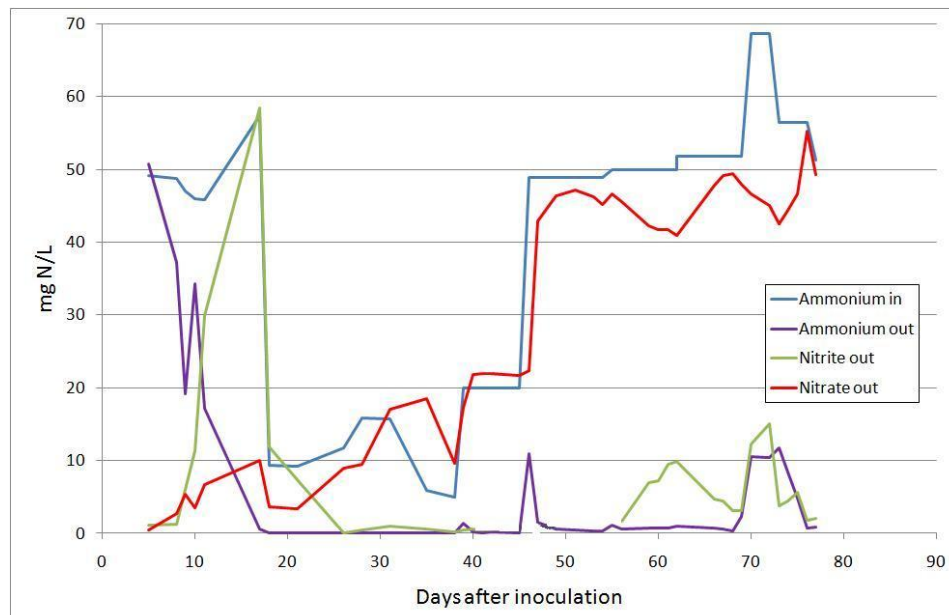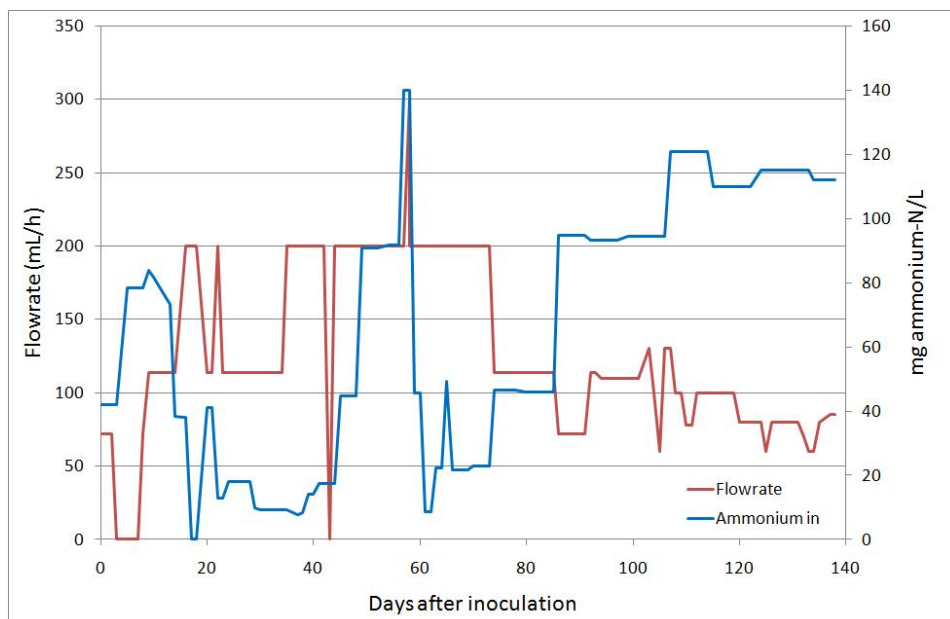Figure 3.6: Flowrate and the concentration of ammonium in the cultivation medium.
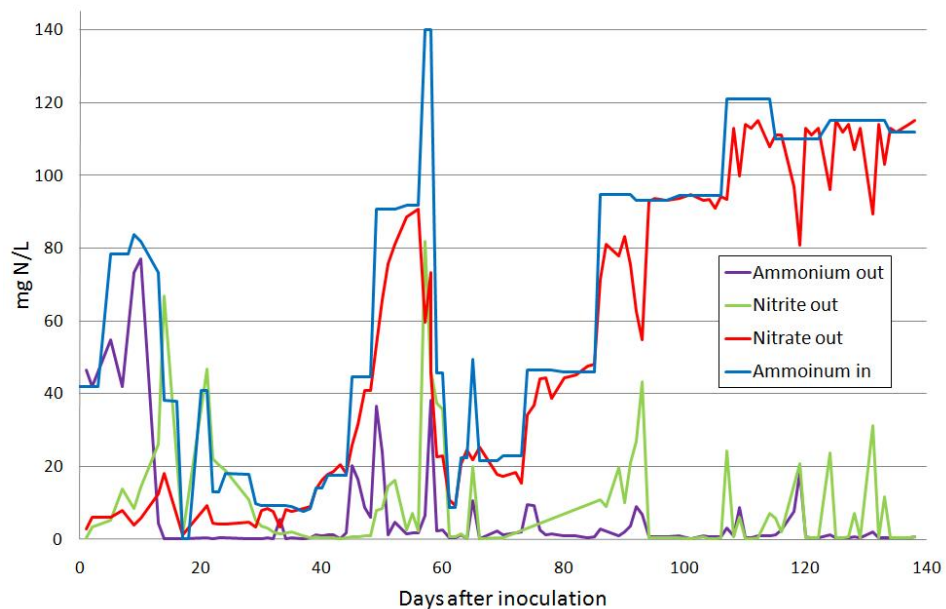


Figure 3.7: The concentration of ammonium in the cultivation medium, and the concentrations of ammonium, nitrite and nitrate in the reactor.

Figure 3.7 shows the concentrations of ammonium, nitrite and nitrate in the reactor, with the corresponding calculated activities in Figure 3.3. As shown in Figure 3.6 the reactor was operated as a batch the first days. Continuous operation was started on day 7, when the ammonium concentration in the reactor started to decrease (Figure 3.7), indicating ammonia oxidation activity (Figure 3.8). The nitrite oxidation activity was still much lower than the ammonia oxidation activity, resulting in nitrite accumulation. As a countermeasure, the flow was increased further on day 8, to dilute the nitrite from the reactor. On day 14, the flow was increased even further, and the concentration of ammonium in the cultivation medium was reduced to zero, to wash out all nitrite and to starve the ammonia-oxidizers. The nitrite was removed, but the effect was only temporary. When the ammonium feeding was started again on day 18 (Figure 3.6), the nitrite accumulated to well above the inhibitory level. Therefore, the ammonium concentration in the cultivation medium was reduced, and the flow was increased over-night. The reactor was operated with low ammonium concentration in the cultivation medium for many days, keeping the nitrite concentration low. From day 34, the feeding rate was gradually increased again to enhance the nitrification activity. The nitrification activity increased accordingly, but from day 51, the nitrite oxidation activity seemed to lag behind, causing nitrite accumulation. It seemed like the nitrite-oxidizing capacity had been surpassed. A temporary solution was to increase the flow over-night to dilute the nitrite from the reactor. At this point, the NaOH pump broke down, causing a serious pH shock in the reactor. Some foaming in the reactor indicated cell lysis. The nitrogen load was reduced, and during the rest of the operation period, the feeding rate was increased carefully to promote high nitrification activity without nitrite accumulation. The activity increased gradually, but it seemed difficult to obtain higher nitrite oxidation activity than 5-10 mg N/L. The nitrite oxidation was unstable towards the end of the operation, evident in Figure 3.9, showing the percentage of available ammonia and nitrite that was oxidized. While the ammonia oxidation was near 100 %, the nitrite oxidation frequently fell below 90-80 %. Transient accumulations of nitrite were solved by temporarily decreasing the flow rate until the nitrite was removed.

Higher activities might have been reached if the reactor was operated for a longer time, giving better time for biofilm maturation after the pH shock. Since the concentration of dissolved oxygen was not measured, it is difficult to know whether the oxygen supply was stable or not. The air supply was in some occasions turned off and on again, and since the air valve was not graded, the level of aeration was only evaluated visually. The DO concentration might have influenced the nitrite oxidation capacity in the reactor. If the air supply was lower towards the end of the operation, this may have been the reason for the difficulties in obtaining similar nitrite oxidation activity as prior to the pH shock.
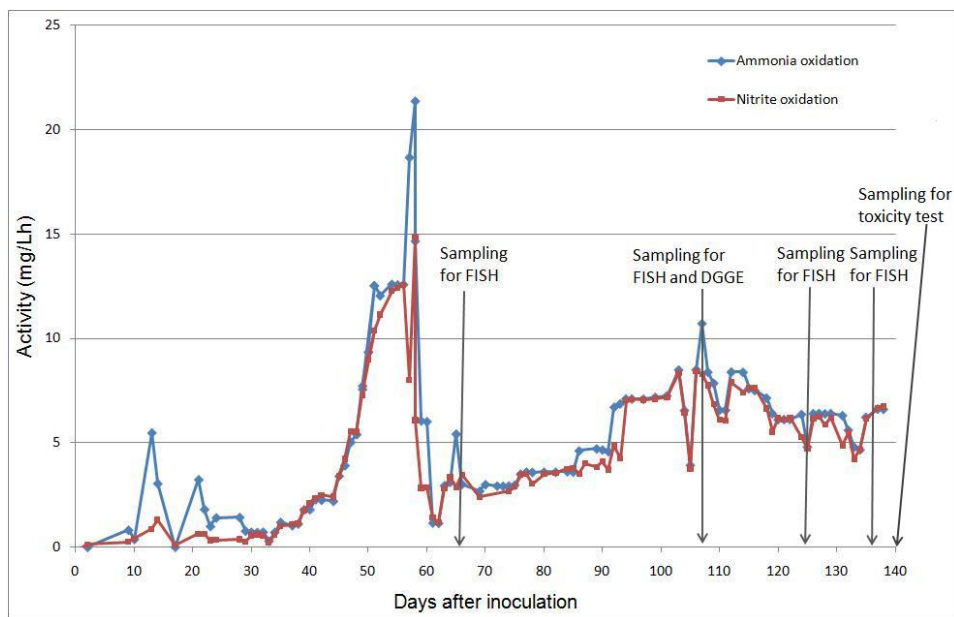
Figure 3.8: The nitrifying activity in the reactor during the operation period. The activities are given as rate of ammonium removal and rate of nitrate production.
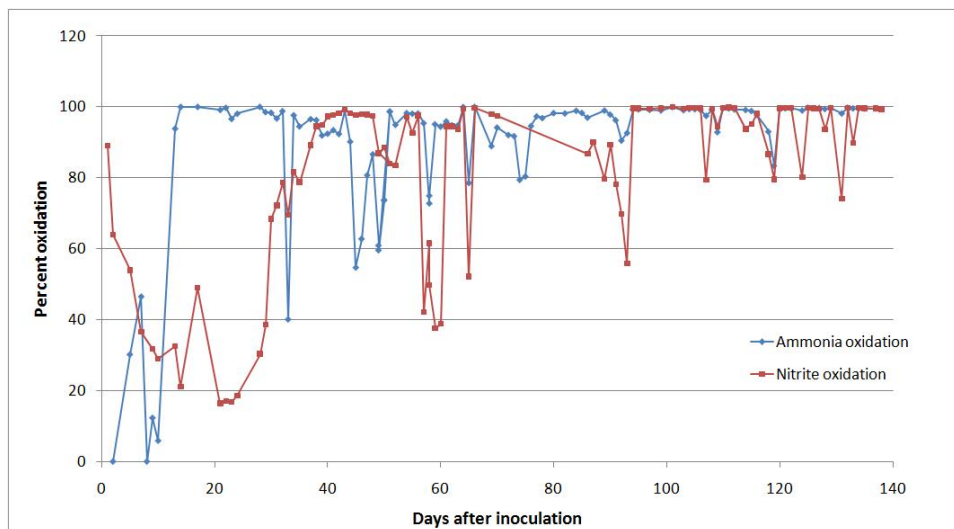


Figure 3.9: The percentage of the available ammonium-N and nitrite-N that was oxidized.

Generally, it seemed difficult to achieve a process where the ammonium oxidation and nitrite oxidation processes remained balanced. The nitrite oxidation was always the limiting step. The ammonia oxidation had to be

50

substrate-limited to avoid nitrite accumulation.

**Data quality**

Figure 3.10 shows the mass balance for nitrogen, i.e. $N_{in}$-$N_{out}$, during the operation period.
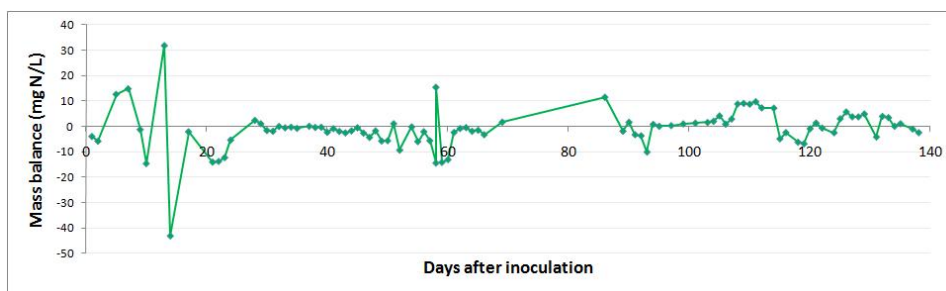


Figure 3.10: The mass balance of nitrogen during the operation of the reactor.

The average mass balance during the experimental period was $-0.9 \pm 0.8$ mg N/L, with a standard deviation of 8 mg N/L, and these deviations can be considered insignificant for the purpose of this investigation. Some correlations could be found between changes in the nitrogen loading and the major deviations in Figure 3.5, however measurements were usually taken 4–5 hydraulic retention times after adjustments of nitrogen loading, by which the mass balance would have adjusted to steady state. The chloride elimination procedure may have affected the accuracy of the Dr. Lange assays for nitrogen measurements, resulting in higher mass balance deviations in the seawater-based reactor compared to the tapwater-based reactor.

## 3.2 Batch culture salinity response test

A batch culture salinity response test was carried out to test the acute effect of different salinities on the nitrification activity in the biofilm adapted to 2/3 seawater. This experiment was conducted as described by Kristoffersen (2004), who in addition tested the inhibiting effect of salt on a nitrifying culture adapted to low salinity (see section 1.8). Experiments with cultivation media with different seawater content were carried out sequentially on the same biofilm carriers, in decreasing order of seawater content. See appendix C for concentration measurements of ammonium, nitrite and nitrate. Figure 3.11 shows the rates of ammonia oxidation and nitrite oxidation at different salinities.
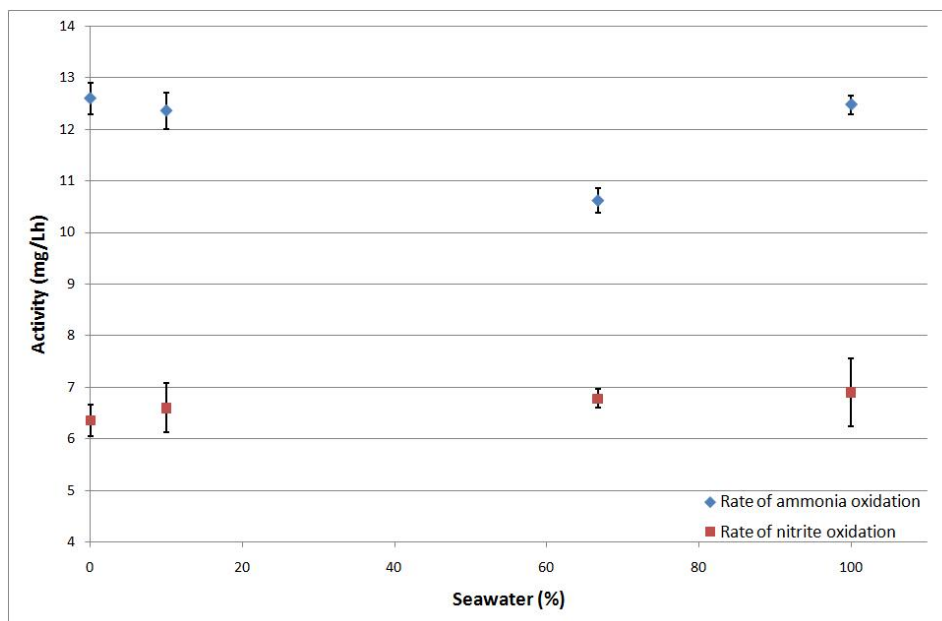
Figure 3.11: Rates of ammonia oxidation and nitrite oxidation at different salinities. The standard errors are indicated.

The salinity did not seem to affect the nitrification activities much. The ammonia oxidation activity stayed between 10-13 mg/Lh during the whole experiment. The nitrite oxidation activity was significantly lower, resulting in accumulation of nitrite. This is in accordance with the results from Kristoffersen (2004) (section 1.8). These results indicate a physiological capacity of the culture to cope with high salinity. The culture seemed to be halotolerant, but not obligately, since the nitrifying activity was equally high at low salinity. Kristoffersen (2004) showed that a nitrifying culture, that was adapted to low salinity, was inhibited when the salinity was increased (see section 1.8). Similar results were reported by Campos et al. (2002), in which adapted activated sludge were found to be less sensitive to high concentrations of salts.

The physiological capacity of the culture adapted to high salinity to tolerate high salinities indicates a microbial composition of species that are halotolerant, and therefore have a competitive advantage in saline environments. However, one possibly important difference between the experiments on the culture adapted to low salinity and the culture adapted to high salinity must be mentioned. The culture adapted to high salinity was exposed to cultivation media with decreasing seawater contents. When cultivation medium was changed, significant amounts of salt may have remained in the biomass, continuing to have an effect. This could have concealed a possible effect of salt. The effect of different salinities may also have had physiological effects on a longer term than the time span of the experiment, i.e.

3 hours for each salinity. Moussa et al. (2006) reported that there was no significant effect of adaptation on the salt tolerance, although microbial community changes were observed after one year of adaption.

During the toxicity test, nitrite accumulated to high levels. Kristoffersen (2004) also showed nitrite accumulation in the culture adapted to high salinity, but this did not occur in the culture adapted to low salinity, even at high salinities. The reason for this may be that the ammonia oxidation activity was lower in the tapwater-adapted culture, and less nitrite was produced. It is difficult to compare activity levels because the cultures were in different shape prior to the toxicity test, and the degree of aeration might have been significantly different.

## 3.3  PCR-DGGE analysis of bacterial 16S rRNA sequences

### 3.3.1  DGGE gel analysis

DNA fragments of correct length were successfully amplified by PCR with the primers 338f-GC and 517r (results not included). The PCR product was analyzed on DGGE gels with different gradients, first on a 30-60 % denaturing gradient gel, in which the bands positioned between 30 and 50 %. For better separation of the bands, the denaturing gradient was confined to 30-50 % (Figure 3.12). After sequencing of bands from the 30-50 % gel (see section 3.3.2), regions with bands belonging to nitrifying species were investigated further by restricting the denaturing gradient to these regions. A DGGE gel with a 30-40 % denaturing gradient was set up to analyze some interesting bands with low melting point (Figure 3.14), while a 35-50 % denaturing gradient gel was used to analyze bands with medium to high melting points (Figure 3.13). Bands were cut out, re-amplified and sequenced from these DGGE gels as well. The results from band pattern analysis of the 30-50 %, 35-50 % and 30-40 % DGGE gels are presented in Figures 3.12, 3.13 and 3.14, respectively. An important assumption for the band pattern analysis was that bands in different lanes with identical position in the gel was similar. Only one band from one of the lanes were sequenced, at that the corresponding bands in the other lanes really were of similar origin could not be proved, but it is reasonable to assume so.

| Band | Peak area (%) | | | |
|---|---|---|---|---|
| | 1F | 2F | 1S | 2S |
| B1 | 0.3 | 0.6 | 1.0 | 1.3 |
| B2 | 0.9 | 2.6 | 0.3 | 0.3 |
| B3 | 0.7 | 2.0 | 0.0 | 0.0 |
| B4 | 0.8 | 1.7 | 0.3 | 0.2 |
| B5 | 0.1 | 0.5 | 0.0 | 0.0 |
| B6 | 0.9 | 3.6 | 0.0 | 0.0 |
| B7 | 0.0 | 0.0 | 0.1 | 0.2 |
| B8 | 0.4 | 1.8 | 0.0 | 0.0 |
| B9 | 0.0 | 0.0 | 0.1 | 0.3 |
| B10 | 0.6 | 0.8 | 1.5 | 0.5 |
| B11 | 0.2 | 1.1 | 0.0 | 0.0 |
| B12 | 1.0 | 4.1 | 0.0 | 0.0 |
| B13 | 1.8 | 0.3 | 0.0 | 0.0 |
| B14 | 5.4 | 9.3 | 0.0 | 0.0 |
| B15 | 0.0 | 0.0 | 22.8 | 25.4 |
| B16 | 2.3 | 1.1 | 0.0 | 0.0 |
| B17 | 0.0 | 0.0 | 0.6 | 1.0 |
| B18 | 3.3 | 3.6 | 0.0 | 0.0 |
| B19 | 0.0 | 0.0 | 11.8 | 11.5 |
| B20-1 | 5.5 | 2.9 | 0.0 | 0.0 |
| B20-2 | 0.0 | 0.0 | 5.0 | 2.3 |
| B21 | 3.1 | 0.7 | 1.4 | 0.8 |
| B22 | 3.8 | 1.5 | 2.7 | 2.4 |
| B23 | 4.1 | 3.8 | 0.0 | 0.0 |
| B24 | 0.0 | 0.0 | 13.7 | 9.2 |
| B25 | 11.2 | 9.7 | 0.0 | 0.0 |
| B26 | 0.0 | 0.0 | 1.5 | 1.5 |
| B27 | 4.1 | 3.6 | 0.0 | 0.0 |
| B28 | 0.0 | 0.0 | 1.3 | 1.9 |
| B29 | 0.0 | 0.0 | 8.5 | 8.8 |
| B30 | 0.0 | 0.8 | 0.7 | 1.9 |
| B31 | 1.3 | 0.2 | 0.7 | 0.6 |
| B32 | 1.9 | 2.6 | 1.1 | 0.7 |
| B33 | 1.5 | 0.8 | 0.8 | 0.7 |
| B34 | 1.4 | 0.7 | 1.2 | 1.7 |
| B35 | 1.8 | 1.8 | 1.3 | 1.4 |
| B36 | 1.8 | 0.8 | 0.2 | 0.0 |
| B37 | 2.1 | 2.3 | 1.0 | 1.3 |
| B38 | 1.9 | 1.7 | 0.2 | 0.0 |
| B39 | 0.0 | 0.0 | 6.4 | 7.9 |
| B40 | 6.6 | 8.5 | 0.0 | 0.0 |
| B41 | 2.2 | 2.0 | 0.0 | 0.0 |
| B42 | 0.0 | 0.0 | 2.8 | 2.8 |
| B43 | 4.5 | 6.8 | 0.6 | 1.3 |
| B44 | 1.6 | 0.8 | 0.0 | 0.0 |
| B45 | 0.0 | 0.0 | 9.3 | 11.0 |
| B46 | 0.0 | 0.0 | 0.8 | 0.4 |
| B47 | 4.5 | 1.8 | 0.2 | 0.3 |
| B48 | 15.5 | 12.1 | 0.0 | 0.0 |
| B49 | 0.0 | 0.0 | 0.2 | 0.2 |
| B50 | 0.4 | 0.5 | 0.0 | 0.0 |
| B51 | 0.7 | 0.4 | 0.0 | 0.0 |

Figure 3.12: Left: The DGGE gel after separation of the 338f-GC/517r DNA fragments in a 30-50 % denaturing gradient. F and S refer to replicate samples from the tapwater-based and the seawater-based reactors, respectively. The numbering indicates the bands that were cut out and sequenced. The bands 20-1 and 20-2 were initially identified as equal, and were named B20. Later, sequencing revealed that these bands were not identical (section 3.3.2), and they were therefore renamed. Middle: The DGGE bands identified by GEL2k. The grey rectangles indicate the bands, while the black areas indicate the histogram peaks. Histogram peaks in the same grey area are thus assumed to be of the same bacterial origin. Right: The histogram peak area for each band in the DGGE gel, given as percentage of total peak area in the lane.

35-50 %

| | Peak area (%) | | | |
|---|---|---|---|---|
| Band | 1F | 2F | 1S | 2S |
| B1 | 1.8 | 1.3 | 3.7 | 4.5 |
| B2 | 2.0 | 2.1 | 0.6 | 1.3 |
| B3 | 4.3 | 6.6 | 0.0 | 0.0 |
| B4 | 2.0 | 1.4 | 6.1 | 9.2 |
| B5 | 36.6 | 28.4 | 25.1 | 21.1 |
| B6 | 2.7 | 1.3 | 0.0 | 0.0 |
| B7 | 0.0 | 0.0 | 1.6 | 1.7 |
| B8 | 0.0 | 0.0 | 12.7 | 8.7 |
| B9 | 0.1 | 0.3 | 0.0 | 0.0 |
| B10 | 0.1 | 0.4 | 1.7 | 1.8 |
| B11 | 0.0 | 0.0 | 1.2 | 0.9 |
| B12 | 1.9 | 2.1 | 2.3 | 1.2 |
| B13 | 0.9 | 0.6 | 0.0 | 0.0 |
| B14 | 0.4 | 0.1 | 0.8 | 0.7 |
| B15 | 1.5 | 1.7 | 0.0 | 0.0 |
| B16 | 0.0 | 0.0 | 1.2 | 1.7 |
| B17 | 1.3 | 1.9 | 0.0 | 0.0 |
| B18 | 3.2 | 2.8 | 4.8 | 4.4 |
| B19 | 3.4 | 2.9 | 1.3 | 1.8 |
| B20 | 0.0 | 0.0 | 1.0 | 1.0 |
| B21 | 2.3 | 2.3 | 0.0 | 0.0 |
| B22 | 0.0 | 0.0 | 0.7 | 0.0 |
| B23 | 0.0 | 0.0 | 0.5 | 0.1 |
| B24 | 0.0 | 0.0 | 8.5 | 11.3 |
| B25 | 6.6 | 12.0 | 0.0 | 0.0 |
| B26 | 0.0 | 0.0 | 1.8 | 1.7 |
| B27 | 2.5 | 3.8 | 0.0 | 0.0 |
| B28 | 0.0 | 0.0 | 7.1 | 6.8 |
| B29 | 10.4 | 10.1 | 0.8 | 0.4 |
| B30 | 0.0 | 0.0 | 3.7 | 5.8 |
| B31 | 0.7 | 1.5 | 0.0 | 0.0 |
| B32 | 0.0 | 0.0 | 9.0 | 9.9 |
| B33 | 0.0 | 0.0 | 1.8 | 1.6 |
| B34 | 0.5 | 0.6 | 0.0 | 0.0 |
| B35 | 0.0 | 0.0 | 0.4 | 0.3 |
| B36 | 0.7 | 0.7 | 0.0 | 0.0 |
| B37 | 0.0 | 0.0 | 0.9 | 0.9 |
| B38 | 0.3 | 0.4 | 0.0 | 0.0 |
| B39 | 0.0 | 0.0 | 0.6 | 0.5 |
| B40 | 0.2 | 0.1 | 0.0 | 0.0 |
| B41 | 4.7 | 7.0 | 0.0 | 0.0 |
| B42 | 0.0 | 0.0 | 0.4 | 0.4 |
| B43 | 8.8 | 7.3 | 0.0 | 0.0 |

Figure 3.13: Left: The DGGE gel after separation of the 338f-GC/517r DNA fragments in a 35-50 % denaturing gradient. F and S refer to replicate samples from the tapwater-based and the seawater-based reactors, respectively. The numbering indicates the bands that were cut out and sequenced. Middle: The DGGE bans identified by GEL2k. Right: The histogram peak area for each band in the DGGE gel, given as percentage of total peak area in the lane.

Figure 3.14: Left: The DGGE gel after separation of the 338f-GC/517r DNA fragments in a 30-40 % denaturing gradient. F and S refer to replicate samples from the tapwater-based and the seawater-based reactors, respectively. The numbering indicates the bands that were cut out and sequenced. Middle: The DGGE bans identified by GEL2k. Right: The histogram peak area for each band in the DGGE gel, given as percentage of total peak area in the lane.

| Band | Peak area (%) | | | |
| --- | --- | --- | --- | --- |
| | 1F | 2F | 1S | 2S |
| B1 | 3.4 | 1.7 | 3.7 | 1.9 |
| B2 | 5.6 | 7.4 | 0.6 | 0.9 |
| B3 | 0.6 | 0.7 | 0.0 | 0.0 |
| B4 | 5.3 | 3.8 | 2.3 | 1.7 |
| B5 | 0.0 | 0.0 | 0.3 | 0.0 |
| B6 | 2.4 | 2.7 | 0.0 | 0.0 |
| B7 | 0.0 | 0.0 | 0.5 | 0.3 |
| B8 | 31.7 | 32.2 | 23.1 | 28.0 |
| B9 | 0.0 | 0.0 | 0.5 | 0.4 |
| B10 | 0.0 | 0.0 | 0.7 | 0.2 |
| B11 | 1.1 | 0.8 | 0.0 | 0.0 |
| B12 | 0.1 | 1.4 | 0.0 | 0.0 |
| B13 | 8.2 | 8.4 | 0.0 | 0.0 |
| B14 | 0.0 | 0.0 | 12.0 | 23.2 |
| B15 | 4.0 | 3.7 | 0.0 | 0.0 |
| B16 | 0.0 | 0.0 | 16.2 | 12.7 |
| B17 | 2.0 | 2.1 | 0.0 | 0.0 |
| B18 | 20.1 | 20.0 | 22.7 | 17.4 |
| B19 | 3.1 | 5.2 | 2.4 | 1.5 |
| B20 | 0.0 | 0.0 | 9.5 | 5.6 |
| B21 | 1.6 | 1.7 | 0.0 | 0.0 |
| B22 | 0.5 | 0.7 | 1.6 | 1.7 |
| B23 | 0.0 | 0.0 | 0.3 | 0.3 |
| B24 | 0.7 | 0.6 | 0.0 | 0.0 |
| B25 | 0.3 | 0.3 | 0.2 | 0.3 |
| B26 | 0.7 | 0.1 | 0.0 | 0.0 |
| B27 | 4.9 | 4.8 | 2.8 | 3.1 |
| B28 | 2.1 | 1.1 | 0.4 | 0.3 |
| B29 | 0.0 | 0.0 | 0.5 | 0.5 |
| B30 | 0.5 | 0.2 | 0.0 | 0.0 |
| B31 | 1.1 | 0.5 | 0.0 | 0.0 |

Samples from the same reactor looked very similar when analyzed by DGGE (Figures 3.12-3.14). Although sampled simultaneously, they were from different biofilm carriers, and DNA extraction and PCR had been performed separately. The similarity between replicate samples was confirmed by calculations of dissimilarities (see below).

Differences between samples from the tapwater-based and the seawater-based reactors were evident by visual inspection of the 30-50 % gel (3.12). The bands from the tapwater-based reactor were distributed over a wider gradient than the bands from the seawater-based reactor. Most bands from the seawater-based reactor were distributed between 38 % and 45 %, while the bands from the tapwater-based reactor occupied higher denaturing re-

gions in gel, and had more bands in the top of the gel than the samples from the seawater-based reactor. Higher band richness in the samples from the tapwater-based reactor was confirmed by analysis in GEL2k (see below). As shown in Figure 3.12, the most dominating bands in the 30-50 % gel, e.g. B15, B19, B24, B25 and B48, were only present in one of the samples, indicating that the microbial communities in the tapwater-based and the seawater-based reactors were dominated by different species. Very intense bands can be composed of several DNA fragments that have not been separated properly. Some of the most dominating bands in the gel, especially B48 which was very wide, could have contained several sequences.

In the 35-50 % and 30-40 % gels (Figures 3.13 and 3.14) the most dominating bands B5 and B8, were present in all samples at roughly similar intensities. Such a band could not be identified in the 30-50 % DGGE gel.

Several other dominating bands could be detected in the 35-50 % DGGE gel, and most of the bands seemed to be unique to either the tapwater-based reactor or the seawater-based reactor.

It was more difficult to analyze the 30-40 % denaturing gradient gel, shown in Figure 3.14, because the bands in the lower part of the gel were smeared and not properly separated. The lower part of the gel seemed to be bent, probably because the denaturing gradient had been cast between glass plates that were not adjusted correctly. The bands in the upper part of the gel, however, seemed to be better separated than in the other gels, which was the purpose of this DGGE run.

By comparing the three DGGE gels in Figures 3.12-3.14, it was evident that narrowing the denaturing gradient did not simply give a close-up of parts of the wider denaturing gradient. It was difficult to compare the gels and identify redundant bands in the different denaturing gradients.

**Calculation of dissimilarities and molecular diversity indices**

The Bray Curtis dissimilarities between different samples, based on their band pattern in the DGGE gels, are shown in Table 3.1. In all gels, the dissimilarity between samples from different reactors were larger than the dissimilarity between samples from similar reactor. The 30-50 % DGGE gel was the only gel that, in theory, had a wide enough denaturing gradient to separate all sequences in the PCR product, and hence could represent the whole microbial community. The dissimilarity between replicate samples was around 0.2, while the dissimilarity between samples from different reactors was above 0.8. The dissimilarity between the samples in the different gels generally decreased with decreasing width of the denaturing gradient.

Figure 3.15 shows Pareto-Lorenz curves calculated from the distribution of bands in the different lanes in the 30-50 % DGGE gel (Figure 3.12). A steeper slope initially means that a smaller fraction of the bands is responsible for a larger fraction of the peak area, compared to the 45° "perfect

Table 3.1: Bray Curtis dissimilarities between different samples, based on their band pattern in the 30-50 % (top), 35-50 % (middle) and 30-40 % (bottom) DGGE gels (Figures 3.12-3.14). Calculations were based on fractional histogram peak areas, and not binary data. 1F and 2F refer to replicate samples from the tapwater-based reactor, while 1S and 2S refer to replicate samples from the seawater-based reactor.

| 30-50 % | 1F | 2F | 1S | 2S |
|---|---|---|---|---|
| 1F | 0 | | | |
| 2F | 0.233 | 0 | | |
| 1S | 0.822 | 0.859 | 0 | |
| 2S | 0.855 | 0.863 | 0.180 | 0 |

| 35-50 % | 1F | 2F | 1S | 2S |
|---|---|---|---|---|
| 1F | 0 | | | |
| 2F | 0.140 | 0 | | |
| 1S | 0.629 | 0.641 | 0 | |
| 2S | 0.666 | 0.681 | 0.118 | 0 |

| 30-40 % | 1F | 2F | 1S | 2S |
|---|---|---|---|---|
| 1F | 0 | | | |
| 2F | 0.066 | 0 | | |
| 1S | 0.443 | 0.460 | 0 | |
| 2S | 0.444 | 0.445 | 0.170 | 0 |

58

evenness" curve (Marzorati et al. 2008). The Pareto-Lorenz curves for samples from the same reactor were very similar, but the two samples from the seawater-based reactor clearly differed from the samples from the tapwater-based reactor. The Pareto-Lorenz curves indicate that the microbial community in the seawater-based reactor was more uneven than the microbial community in the tapwater-based reactor.
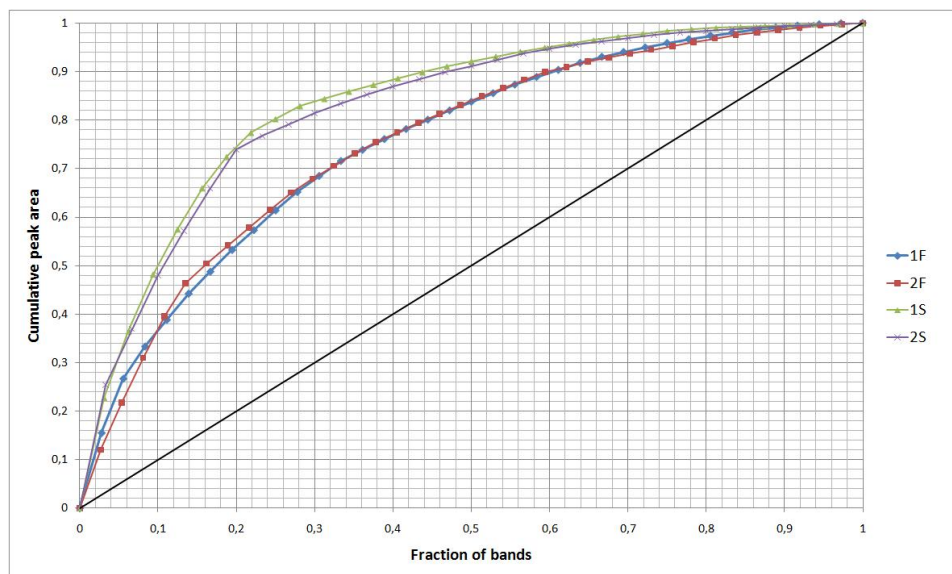


Figure 3.15: Pareto-Lorenz curves showing the cumulative peak area in each lane from the 30-50 % denaturing gradient gel, vs. the cumulative proportion of bands. The black line indicates the scenario where all bands in the lane have equal peak areas.

Various calculated indicators of community composition is given in Table 3.2. The Gini coefficients, based on the curves in Figure 3.15, were higher for the seawater-based reactor than for the tapwater-based reactor, indicating higher evenness in the tapwater-based reactor. The samples from the tapwater-based reactor had higher band richness than the samples from the seawater-based reactor, indicating higher species richness in the tapwater-based reactor.

59

Table 3.2: Band richness, range-weighted richness (Rr), the Shannon-Weaver index (H'), Pielou's evenness index (J') and the Gini coefficient based on the band patterns for each sample in the 30-50 % denaturing gradient gel.

| Sample | Band richness | Rr | H' | J' | Gini |
|---|---|---|---|---|---|
| 1F | 36 | 240 | 3.12 | 0.87 | 0.51 |
| 2F | 37 | 253 | 3.17 | 0.88 | 0.51 |
| 1S | 32 | 179 | 2.61 | 0.75 | 0.67 |
| 2S | 30 | 158 | 2.59 | 0.76 | 0.65 |

Because the bands from the tapwater-based reactor were distributed over a wider denaturing gradient, the range-weighted richness was also higher in the samples from the tapwater-based reactor. All indices indicated the same; higher species richness, higher diversity and higher evenness in the tapwater-based reactor. The higher band richness, occupation of a larger denaturing range and lower dominance of some bands in the samples from the tapwater-based reactor resulted in the fact that all calculated evenness and diversity indices indicated higer diversity and evenness in the tapwater-based reactor.

### 3.3.2 Sequence analysis of the 338f-GC/517r fragment

Table 3.3 shows the result from sequence analysis of the 338f-GC/517r DGGE bands, and the corresponding DGGE histogram peak areas. The similarity between the DGGE sequences and the nearest database neighbour is given as the percentage of shared 7-mers, and not as percent sequence similarity. According to Greengenes (DeSantis et al. 2006), two sequences will often have a lower percentage of shared 7-mers than % sequence similarity (e.g. sequences with 95 % sequence similarity may only share 78 % of their 7-mers).

Some sequences, most of them from the 30-50 % DGGE gel, did not pass the quality standards from Eurofins-DNA, and were not analyzed further. The reason for this was probably that the UV lamp in the gel documentation system destroyed DNA in the gel, due to long processing time and high intensity in the UV lamp. The intensity of the UV lamp was unnecessarily high when bands were cut out of the 30-50 % DGGE gel. Most of the sequences that did not pass the quality requirements were from the bottom of the gel. These bands were cut out last and had been exposed to the UV light for more than 15 minutes. Some bands also seemed to consist of several DNA sequences. This could be seen from the sequence chromatograms, where many peaks were ambiguous. The results from chimera detection did not indicate chimeric sequences (results not included), but chimera detection

is difficult for short sequences like the 338f-GC/517r fragment. The presence of chimeric sequences in the dataset cannot be completely ruled out.

As shown in Table 3.3, most of the sequences belonged to the phylum *Proteobacteria*. Representatives from $\alpha$-, $\beta$ and $\gamma$-proteobacteria were found. 13 out of 44 sequences were affiliated with nitrifying bacteria. Of these, eight were related to ammonia-oxidizers, while five were related to nitrite-oxidizers.

Table 3.3: The Greengenes phylogeny of sequenced 338f-GC/517r fragments. The % identity refers to the percentage of 7-mers shared by the query sequence and the database sequence. The peak area is the peak area from the grey level histograms generated in GEL2k, given as percentage of total peak area in the lane. The average between the replicate samples (1F and 2F, 1S and 2S) is given. The peak area cannot be directly compared between gels with different denaturing gradients, because the narrower gradients had fewer bands than the 30-50 % gel. (F=sample from the tapwater-based reactor, S=sample from the seawater-based reactor)

| Band | Phylogenetic affiliation | % identity | Peak area (%) | |
| --- | --- | --- | --- | --- |
| | | | F | S |
| **30-50 %** | | | | |
| B2 | Dechloromonas denitrificans str. ED1 | 83.5 | 1.8 | 0.3 |
| B3 | Dechloromonas sp. str. SIUL | 96.4 | 1.3 | 0.0 |
| B4 | Methylobacterium sp. OS-16.b | 98.8 | 1.3 | 0.3 |
| B6 | Unclassified clone sequence | 90.6 | 2.3 | 0.0 |
| B8 | Azospirillum species | 77.5 | 1.1 | 0.0 |
| B10 | Inquilinus limosus str. AU430 | 81.4 | 0.7 | 1.0 |
| B12 | Thalassospira sp. str. MCCC 1A02843 | 86.6 | 2.5 | 0.0 |
| B14 | Thalassospira sp. Bp123 str. BP123 | 86.1 | 7.4 | 0.0 |
| B15 | Nitrosomonas halophila | 80.2 | 0.0 | 24.1 |
| B18 | Nitrosomonas ureae | 81.9 | 3.5 | 0.0 |
| B19 | Thalassolituus oleivorans str. MIL-1 | 72.8 | 0.0 | 11.6 |
| B20-1 | Unclassified nitrosomadaceae | 79.1 | 4.2 | 0.0 |
| B20-2 | Thalassolituus oleivorans str. MIL-1 | 75.2 | 0.0 | 3.6 |
| B22 | Aleurodicus dugesii | 83.3 | 2.7 | 2.6 |
| B24 | "Nitrospira moscoviensis" | 67.0 | 0.0 | 11.5 |
| B39 | Afipia broomeae str. F186 | 68.4 | 0.0 | 7.2 |
| B45 | Thermoanaerobacter sp. str. MET-G | 47.3 | 0.0 | 10.2 |
| B48 | Nitrospira cf. moscoviensis str. SBR2016 | 100.0 | 13.8 | 0.0 |
| **35-50 %** | | | | |
| B3 | Nitrosomonas sp. Is343 | 85.0 | 5.5 | 0.0 |
| B4 | Nitrosomonas halophila | 80.2 | 1.7 | 7.7 |

*Continued on next page*

*Table 3.3 continued*

| Band | Phylogenetic affiliation | % identity | Peak area (%) | |
| --- | --- | --- | --- | --- |
| | | | F | S |
| B5 | Nitrosomonas oligotropha | 96.5 | 32.5 | 23.1 |
| B6 | Dechloromonas denitrificans str. ED1 | 87.0 | 2.0 | 0.0 |
| B7 | Aquaspirillum subsp. peregrinum str. IFO 14922 | 84.9 | 0.0 | 1.7 |
| B8 | strain isolate str. rJ15 | 78.6 | 0.0 | 10.7 |
| B10 | isolate str. BH203 | 90.9 | 0.3 | 1.8 |
| B11 | isolate str. BH204 | 88.2 | 0.0 | 1.0 |
| B12 | Dechloromonas sp. str. SIUL | 85.9 | 2.0 | 1.8 |
| B15 | Nitrosomonas sp. Is343 | 88.3 | 1.6 | 0.0 |
| B16 | Aquaspirillum peregrinum subsp. integrum str. IAM 14946 subsp. | 89.9 | 0.0 | 1.5 |
| B17 | Azospirillum species | 79.0 | 1.6 | 0.0 |
| B18 | Dechloromonas sp. str. SIUL | 84.3 | 3.0 | 4.6 |
| B19 | Inquilinus sp. str. ZY061 | 72.0 | 3.2 | 1.6 |
| B24 | Agrobacterium larrymoorei str. 3-10 | 86.9 | 0.0 | 9.9 |
| B25 | Sphingomonas sp. K101 | 77.2 | 9.3 | 0.0 |
| B28 | Azospirillum species | 82.8 | 0.0 | 7.0 |
| B29 | Nitrospira cf. moscoviensis str. SBR2016 | 64.7 | 10.3 | 0.6 |
| B31 | rice rhizoplane isolate str. RRP-E4 | 68.9 | 1.1 | 0.0 |
| B36 | Nitrifying sludge clone RC73 | 80.4 | 0.7 | 0.0 |
| B41 | Nitrospira cf. moscoviensis str. SBR2016 | 96.3 | 5.9 | 0.0 |
| B43 | Nitrospira cf. moscoviensis str. SBR2016 | 100.0 | 8.1 | 0.0 |
| **30-40 %** | | | | |
| B1 | Lysobacter sp. str. GH41-7 | 81.2 | 2.5 | 2.8 |
| B2 | Dechloromonas sp. str. SIUL | 85.9 | 6.5 | 0.8 |
| B4 | Nitrosomonas sp. str. Nm84 | 80.0 | 4.6 | 2.0 |
| B6 | Roseospira thiosulfatophila AT2115 | 88.4 | 2.6 | 0.0 |

## AOB-affiliated sequences

Table 3.4 summarize the findings of sequences related to AOB and NOB. Only ammonia-oxidizers within the *Nitrosomonas* cluster were identified. Sequences related to *Nitrosomonas halophila* and *Nitrosomonas oligotropha* seemed to be the only AOB sequences dominating in the PCR product from the seawater-based reactor. In the tapwater-based reactor, *Nitrosomonas halophila* affiliated sequences were only found in small amounts. *Nitrosomonas oligotropha*-affiliated sequences seemed to dominate in all samples in the 35-50 % DGGE gel, but this DGGE band was not identified in the 30-50 % gel. The sequence might not have been localized in a clear DGGE

band, or the DGGE band was cut out and sequenced, but did not pass the quality standards. A band that looked similar to the *Nitrosomonas oligotropha* band in the 35-50 % gel was found in the 30-40 % gel (B8), but this band was not sequenced.

Table 3.4: DGGE sequences affiliated with nitrifying species. The abundance of different sequences in the DGGE gels are indicated[1]. The % identity refers to the percentage of sheared 7-mers between the query sequence and the nearest neighbour.

| Band | Phylogenetic affiliaton | %identity | F | S |
|------|------------------------|-----------|---|---|
| **Ammonia oxidizers** | | | | |
| 30-50 % B15 | Nitrosomonas halophila | 80.2 | - | ++++ |
| 35-50 % B4 | Nitrosomonas halophila | 80.2 | + | ++ |
| 35-50 % B15 | Nitrosomonas sp. Is343 | 88.3 | + | - |
| 35-50 % B3 | Nitrosomonas sp. Is343 | 85.0 | ++ | - |
| 35-50 % B5 | Nitrosomonas oligotropha | 96.5 | ++++ | ++++ |
| 30-50 % B18 | Nitrosomonas ureae | 81.9 | + | - |
| 30-40 % B4 | Nitrosomonas sp. str. Nm84 | 80.0 | + | + |
| 30-50 % B20-1 | Unclassified Nitrosomonadaceae | 79,1 | + | - |
| **Nitrite oxidizers** | | | | |
| 30-50 % B24 | "Nitrospira moscoviensis" | 67.0 | - | +++ |
| 30-50 % B48 | Nitrospira moscoviensis str. SBR2016 | 100.0 | +++ | - |
| 35-50 % B29 | Nitrospira moscoviensis str. SBR2016 | 64.7 | +++ | + |
| 35-50 % B41 | Nitrospira moscoviensis str. SBR2016 | 96.3 | ++ | - |
| 35-50 % B43 | Nitrospira moscoviensis str. SBR2016 | 100.0 | ++ | - |

[1] Scale is based on relative peak areas, where 0 % = -, 0–5 % = +, 5–10 % = ++, 10–15 % = +++, >15 % = ++++.

In addition to sequences affiliated with *Nitrosomonas halophila* and *Nitrosomonas oligotropa*, sequences affiliated with *Nitrosomonas sp. Is343*, *Nitrosomonas sp. str. Nm84* and *Nitrosomonas ureae* were found. *Nitrosomonas Is343* and *Nitrosomonas ureae*-like sequences were only found in the tapwater-based reactor, while the *Nitrosomonas sp. str. Nm84*-like sequence was found in smaller amounts in PCR product from both reactors.

When comparing the sequence affiliated with *Nitrosomonas sp. str. Nm84* and the *Nitrosomonas sp. Is343* sequence from B3 in the 35-50 % DGGE gel, it turned out that these sequences were identical. The *Nitrosomonas sp. str. Nm84*-related sequence was slightly longer, which was the

reason why these sequences had been classified differently. Since these two bands were located similarly in the 35-50 % and the 30-40 % DGGE gel, it is likely that these two sequences originated from the same organism.

One sequence, 30-50 % B20-1, showed highest match with an unclassified sequence belonging to the *Nitrosomonadaceae*. An NCBI nucleotide BLAST search of this sequence gave high similarity values to different uncultured *Nitrosomonas*. Some regions of this sequence were of low quality with ambiguous nucleotides, and it is likely that database querying would have given closer matches if these regions were of better quality.

All Nitrosmononas-related sequences sheared around 80 % or more of their 7-mers with their closest database match (Table 3.4). It is difficult to compare this similarity with the 97 % sequence similarity value that is often used as a functional measure for microbial species. A BLAST search on the AOB-related 338f-GC/517r sequences generally gave high similarity scores (>97 %) with different *Nitrosomonas* species.

**NOB-affiliated sequences**

Only *Nitrospira*-affiliated NOB sequences were identified, and most of these sequences were only present in the PCR-product from the tapwater-based reactor. One dominating *Nitrospira moscoviensis*-like band was identified from the seawater-based reactor (30-50 % B24), but the similarity to the database sequence was not high. When querying the sequence in BLAST, the closest match with an isolated organism was with *Nitrospira marina*, which had 97 % sequence similarity. Investigation of the sequence chromatogram showed that the sequence was of bad quality. Several double peaks indicated that more than one sequence was present in the DGGE band. The other *Nitrospira moscoviensis* band with low similarity score, B29 from the 35-50 % DGGE gel, also had a chromatogram with several double peaks. Comparison of the chromatograms for these two sequences showed that the ambiguous bases were located in the same regions. These regions were probably at variable locations in the 16S rRNA sequence, because the occurrence of more than one sequence in a DGGE band will be evident in variable regions where there are sequence differences.

The other *Nitrospira moscoviensis*-affiliated sequences had high similarity values. Comparison of these sequences revealed that the B48 sequence in the 30-50 % gel were identical to the B43 sequence in the 35-50 % gel. The B41 sequence in the 35-50 % gel had one mismatch. The B48 band in the 30-50 % gel might have consisted of both *Nitrospira moscoviensis* sequences.

Figure 3.16 is a neighbour-joining phylogenetic tree constructed from the 338f-GC/517r sequences in Table 3.3, and AOB and NOB reference sequences from GenBank. The AOB- and NOB-related sequences clustered within the $\beta$-proteobacteria and the *Nitrospira* lineage, respectively.

The phylogenetic tree do not show much difference between different $\beta$-proteobacteria. The two $\beta$-proteobacterial *Nitrosospira* sequences clustered together, but none of the DGGE sequences seemed to be related to *Nitrosospira*. The *Nitrosomonas sp. str. Nm48* sequence from B4 in the 30-40 % gel clustered together with B8 from the 30-50 % gel and B17 from the 35-50 % gel. These two sequences were affiliated with *Azospirillum sp.* Manual investigation of these sequences revealed that the *Azospirillum*-like sequences were identical, except that the B8 sequence was three nucleotides longer, resulting in a slightly different similarity score. The *Nitrosomonas sp. str. Nm48* sequence had three mismatches to the *Azospirillum* sequences. Since the *Nitrosomonas sp. str. Nm48* sequence was identical to the *Nitrosomonas sp. Is343* sequence from B3 in the 35-50 % gel, this clustering might not be of much significance.

The three sequences with high similarity to *Nitrospira moscoviensis* clustered within the *Nitrospira* lineage (Figure 3.16). The two *Nitrospira*-related sequences with low similarity scores (30-50 % B24 and 35-50 % B29) showed some relationship to the *Nitrospira* lineage, but were positioned some distance away from the other *Nitrospira* sequences, especially the B29 sequence from the 35-50 % gel. As reported previously, these sequences had some ambiguous bases.

| | N. multiformis 24C 16S ribosomal RNA | Nitrosospira |
| 50 | N. briensis | |

N. cryotolerans Nm55 16S rRNA
29792 AF2872971 Nitrosococcus mobilis...
● 35-50 B11
6702 AF1703561 Dechloromonas sp str SIUL
● 35-50 B10
N. eutropha C91 Nm57 16S rRNA
● 30-50 B3
● 35-50 B15
105569 AJ6210261 Nitrosomonas sp ls79A3
● 30-50 B20 1
N. aestuarii 16S ribosomal RNA
16548 AF2724161 Nitrosomonas sp NM 107
100972 AY2776211 Dechloromonas agitat...
● 35-50 B5
N. europaea
● 35-50 B6
N. halophila Nm1 16S rRNA
● 35-50 B18
● 35-50 B3
106023 AJ6210291 Nitrosomonas sp ls425
N. oligotropha 16S ribosomal RNA
● 35-50 B12
N. mobilis M93 16S ribosomal RNA
● 35-50 B4
18274 AF2724151 Nitrosomonas sp NM 104
N. europaea ATCC19178 16S ribosomal RNA
49602 AF2724141 Nitrosomonas ureae
● 30-50 B8
● 35-50 B17
● 30-40 B4
101077 AJ6210321 Nitrosomonas sp ls343
28030 AF3867571 Nitrosomonas sp R7c187
● 30-50 B2
● 30-40 B2
N. marina 16S ribosomal RNA
● 30-50 B15
69852 AY1237941 Nitrosomonas sp str N...
N. halophila 16S ribosomal RNA
17356 AF2724241 Nitrosomonas sp Nm51
● 30-50 B18
35231 AF2724171 Nitrosomonas communis
6658 M964031 Nitrosococcus mobilis st...
N. communis Nm2 16S rRNA
351746 EU8339881 Lysobacter sp str RC...
● 30-40 B1
● 35-50 B7
● 35-50 B16
● 30-50 B12
326754 EU9828431 Rhodobium sp str 2
● 35-50 B8
N. oceani
182472 AB2861791 Rhodanobacter thioox...
107836 AJ5804971 Luteibacter rhizovic...
● 30-50 B19
● 30-50 B20 2
E. coli 16S ribosomal RNA
101731 AY5447681 Aquamonas vora str B...
● 35-50 B31
● 35-50 B25
● 30-50 B10
145538 AB2453521 Inquilinus ginsengis...
● 30-50 B6
● 35-50 B28
77884 AJ4012081 Roseospira thiosulfat...
101335 AY6609631 Azospirillum irakens...
● 30-40 B6
102265 AY5634411 Sphingomonas phyllos...
227483 EF5404861 Devosia sp c4M
● 30-50 B4
● 35-50 B24
N. hamburgensis X14 X14 DSM 10229 16S...
150542 D144272 Rhodopseudomonas sp st...
N. sp. LL 16S rRNA
101778 AY7417251 Methylobacterium sp ...
165499 AJ9686921 Bosea sp str STM 358
● 35-50 B19
● 30-50 B14
● 30-50 B39
● 30-50 B22
● 35-50 B29
108977 AY8001041 Thermoanaerobacter s...
● 35-50 B36
● 30-50 B24
● 30-50 B45
3301 AF1327921 Prochlorothrix hollandica
● 35-50 B43
● 35-50 B41
N. cf. moscoviensis SBR1015 SBR1015 1...
● 30-50 B48
1451 L355011 Nitrospira marina
N. sp. 16S rRNA
1443 X825591 Nitrospira marina str 295

Betaproteobacteria
Nitrosomonas
Nitrosococcus
Gammaproteobacteria
Alfaproteobacteria
Nitrobacer
Nitrospira

Caption on following page

0.02

Figure 3.16: Phylogenetic Neighbour-Joining maximum composite likelihood tree with 338f-GC/517r DGGE sequences and some sequences belonging to nitrifying species from GenBank. Sequences from the nearest isolated neighbours according to the Greengenes NAST alignment are also represented in the tree. The DGGE sequences (indicated by bullets) are referred to by the denaturing gradient of the gel from which they were taken, and their band number. Sequences that were related to ammonia-oxidizers are indicated by green bullets, while sequences related to nitrite-oxidizers are indicated by red bullets. The bootstrap values for each branch after 100 replicates are shown. All positions containing gaps and missing data were eliminated from the dataset (complete deletion option).



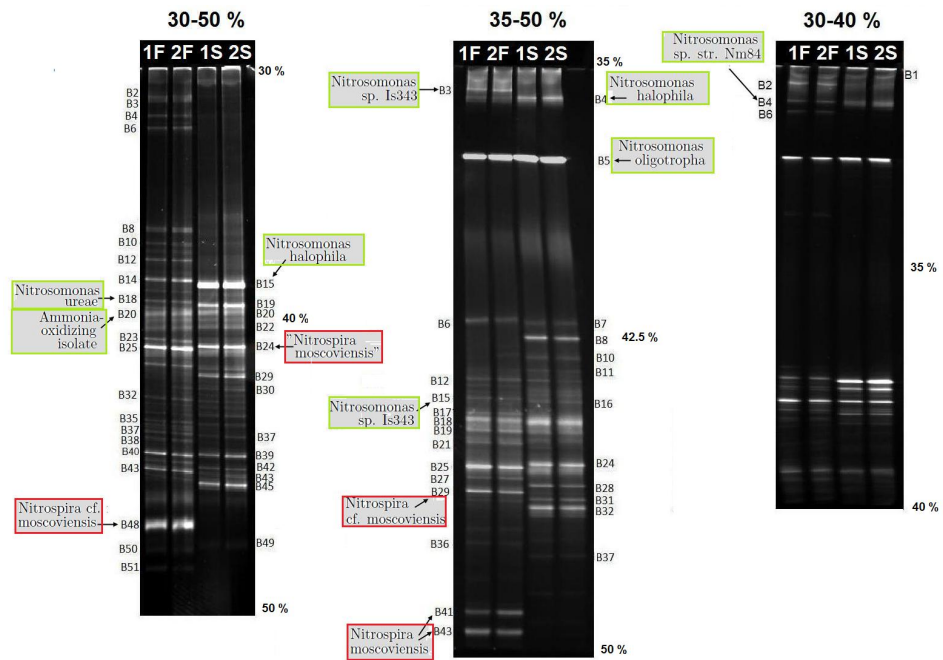Figure 3.17: The 30-50%, 35-50 % and 30-40 % DGGE gels from which bands were sequenced. The bands affiliated with nitrifying bacteria are indicated.

The DGGE bands affiliated with AOB and NOB are indicated on the DGGE gel in Figure 3.17. The *Nitrosomonas*-related bands were distributed in the upper part of the gels, from 30 % to around 40 %. *Nitrospira* bands were in the lower part of the gels, from around 40 % to 50 %.

67

## 3.4 PCR amplification of bacterial *amoA* sequences

Several PCR primers for amplification of *amoA* sequences were tested. Some of the primers did not give satisfactory PCR products. In the following sections, the results from primer trials and optimization of annealing temperatures and MgCl$_2$ concentrations are described. Two primers gave PCR product that were considered good enough for DGGE analysis; the traditional amoA-1F-GC/amoA-2R primers, and the newer amoA121f-GC/amoA359rC primers. DGGE analysis was mainly performed with the amoA121f-GC/amoA359rC fragment. DGGE results are presented in section 3.5.

### 3.4.1 PCR with the primers A189f and A682r-GC

Temperature gradient PCR was used in order to evaluate the optimal annealing temperature. Figure 3.18 shows the PCR products after gel electrophoresis. The annealing temperature did not seem to affect the quality of the PCR product in the temperature range that was tested. Several bands could be seen in the agarose gel, especially from the sample from the seawater-based reactor. The concentration of MgCl$_2$ in the PCR reaction mixture was lowered as an attempt to avoid amplification of the unwanted bands. Figure 3.19 shows the agarose gel with PCR products after amplification with lowered MgCl$_2$ concentration.
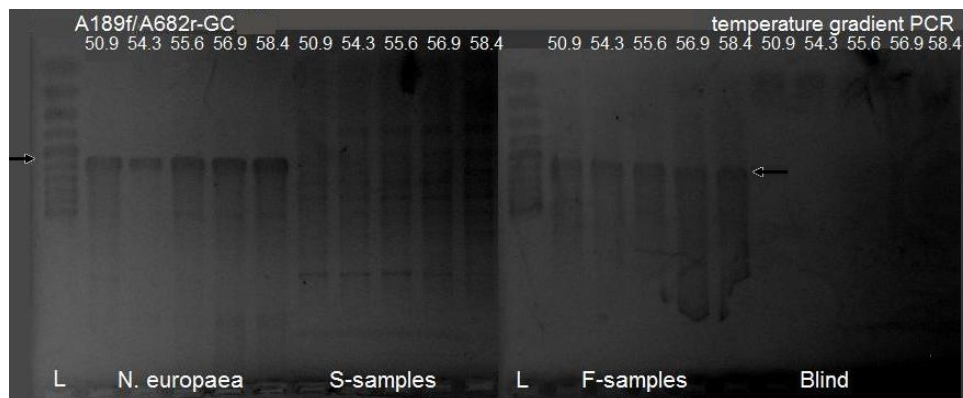


Figure 3.18: PCR products after temperature gradient PCR with the primers A189f and A682r-GC. The arrows show the correct PCR product length. The annealing temperatures are indicated above the DNA bands. F=sample from the tapwater-based reactor, S=sample from the seawater-based reactor, Blind=no-template control, L=100 bp ladder
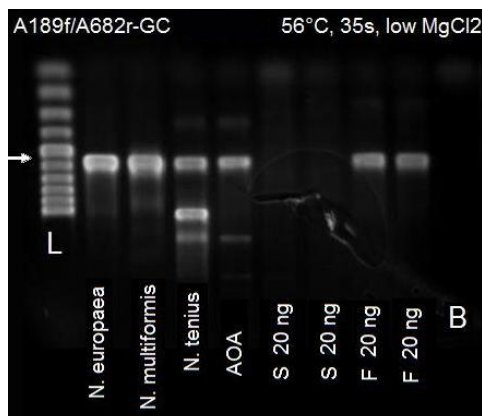
Figure 3.19: PCR products after amplification with the primers A189f and A682r-GC and lowered MgCl$_2$ concentration. The arrow indicates the correct PCR product length. The amount of template per 25 $\mu$L reaction volume is shown. AOA=archaeal amoA, F=sample from the tapwater-based reactor, S=sample from the seawater-based reactor, B=no-template control, L=100 bp ladder

Lowering the MgCl$_2$ concentration reduced the presence of unspecific products, but the PCR product still contained several unwanted bands. The effect of the amount of template in the PCR reaction and the number of PCR cycles were tested, but no improvement could be seen. The A189f/A682r-GC fragment was not analyzed further by DGGE.

The A189f/A682r primers were originally designed by Holmes et al. (1995) to target AOB *amoA* genes and MOB *pmoA* genes. These primers have been thought of as specific for $\gamma$-AOB within the ammonia-oxidizing bacteria (Wuchter et al. 2006), but a more recent primer evaluation by Junier et al. (2008), revealed that the A682r primer has perfect match only with some *Nitrosospira amoA* genes. In spite of this, products of correct length were amplified from the *N. europaea amoA* plasmid, and even from the archaeal *amoA* fosmid. Primer-BLAST was used to check the primer specificity *in silico*. It turned out that *N. europaea* ATCC19718 have one mismatch with the forward primer and one mismatch with the reverse primer. The ammonia-oxidizing crenarchaeon *Nitrosopumilus maritimus* had more than four mismatches with the primers, and is therefore not a plausible target for the A189f/A682r primers. However, *in silico* analysis is not enough to reliably evaluate the specificity of primers. The primer specificity was also checked towards the *E. coli* genome, which was co-extracted with the plasmids, but no probable target sequence of correct length was found. It is possible that the *E. coli* culture with the archaeal *amoA* fosmid, or DNA extracts from the culture, was contaminated, possibly with the other *amoA* plasmids.

No PCR product was detected in the samples from the seawater-based reactor. Due to the uncertain specificity of the primers, it is difficult to interpret these results. It is likely that the amplification efficiency was higher for the *amoA* genes in the plasmid controls than for the biofilm samples, due to higher copy number of the *amoA* genes and lower presence of competing sequences. The fact that no PCR product could be detected in the replicate samples from the seawater-based reactor, does not necessarily mean that *N. europaea, N. multiformis* and *N. tenius* was not present, but it is likely that these were absent or in low numbers.

### 3.4.2 PCR with the primers amoA-1F-GC and amoA-2R

The result from temperature gradient PCR with the primers amoA1F-GC and amoA-2R is shown Figure 3.20. At the lowest annealing temperatures, some secondary product seemed to be amplified. At the highest annealing temperature, no product could be detected from the tapwater-based reactor sample. To avoid secondary products, but still get a sufficient amplification efficiency for the reactor samples, an annealing temperature at 59 °C was chosen, and the template concentration was increased. Figure 3.21 shows the result from PCR under these conditions.

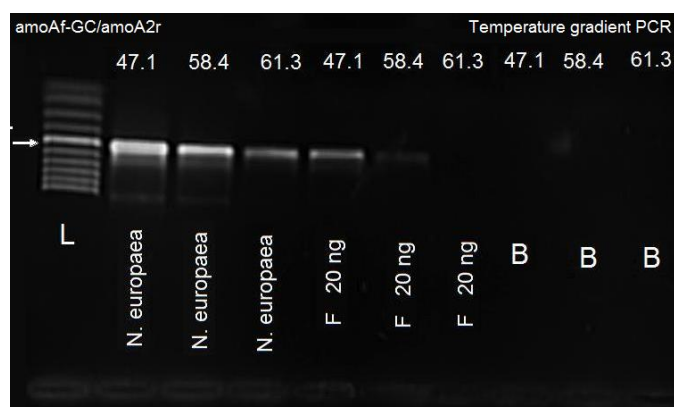

Figure 3.20: PCR products after temperature gradient PCR with the primers amoA-1F-GC and amoA-2R. The annealing temperatures are indicated at the top. The arrow indicates the correct product length. The amount of template per 25 $\mu$L reaction volume is indicated for the samples from the tapwater-based reactor. F=sample from the tapwater-based reactor, B=non-template control, L=100 bp ladder
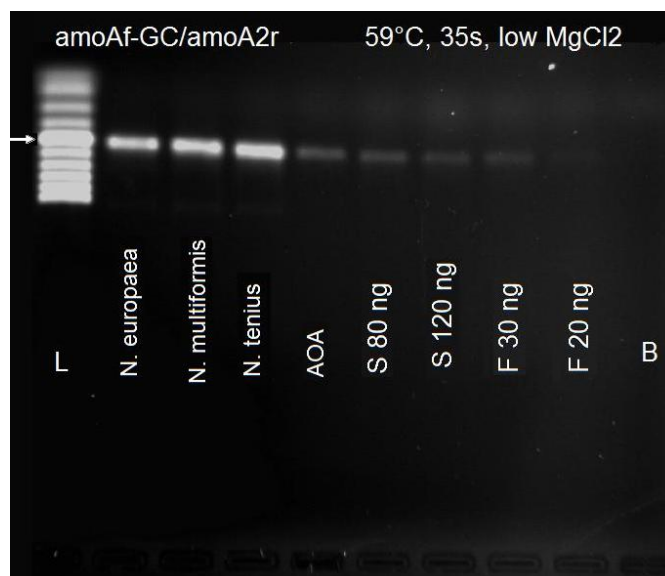
Figure 3.21: PCR products after amplification with the primers amoA1F-GC and amoA-2R, with 59 °C annealing temperature and increased concentration of template. The arrow indicates the correct product length. The amount of template per 25 $\mu$L reaction volume is indicated for the reactor samples. AOA=archaeal amoA, F=sample from the tapwater-based reactor, S=sample from the seawater-based reactor, B=non-template control, L=100 bp ladder.

The archaeal *amoA* gene was also amplified, as with the A189f/A682r-GC primer pair, although lower amounts of PCR product could be detected compared to the other *amoA* controls. This indicates that the amplification efficiency was lower, because of mismatch between primers and template or, if the AOA control was contaminated with AOB controls, because of lower copy numbers of the *amoA* plasmid contamination. The amoA-1F/amoA-2R primers should be specific to $\beta$-AOB. Since the archaeal *amoA* gene is not closely related to bacterial *amoA*, the PCR product from the 54d9 fosmid is difficult to explain. The primer specificity was checked in Primer-BLAST. The results showed that the primers have full complementarity to *N. europaea, N. multiformis* and *N. tenius*, but more than four mismatches to the archaeon *Nitrosopumilus maritimus*. The primer specificity was also checked towards the *E. coli* genome, which was co-extracted with the plasmids, but no probable target sequence of correct length was found.

The PCR products detected from the archaeal *amoA* control after PCR with the primer pairs A189f/A682r-GC and amoA-1F-GC/amoA-2R was not sequenced, and the origin of this PCR product is therefore unknown, but the AOA control was possibly contaminated. This suspicion was reinforced when sequences from the amoA-1F-GC/amoA-2R PCR product was

separated by DGGE (section 3.5.1).

### 3.4.3   PCR with the primers amoA121f-GC and amoA359rC

After experiencing problems with separation of DNA fragments of approximately 500 bp by DGGE (section 3.5.1), the primers amoA121f-GC and amoA359rC were chosen for further *amoA*-based analysis. This primer pair targets a 279 bp region from the $\beta$-AOB *amoA* gene.

As shown in Figure 3.22, DNA fragments of correct length were amplified from the reactor samples, but not from the *amoA* controls. PCR was run with different $MgCl_2$ concentrations, annealing temperatures and template amounts, but no product of correct length could be detected from the *amoA* controls. This gave rise to concern about the specificity of the amoA121f-GC/amoA359r primers. The amoA121f and amoA359rC primers have, according to Junier et al. (2008), no mismatches with different *Nitrosospira*, e.g. *N. briensis, N. multiformis* and *N. tenuis*, and 0–2 mismatches with different *Nitrosomonas* species. Based on sequence data, one could therefore expect PCR product from the *N. multiformis* and the *N. tenius amoA* controls. The amoA359rC primer has one mismatch with *N. europaea*. Junier et al. (2009) tested these primers on environmental samples. Most of the sequences obtained from PCR-DGGE were affiliated with the *Nitrosospira*. Primer-BLAST confirmed that the amoA121f/amoA359rC primers have no mismatches with *N. multiformis* and *N. tenius*, and one mismatch with *N. europaea* ATCC 19718. Since PCR products were obtained with the amoA-1F/amoA-2R and A189f/A682r, there is no reason to believe that inhibiting substances hampered the PCR reaction. It is therefore difficult to explain the missing product. The GC-clamp might have affected the amplification.



Figure 3.22: PCR products after amplification with the primers amoA121f-GC and amoA359rC. The arrow indicates the products of correct length. AOA=archaeal amoA, F=sample from the tapwater-based reactor, S=sample from the seawater-based reactor, B=no-template control, L=100 bp ladder.

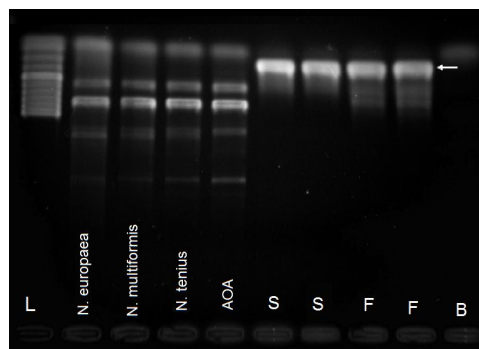## 3.5  DGGE analysis of bacterial *amoA* sequences

### 3.5.1  DGGE analysis of the amoA-1F-GC/amoA-2R fragment

The PCR products from amplification with the primers amoA-1F-GC and amoA-2R were analyzed on a wide denaturing gradient from 25-50 %. Figure 3.23 shows the DGGE gel after staining with SYBRGold. Separation of amoA-1F-GC/amoA-2R sequences were difficult due to their lenght. Some bands could be detected, but they were smeared, and attempts to sequence these bands would probably have failed, due to insufficient separation of different sequences. The same problem had been experienced by others at the department, trying to analyze PCR products of around 500 bp or longer with the Ingeny phorU system.

Some bands could be detected on the DGGE gel (Figure 3.23), and most of them were from the *N. multiformis, N. tenius* and archaeal *amoA* controls. These bands had migrated further than the smear in the upper part of the gel. Nitrifying bacteria often have several copies of the *amoA* gene, and different copies can have slightly different sequence (Koops & Pommerening-Röser 2005), resulting in several DGGE bands. It seemed like the archaeal *amoA* control had the same bands as the *N. multiformis* and *N. tenius* controls. The archaeal *amoA* control might have been contaminated with *N. multiformis* and *N. tenius amoA*. No similar bands were detected from the reactor samples, even though one could expect many different sequences from these environmental samples. The presence of many different sequences may have effected the separation, maybe due to interaction between the sequences, having co-migrational effects, in which different sequences tend to migrate together in the gel (Gafan & Spratt 2005).

Reducing the concentration of acrylamide in the DGGE gel from 8 % to 6 % did not give better separation of bands. Therefore, the DGGE analysis of *amoA* sequences was instead focused on the shorter amoA121f-GC/amoA359rC fragment.

### 3.5.2  DGGE analysis of the amoA121f-GC/amoA359rC fragment

After PCR with the primer pair amoA121f-GC/amoA359rC, the PCR product was analyzed by DGGE. A 30-50 % denaturing gradient was found to be wide enough to represent all sequences in the PCR product, while giving optimal separation of bands. Figure 3.24 shows the 30-50 % denaturing gradient gel after separation of *amoA* sequences.
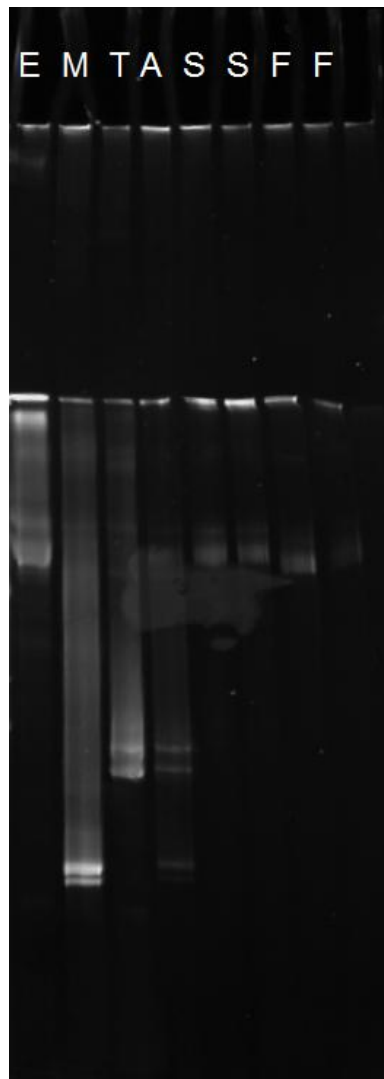
Figure 3.23: Separation of DNA sequences in a 25-60 % denaturing gradient after PCR with the primer pair amoA-1F-GC/amoA-2R. E=*N. europaea amoA*, M=*N. multiformis amoA*, T=*N. tenius amoA*, A=archaeal *amoA*, S=sample from the seawater-based reactor, F=sample from the tapwater-based reactor.

Samples from the same reactor looked very similar when analyzed by DGGE. Although sampled simultaneously, they were from different biofilm carriers, and DNA extraction and PCR had been performed separately. The similarity between replicate samples were confirmed by dissimilarity calculations (see below).

The bands in the gel (Figure 3.24) were generally quite smeared, and it seemed like DNA was distributed over large parts of the denaturing gradi-

| | Peak area (%) | | | |
|------|------|------|------|------|
| Band | 1F | 2F | 1S | 2S |
| B1 | 0.2 | 1.4 | 0.0 | 0.0 |
| B2 | 1.4 | 0.8 | 0.0 | 0.0 |
| B3 | 2.9 | 2.1 | 0.0 | 0.0 |
| B4 | 0.0 | 0.0 | 14.1 | 12.1 |
| B5 | 0.0 | 0.0 | 7.5 | 8.8 |
| B6 | 0.0 | 0.0 | 13.8 | 17.2 |
| B7 | 0.0 | 0.0 | 2.4 | 9.3 |
| B8 | 2.1 | 9.3 | 0.0 | 0.0 |
| B9 | 4.8 | 8.5 | 0.7 | 0.7 |
| B10 | 0.0 | 0.0 | 2.7 | 2.5 |
| B11 | 2.0 | 1.7 | 0.0 | 0.0 |
| B12 | 0.8 | 1.1 | 5.9 | 2.2 |
| B13 | 15.0 | 9.3 | 2.3 | 2.5 |
| B14 | 0.0 | 0.0 | 4.3 | 5.0 |
| B15 | 1.6 | 1.9 | 0.0 | 0.0 |
| B16 | 0.0 | 0.0 | 3.7 | 4.3 |
| B17 | 0.0 | 0.0 | 2.7 | 1.6 |
| B18 | 0.0 | 0.0 | 0.6 | 0.0 |
| B19 | 2.3 | 3.6 | 17.0 | 19.9 |
| B20 | 0.0 | 0.0 | 17.3 | 7.2 |
| B21 | 13.5 | 13.0 | 1.9 | 2.5 |
| B22 | 0.0 | 0.0 | 1.9 | 2.3 |
| B23 | 11.8 | 12.0 | 0.0 | 0.0 |
| B24 | 10.3 | 7.6 | 0.0 | 0.0 |
| B25 | 15.9 | 11.8 | 0.0 | 0.0 |
| B26 | 3.2 | 2.6 | 1.4 | 1.8 |
| B27 | 4.7 | 5.8 | 0.0 | 0.0 |
| B28 | 7.5 | 7.5 | 0.0 | 0.0 |

Figure 3.24: Left: The DGGE gel after separation of DNA fragments from PCR with the primer pair amoA121f-GC/amoA359rC. The numbers indicate the bands that were cut out of the gel and sequenced. Middle: The bands identified in GEL2k. The bands are indicated by black lines. Bands in the same grey area are assumed to be of similar bacterial origin. Right: Normalized peak area for every band in the DGGE gel, given as percentage. These values indicate the percentage of different DNA fragments in the PCR product. F=sample from tapwater-based reactor, S=sample from seawater-based reactor.

ent, giving high background fluorescence. Differences between samples from the tapwater-based and the seawater-based reactors were evident by visual inspection of the DGGE gel. Approximately 19 distinct bands were present in the DGGE gel, 12 of these were from the tapwater-based reactor. None of the most distinct bands seemed to be present in both reactors, suggesting that different nitrifyers dominated in the two reactors. Several other bands were detected by analysis in GEL2k, when less distinct bands were considered. The bands richness turned out to be equal in all samples, although some very weak bands from the seawater-based reactor samples were near the detection limit (B13, B15-B18), and it might have been better if these bands were left out of the analysis. If so, the band richness would have been higher in the samples from the tapwater-based reactor.

The distinct bands from the tapwater-based reactor (Figure 3.24) were distributed over a wider gradient than the bands from the seawater-based reactor. The bands from the tapwater-based reactor were spread between 31 % and 47 %, while the clear bands from the seawater-based reactor occupied denaturing regions from 38 % to 45 %. The smeared region at the top of the gel was not considered to be a band.

**Calculation of dissimilarities and molecular diversity indices**

The normalized distribution of bands in the different lanes (Figure 3.24), was used to calculate the Bray Curtis dissimilarity between the samples (Table 3.5). The dissimilarity between samples from different reactors was around 0.9, while the dissimilarity between samples from similar reactor was below 0.2. These dissimilarities were quite similar to the dissimilarities in the 16S rRNA 30-50 % DGGE gel (Table 3.1).

Table 3.5: Bray Curtis dissimilarities between different samples, based on their band pattern in the DGGE gel. Calculations were based on fractional histogram peak areas for each band. F=sample from tapwater-based reactor, S=sample from seawater-based reactor

|     | 1F    | 2F    | 1S    | 2S  |
| --- | ----- | ----- | ----- | --- |
| 1F  | 0     |       |       |     |
| 2F  | 0.153 | 0     |       |     |
| 1S  | 0.906 | 0.890 | 0     |     |
| 2S  | 0.894 | 0.878 | 0.176 | 0   |

Figure 3.25 shows Pareto-Lorenz curves calculated from the distribution of bands in the different lanes in the DGGE gel. The Pareto-Lorenz curves were quite similar for all samples, indicating a similar degree of evenness of different sequences in the PCR products. Despite the high similarity be-
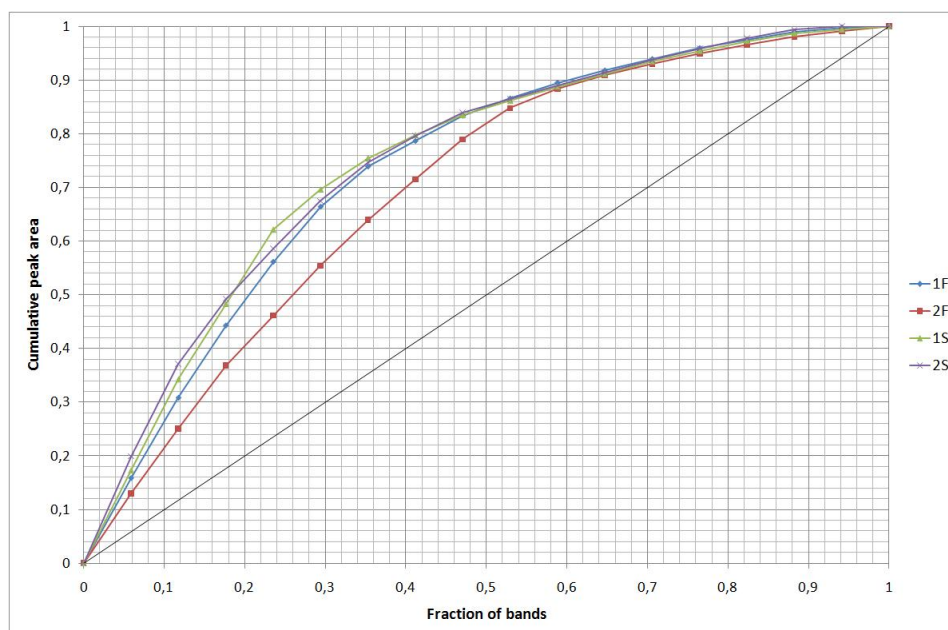
Figure 3.25: Pareto-Lorenz curves showing the cumulative peak area in each lane in the DGGE gel, vs. the cumulative proportion of bands. The black line indicates the scenario where all bands in the lane have equal peak areas. F=replicate samples from the tapwater-based reactor, S=samples from the seawater-based reactor

tween the samples from the tapwater-based reactor (Table 3.5), the Pareto-Lorenz curve for the 2F sample deviated mostly from the others. This was because the most intense bands in the 1F sample (e.g. B25 and B13) were stronger than the corresponding bands in the 2F sample. It was difficult to see this directly from the DGGE gel, but the histogram peaks for these bands, generated in GEL2k, had larger areas in the 1F sample than in the 2F sample. The 1F sample had a slightly lower Pareto-Lorenz curve than the samples from the seawater-based reactor, but the difference was not large.

Various calculated indices of community composition is given in Table 3.6. The seawater-based reactor samples had, as expected, the highest Gini coefficients, indicating lower molecular evenness in the PCR product from these samples. The 1F sample had a Gini coefficient that was more similar to the seawater-based reactor samples than to the 2F sample, as could be seen directly from the Pareto-Lorenz curves.

The range-weighted richness, shown in Table 3.6, was much higher in the samples from the tapwater-based reactor. Even though the band richness was similar in all samples, the DGGE bands from the tapwater-based reactor samples were distributed over a wider denaturing gradient, resulting

77

Table 3.6: Band richness, range-weighted richness (Rr), the Shannon-Weaver index (H'), Pielou's evenness index (J'), and the Gini coefficients calculated from normalized peak areas for the bands in the DGGE gel after separation of amoA121f-GC/amoA359rC fragments.

| Sample | Band richness | Rr | H' | J' | Gini |
|--------|---------------|----|------|------|------|
| 1F | 17 | 46 | 2.46 | 0.87 | 0.47 |
| 2F | 17 | 46 | 2.57 | 0.91 | 0.40 |
| 1S | 17 | 20 | 2.42 | 0.85 | 0.49 |
| 2S | 17 | 20 | 2.41 | 0.85 | 0.50 |

in higher range-weighted richness. This indicated that the genetic diversity was higher in the tapwater-based reactor samples. The Shannon diversity index was also larger for the samples from the tapwater-based reactor; however, the Shannon index for the 1F sample was more similar to the Shannon indices for the samples from the seawater-based reactor than to the 2F sample. The Shannon index will be highest when all bands have equal peak areas, i.e. when there is total evenness. Since the molecular composition of the 2F sample seemed to be most even, as indicated by both the Gini coefficient and Pielou's evenness index, the Shannon index was largest for the 2F sample. All indices indicated the same; larger diversity and larger evenness in the tapwater-based reactor. The occupation of a larger denaturing range and lower dominance of some bands in the samples from the tapwater-based reactor resulted in this.

### 3.5.3 Sequence analysis of the amoA121f-GC/amoA359rC fragments

All sequence chromatograms from Eurofins MWG Operon were checked to evaluate the quality of the sequences. The sequences from bands B1, B2, B3, B9 and B21 were not analyzed further because the chromatograms for these sequences had many double peaks, indicating that more than one sequence was present in these bands. The rest of the sequences were analyzed further, but to avoid ambiguous bases in the dataset, they were shortened to include only regions of high quality. The resulting dataset consisted of sequences with around 180 bases. Most of the sequence positions were highly conserved. Sequences B4, B5, B12 and B28 and sequences B6, B7 and B19 were identical.

The nucleotide sequences were also translated to amino acid sequences by using the ExPASy translate tool. At the amino acid level, the similarity between the sequences was even larger. Sequences B4, B5, B6, B7, B12, B14, B19 and B28 were identical. B8, B20, B23 and B24 were also identical, except that some of the sequences were a few amino acids longer. Table

3.7 shows the nearest BLAST hits for the *amoA* nucleotide sequences and translated nucleotide sequences.

All sequences seemed to be affiliated with $\beta$-AOB, either with the *Nitrosomonas* cluster or with the *Nitrosospira* cluster. From Table 3.7 it is evident that the BLAST results from querying nucleotide and protein sequences were not congruent on a more detailed phylogenetic level than the class $\beta$-proteobacteria. Sequences B4, B5, B12, B14, B28, B6, B7 and B19, which were identical on protein-level, seemed to be affiliated with the *Nitrosospira* cluster on the nucleotide-level, but were more similar to species within the *Nitrosomonas* cluster on protein-level. Sequences B8, B20, B23, B24, B25 and B26 were most similar to *Nitrosomonas* on both nucleotide- and protein-level. These sequences had the highest similarity to database sequences, and it seemed like these sequences could be classified more reliably.

The sequences seemed to be too conserved for reliable phylogenetic classification. The *amoA* gene is known to give less resolution than the 16S rRNA gene (Purkhold et al. 2003), and *amoA* sequences as short as 180 bp might be inadequate. A longer *amoA* fragment have traditionally been used for phylogenetic analysis (Holmes et al. 1995, Rotthauwe et al. 1997, Purkhold et al. 2000, Hornek et al. 2006). However, if the sequences were highly conserved, it is reasonable to think that they would have higher similarity to database sequences. On the nucleotide level, most of the sequences had lower than 90 % sequence similarity to database sequences. Also, the separation of the bands on the DGGE gel indicated that there were differences between the sequences, although co-migration of different sequences creating unexpected band patterns have been reported (Sekiguchi et al. 2001, Nicolaisen & Ramsing 2002, Gafan & Spratt 2005).

To get a better impression of the degree of conservation among *amoA* sequences in GenBank, the DGGE sequences were aligned towards reference sequences. First, ambiguous bases in the dataset were replaced with IUB codes (Cornish-Bowden 1985). Some sequences (B8, B19, B25, B26, B27) were left out because they had many ambiguities. Ambiguous bases turned out to be on the same places in the sequences, usually in third codon position, as expected. These ambiguities were probably caused by background DNA in the DGGE gel. The level of background fluorescence in the DGGE gel (Figure 3.24) was relatively high, and it is probable that many bands were contaminated by small amounts of DNA sequences that were not properly separated. The DGGE sequences and *amoA* sequences from GenBank were manually aligned in MEGA4. Only regions corresponding to the DGGE sequences, approximately 180 bp, were used. There were few *amoA* sequences in the databases to compare the DGGE sequences with. Most studies have used *amoA* primers that amplify a region from around position 340 in the *amoA* gene (Rotthauwe et al. 1997, Purkhold et al. 2000, Hoshino et al. 2001, Purkhold et al. 2003, Ebie et al. 2004, Park & Noguera

79

Table 3.7: The phylogenetic affiliation of sequenced *amoA* bands, on nucleotide and translated nucleotide level. The best BLAST match to a classified organism is given. The peak area is the peak area from the grey level histograms generated in GEL2k (Figure 3.24), given as percentage of total peak area in the lane. The average between the replicate samples (1F and 2F, 1S and 2S) is given. (F=sample from the tapwater-based reactor, S=sample from the seawater-based reactor)

| Band | Nucleotide BLAST | | Translated nucleotide BLAST | | Average peak area (%) | |
| --- | --- | --- | --- | --- | --- | --- |
| | Nearest neighbour | Similarity (%) | Nearest neighbour | Similarity (%) | F | S |
| B4 | Nitrosovibrio tenuis | 83 | Nitrosomonas sp. CNS332 | 94 | 0.0 | 13.1 |
| B5 | Nitrosovibrio tenuis | 83 | Nitrosomonas sp. CNS332 | 94 | 0.0 | 8.1 |
| B12 | Nitrosovibrio tenuis | 83 | Nitrosomonas sp. CNS332 | 94 | 0.0 | 4.6 |
| B14 | Nitrosovibrio tenuis | 83 | Nitrosomonas sp. CNS332 | 94 | 1.0 | 4.1 |
| B28 | Nitrosovibrio tenuis | 83 | Nitrosomonas sp. CNS332 | 94 | 7.5 | 0.0 |
| B6 | Nitrosospira sp. NpAV | 83 | Nitrosomonas sp. CNS332 | 94 | 0.0 | 15.5 |
| B7 | Nitrosospira sp. NpAV | 83 | Nitrosomonas sp. CNS332 | 94 | 0.0 | 5.9 |
| B19 | Nitrosospira sp. NpAV | 83 | Nitrosomonas sp. CNS332 | 94 | 2.9 | 18.4 |
| B8 | Nitrosomonas sp. AL212 | 94 | Nitrosomonas sp. AL212 | 98 | 5.7 | 0.0 |
| B20 | Nitrosomonas sp. AL212 | 94 | Nitrosomonas sp. AL212 | 100 | 0.0 | 12.2 |
| B23 | Nitrosomonas sp. AL212 | 93 | Nitrosomonas sp. AL212 | 100 | 11.9 | 0.0 |
| B24 | Nitrosomonas sp. AL212 | 93 | Nitrosomonas sp. AL212 | 100 | 8.9 | 0.0 |
| B13 | Nitrosolobus multiformis | 84 | Nitrosospira sp. NpAV | 93 | 12.1 | 2.4 |
| B25 | Nitrosomonas sp. JL21 | 88 | Nitrosomonas sp. AL212 | 98 | 13.8 | 0.0 |
| B26 | Nitrosomonas europaea | 97 | Nitrosomonas eutropha | 98 | 2.9 | 1.6 |
| B27 | Nitrosomonas europaea | 91 | Nitrosomonas eutropha | 95 | 5.2 | 0.0 |

2006). Most of the *amoA* database sequences were therefore not from a region corresponding to the amoA121f/amoA359rC fragment.

The alignment revealed high similarity between different *amoA* sequences. Sequences from the *Nitrosomonas* and the *Nitrosospira* clusters were very similar. Three of the *Nitrosomonas* sequences from GenBank, *Nitrosomonas eutropha, Nitrosomonas sp. GH22* and *Nitrosomonas CNS332* were identical. An *amoA* sequence from the $\gamma$-protrobacterial *Nitrosococcus* cluster differed significantly from the $\beta$-proteobacterial *Nitrosomonas* and *Nitrosospira* sequences.
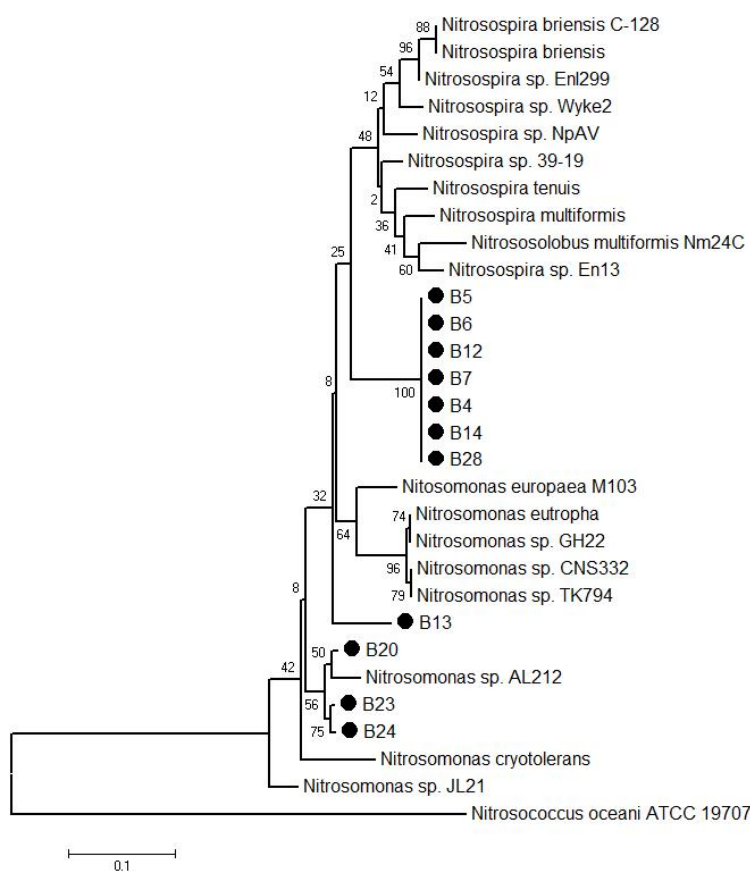


Figure 3.26: A Neighbour-Joining phylogenetic tree with the *amoA* DGGE-sequences and reference sequences from GenBank and from Norton et al. (2002). The percentages of replicate trees in which the associated taxa clustered together in the bootstrap test (100 replicates) are shown next to the branches. The bar indicates the number of base substitutions per site. The evolutionary distances were computed using the Maximum Composite Likelihood method. All positions containing gaps and missing data were eliminated from the dataset (complete deletion option)

81

A Neighbour-Joining phylogenetic tree was constructed from the alignment, where *Nitrosococcus oceani* was used as an out-group (Figure 3.26).

The *Nitrosomonas* and the *Nitrosospira* sequences were distributed in two different clusters, but the distance between these were small. Also, some *Nitrosomonas* sequences clustered away from the other sequences. The DGGE-sequences B4, B5, B6, B7, B12, B14 and B28, which were identical on protein-level, seemed to position between the *Nitrosomonas* and the *Nitrosospira* clusters. B13 positioned close to the *Nitrosomonas* cluster, although it showed higher similarity to *Nitrosospira* sequences in BLAST. Sequences B13, B20, B23 and B24, which were identical on protein-level, clustered together with the *Nitrosomonas sp. AL212* sequence, which was also the closest match in BLAST.

To summarize, the problems with classification based on the *amoA* sequences seemed to arise from several limitations; the sequenced bands had many ambiguous bases due to contamination from background DNA in the DGGE gel. The sequences had to be shortened to avoid regions of bad quality. The remaining sequences were highly conserved, and did not give sufficient resolution for reliable classification. The regions that were taken out of the dataset may have been more variable; it is reasonable that a contamination will have higher influence on the sequence quality in variable regions. In addition, contamination from background DNA may have masked the sequence differences. There were also few corresponding *amoA* sequences in the databases to compare the DGGE sequences with, making classification even more difficult. This may have been the reason for BLAST-similarities under 90 %, despite the high degree of sequence conservation.

## 3.6 Detection of *Archaea*

### 3.6.1 Detection of archaeal 16S rRNA genes

The primers 20Archf and 958Archr were used to amplify a region of the archaeal 16S rRNA gene. After 35 PCR cycles, PCR product could not be detected in the reactor samples, while product was detected from environmental positive control samples known to contain archaea, donated by Anna Synnve Ødegaard Røstad at the Department of Biotechnology, NTNU. Figure 3.27 shows the agarose gel with the PCR product. This result suggest that *Archaea* were less important players in the nitrifying communities in the reactors, or even absent.
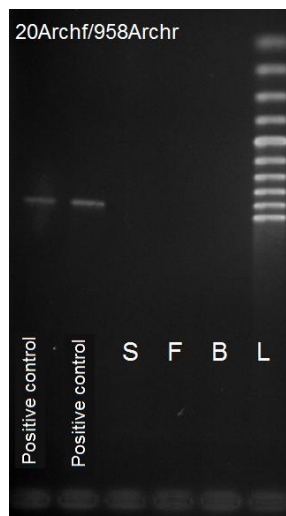
Figure 3.27: PCR products after amplification with the archaeal 16S rRNA primers 20Archf and 958Archr. S=sample from the seawater-based reactor, F=sample from the tapwater-based reactor, L=100 bp ladder.

### 3.6.2 Detection of archaeal *amoA* genes

The archaeal *amoA* gene was also used as a marker gene for the detection of *Archaea*. Figure 3.28 shows the result from temperature gradient PCR with the primers Arch-amoA-for and Arch-amoA-rev-GC. These primers should amplify a 296 bp fragment, but fragments of different lengths were produced. A more distinct band with the expected lenght was amplified from the archaeal *amoA* fosmid. The same band seemed to be amplified from the samples from the seawater-based reactor as well, but not from the *N. europaea amoA* plasmid which was used as a negative control. This result suggest that archaeal ammonia-oxidizers were present in the reactor after all. The PCR product was not analyzed by DGGE and sequenced, so it is difficult to make conclusions about the origin of the amplified sequences. The primers were tested towards *Nitrosospira, Nitrosomonas* and *Nitroso-coccus* sequences in Primer-BLAST, but no primer homology to bacterial *amoA* sequences were found, indicating that the product amplified from the reactor samples originated from archaeal *amoA*.
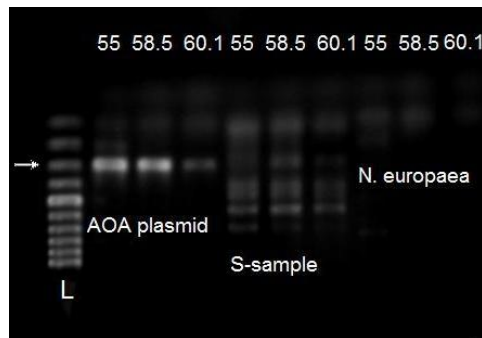
Figure 3.28: PCR products after amplification with the primers Arch-amoA-for and Arch-amoA-rev-GC with different annealing temperatures. The arrow indicates the length of the target sequence.

## 3.7 Fluorescence *in situ* hybridization

Fixated biofilm samples from the seawater-based and the tapwater-based reactors were hybridized with different oligonucleotide probes, and studied by epifluorescence and confocal laser scanning microscopy.

**Epifluorescence microscopy**

Initially, few single cells could be detected by epifluorescence microscopy, because the cells were clustered together (results not included). This made quantification by counting difficult. To resolve this problem, the cells were sonicated prior to hybridization. After sonication, large clusters were still present, but many single cells could be detected. Figure 3.29 shows a sample from the tap-water based reactor, hybridized with the oligonucleotide probes EUBI, EUBII and EUBIII (green) for all bacteria and Nso190 (red) for $\beta$-AOB. The sample was also stained with the nucleic acid stain DAPI (blue).
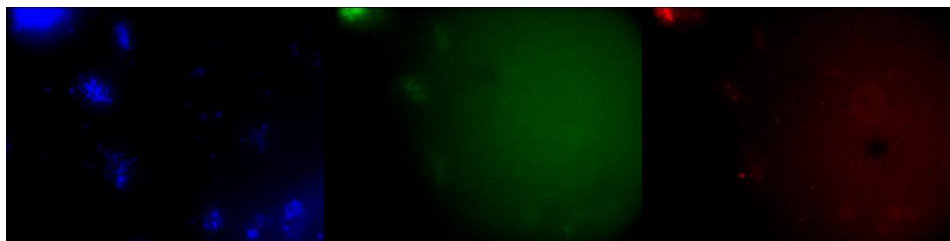


Figure 3.29: Sonicated sample from the tapwater-based reactor, stained with DAPI (blue) and hybridized with the oligonucleotide probes EUB338I-III (green) and Nso190 (red).

When applying a Zeiss Axioplan microscope, the signal from the oligonucleotide probes was very low. When pictures were taken, the exposure time had to be extended, resulting in very high background levels, as evident in Figure 3.29. The microscope lamp was not properly aligned, as seen by the uneven illumination evident in Figure 3.29. Threshold binarization of these pictures was difficult because parts of the pictures were brighter than the cell signals on other parts of the pictures, making quantification difficult. This problem was less evident in the DAPI pictures because the DAPI signal was much stronger.

The same samples were also investigated with a Zeiss Axio Scope microscope. Figure 3.30 shows a sample from the seawater-based reactor, hybridized with the EUB probes for all bacteria, Nso190 for $\beta$-proteobacteria and DAPI.
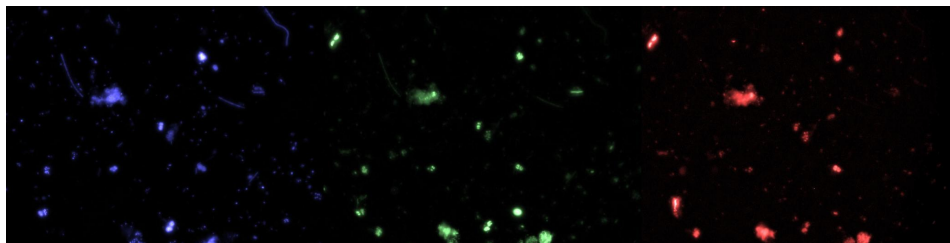


Figure 3.30: Sample from the seawater-based reactor, hybridized with the probes EUBI,II,III (green) and Nso190 (red), and stained with DAPI (blue)

The problem was, however, that the signal intensity from un-hybridized samples was almost as high as the signal from hybridized samples. Figure 3.31 shows a sample without probe or DAPI, viewed with the filters for DAPI, FITC (EUB338 probes) and Cy3 (Nso190 probe).
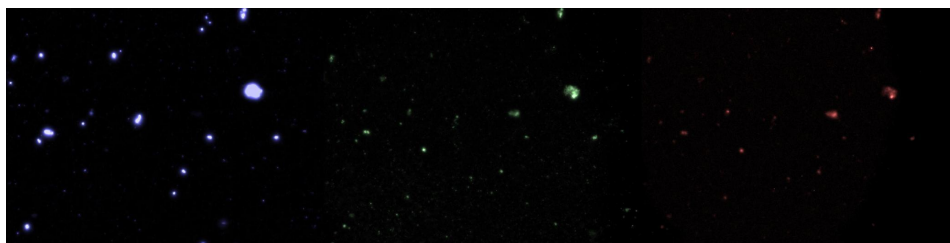


Figure 3.31: Un-hybridized FISH sample from the seawater-based reactor. The sample was viewed in the channels for DAPI (blue), FITC (green) and Cy3 (red).

### 3.7.1 Confocal laser scanning microscopy

**Confocal laser scanning microscopy with Leica TCS SP5**

Confocal laser scanning microscopy was also applied to evaluate FISH samples from the reactors. Problems with low probe-conferred signal above the background noise were still experienced. Figure 3.32 shows an un-hybridized sample viewed with instrument settings, denoted channels, for FITC and Cy3.
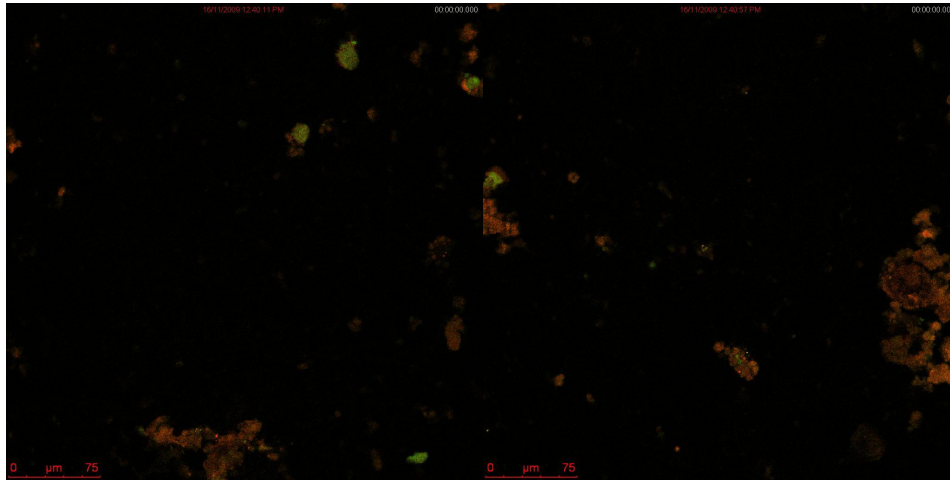


Figure 3.32: Un-hybridized sample excited and viewed in the channels for FITC (green) and Cy3 (red)

To try to solve the background/autofluorescence problem, microscopic adjustments were done on a sample without probes. The laser intensity and gain/offset was adjusted and set to zero signal for the sample without probe. At these adjustments, nearly no signal could be detected from sample with probes. Despite this, changes in the distribution of red and green signal could be detected when an intact biofilm sample was investigated at higher gain. Figure 3.33 shows some of the optical sections in the z-stack through the biofilm, probed with EUB338I,II,III (green) and NIT3 (red) for *Nitrobacter* ssp.
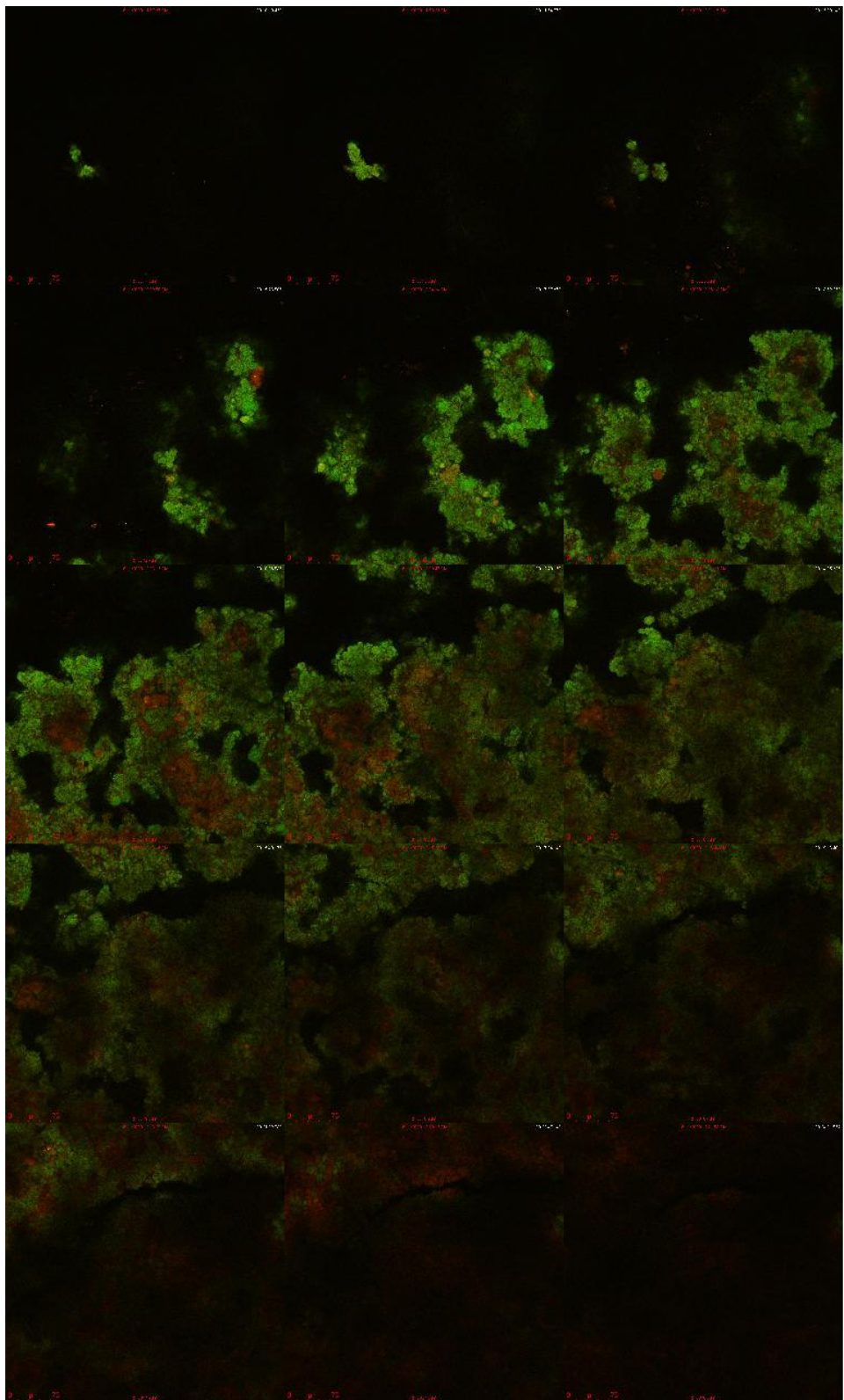
Caption on the following page

Figure 3.33: Sections through an intact biofilm sample from the seawater-based reactor, hybridized with the probes EUBI,II,III (green) and NIT3 (red) for *Nitrobacter*. The biofilm was 140 $\mu$m thick, and 150 pictures were taken through the biofilm. The top of the biofilm is depicted on the top picture to the left, while the bottom of the biofilm is depicted on the bottom picture to the right. This means that there are approximately 10 $\mu$m between each of the pictures shown.

Since the EUB338 probes target (nearly) all bacteria, the NIT3 *Nitrobacter* signal should not exceed the EUB338 signal. However, when the stack pictures in Figure 3.33 were thresholded, and the EUB338 and NIT3 signal quantified as area in pixels, the NIT3 signal exceeded the EUB338 signal in the deeper layers of the biofilm. A high level of red background noise clearly influenced, and made detection if NIT3-targeted cells difficult. However, the distribution of EUB338 signal in the biofilm may indicate that cells in the outer layers of the biofilm were more metabolically active than cells in the deeper levels, due to better access to oxygen and substrates. Metabolic activity is usually correlated with the 16S rRNA levels in cells (Moter & Göbel 2000, Amann & Fuchs 2008).

### Confocal laser scanning microscopy with Zeiss LSM 510 Meta

The samples were also investigated with a Zeiss LSM microscope that had several functions for correcting autofluorescence or background fluorescence problems. The emission from un-probed samples were checked in different parts of the relevant FITC and Cy3 emission spectra, shown in Figure 3.34 and 3.35. If the signal in some parts of the spectra were low, the filters could be adjusted accordingly to detect probe signal in those parts of the spectra. The background emission was unfortunately equally high in all parts of the relevant spectra.

The detector offset and gain was adjusted and set to zero signal on un-probed samples. Possible cross-interference between the FITC and Cy3 channels was investigated by looking at samples probed with one probe, with microscope settings for the fluorochrome that was absent from the sample, at low detector gain for shutting out background fluorescence. Under these conditions, no bleed-through or cross-interference signal could be detected. Figure 3.36 shows a sample from the seawater-based reactor, probed with the EUB338 probes and Nso190, targeting $\beta$-AOB.

Even though Figure 3.36 shows several colonies of what seemed to be EUB338- and Nso190-stained cells, areas with a lot of signal above the background was hard to detect. In several samples, signal above the background could not be detected at all.

In a later experiment, a fixated biofilm sample from a membrane filtration system for filtration of drinking water, donated by Eva Rogne at the
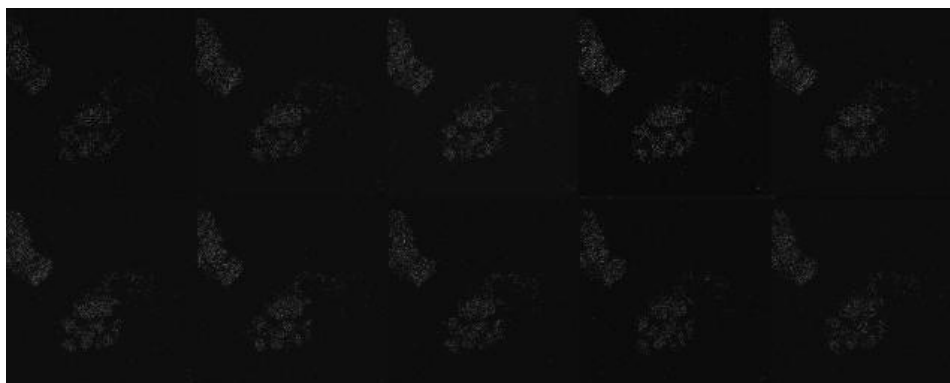
Figure 3.34: Emission from un-hybridized sample in the FITC emission spectrum.
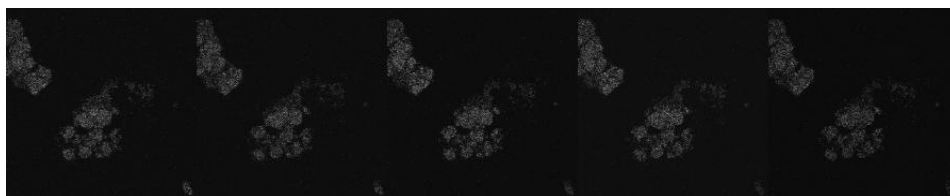


Figure 3.35: Emission from un-hybridized sample in the Cy3 emission spectrum.
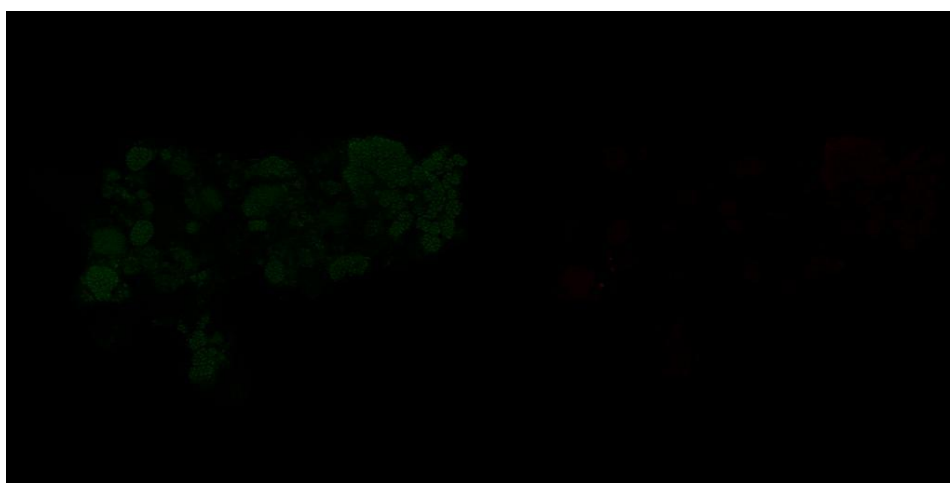


Figure 3.36: Sample from the seawater-based reactor probed with EUB338I,II,II (green) and Nso190 (red) for $\beta$-AOB. The signal from Nso190, measured in area, is approximately 7 %.

Department of Biotechnology, NTNU, was hybridized with the EUB338-FITC probes. Almost no signal above the background fluorescence could be detected. Similar samples from the same membrane filtration system were hybridized by Eva Rogne with the EUB338 probes labelled with Cy5 instead of FITC. These samples were investigated in the same LSM microscope, with approximately the same laser and detector settings. These samples did not seem to give higher signal, but the background fluorescence was lower. These samples could therefore be investigated with a higher detector gain, enabling detection of probe-targeted cells. These samples had been fixated and hybridized according to a protocol modified from Daims et al. (2005). The most important modification of the protocol was the addition of SDS to the washing buffer to avoid precipitation. Vectashield$^\circledR$ mounting media was used instead of Citifluor$^{\text{™}}$ AF1 as antifadent. It is difficult to imagine that these differences could cause such difference in hybridization outcome. However, the use of Cy5 instead of FITC as a fluorescent probe label may have had an effect.

To summarize, some probe-conferred signal could be detected above the background fluorescence, but the signal was very low. The signal intensity and background noise seemed to vary between samples and between experiments. Some hybridized samples could have been used for quantification of probe-targeted cells, but in other samples, the probe-conferred signal seemed to be too low, or the background too high. Methodological and optical limitations were probably the cause of the FISH difficulties.

# Chapter 4

# General discussion and conclusions

## 4.1 Comparison of nitrifying activities in the seawater-based and the tapwater-based reactors

The nitrification process in the seawater-based reactor was more unstable than in the tapwater-based reactor (section 3.1). It was difficult to obtain a stable process with high activity without accumulation of nitrite. In the tapwater-based reactor, stable operation with nitrification activities up to 20 mg N/L were obtained, while the nitrification activity remained below 10 mg N/L during stable operation of the seawater-based reactor.

The ammonium oxidation seemed to have a larger activity potential than the nitrite oxidation in both reactors. It is likely that the oxygen concentration will be the limiting factor in mature biofilms (de Beer et al. 1994, Vogelsang et al. 1997). It has also been reported that nitrite-oxidizers are more sensitive to low oxygen levels than ammonia-oxidizers, because they have higher oxygen half-saturation constants (Tanaka & Dunn 1982, Hanaki et al. 1990). This may be the reason for nitrite accumulation at higher nitrification activities when the competition for oxygen in the biofilm was higher. Hanaki et al. (1990) reported that oxygen limitation in a biofilm reactor resulted in high effluent nitrite concentrations.

The nitrite oxidation was more unstable, and the potential nitrite oxidation activity seemed to be lower in the seawater-based reactor. Similar problems have been reported in wastewater treatment plants treating high salinity wastewater (Nijhof & Bovendeur 1990, Dincer & Kargi 1999, Kim et al. 2000, Yu et al. 2002, Campos et al. 2002, Uygur & Kargi 2004). It has been reported that the nitrite-oxidizing bacteria are more sensitive to high salinity than the ammonia-oxidizing bacteria, even at salinities below 10 ‰ (Vredenbregt et al. 1997, Dincer & Kargi 1999). This may be the reason for problems with nitrite accumulation in wastewater treatment processes at high salinity. However, according to Moussa et al. (2006), these reported effects were probably related to oxygen limitation, since salt reduces the solubility of oxygen gas, and the oxygen transfer rate. Campos et al. (2002) also reported this as a probable mechanism for nitrite accumulation at high salt concentrations. The concentration of dissolved oxygen was not measured in the reactors. Since the air supply was not strictly controlled in the two reactors, better air supply to one of the reactors cannot be ruled out.

## 4.2 The effect of salinity on microbial community composition

The results from the salinity response test (section 3.2), combined with the results from Kristoffersen (2004), suggest that the culture that was adapted to 2/3 seawater tolerated high salinities better. This indicates a difference in the microbial community composition of the reactors. DGGE band patterns

(section 3.3) revealed differences in genetic composition of the two cultures, indicating higher microbial diversity and evenness in the tapwater-based reactor. The microbial diversity in "extreme" environments is often low due to selective stress, and the loss of diversity of nitrifying bacteria related to increasing salinity have previously been shown (Bollmann & Laanbroek 2002, Bernhard et al. 2005, Grommen et al. 2006, Sahan & Muyzer 2008).

Sequence analysis of 16S rRNA DGGE bands also showed a higher species richness of nitrifying bacteria in the tapwater-based reactor compared to the seawater-based reactor. Only *Nitrosomonas*-related AOB sequences were found, seven of these were detected in the tapwater-based reactor, while only four were detected in the seawater-based reactor (section 3.3.2). *Nitrosomonas oligotropha*- and *Nitrosomonas sp. Is343*-affiliated sequences seemed to dominate in the tapwater-based reactor. *N. sp. Is343*-related sequences were not found in the seawater-based reactor, but *N. oligotropha*-like sequences were also the most dominating sequences in the seawater-based reactor, in addition to *Nitrosomonas halophila*, which was only found in small amounts in the tapwater-based reactor. *N. oligotropha* has been recognized as a salt-sensitive lineage within the nitrosomonads (Koops & Pommerening-Röser 2005). The effect of salinity on microbial community composition of ammonia-oxidizing bacteria has been investigated in several studies, and it has repeatedly been demonstrated that *N. oligotropha* was replaced by other AOB at increased salinities (Bollmann & Laanbroek 2002, Chen et al. 2003, Bernhard et al. 2005, Coci et al. 2005, Moussa et al. 2006). In most of these studies, *Nitrosococcus mobilis* and *Nitrosomonas marina* were found to be the dominating AOB at higher salinities. However, Chen et al. (2003) detected *N. oligotropha* in a nitrifying culture adapted to up to 30 g $Cl^-$/L. *N. halophila* is known to be salt tolerant (Koops & Pommerening-Röser 2005), and have been isolated from soda lakes with salt concentrations of up to 360 g/L (Sorokin et al. 2001).

Five different NOB-affiliated DGGE-bands were recognized in the 16S rRNA-based analysis. Four of these were present in the tapwater-based reactor, while only two were present in the seawater-based reactor, indicating higher NOB diversity in the tapwater-based reactor. All NOB-affiliated sequences were related to *Nitrospira moscoviensis*, but the two sequences that were identified from the seawater-based reactor were not closely related. These sequences may belong to other lineages within the *Nitrosopira*. *Nitrospira* is often found to be the dominating nitrite oxidizer in wastewater treatment plants (Juretschko et al. 1998, Daims et al. 2001, Gieseke et al. 2001, Wagner et al. 2002), and is often described as a K-strategist, with low $\mu_{max}$, but well adapted to low substrate concentrations. *Nitrobacter*, on the other hand, is an r-strategist with the ability to grow relatively fast when substrate concentrations are high (Schramm et al. 1999, Wagner et al. 2002, Kim & Kim 2006). The nitrite concentrations in wastewater treatment plants are usually low, giving *Nitrospira* a competitive advantage. In

the tap-water and seawater-based reactors, however, the nitrite concentration often accumulated, and one might expect this to favour the growth of *Nitrobacter*. Chen et al. (2003) and Moussa et al. (2006) investigated the microbial composition in nitrifying reactors with increasing salinity, and could detect a community shift from *Nitrospira* to *Nitrobacter* when the salt concentration was above 10 g/L. Despite of this, *Nitrobacter* was not detected in the seawater-based reactor analyzed in this work.

The main differentiating factor between the seawater-based and the tapwater-based reactors was the salinity. However, the concentration of oxygen in the reactors was not measured, and differences in oxygen supply cannot be ruled out, having a potential effect on the microbial communities. However, Bollmann & Laanbroek (2002) investigated the influence of oxygen concentration and salinity on microbial communities, and found that it was the salinity, and not the oxygen concentration that was the regulating factor for population shifts.

The microbial community was not investigated over time, and the stability of the microbial composition cannot be verified. Graham et al. (2007) demonstrated chaotic instability of abundances of the AOB and NOB guilds over time in chemostats, and postulated that nitrification is particularly unstable due to a strong interdependence between AOB and NOB and low diversity, causing a fragile AOB-NOB mutualism.

## 4.3 Evaluation of the molecular methods

Both the 16S rRNA and the *amoA* based DGGE analyses turned out to be useful for analysis of the microbial community organization, such as diversity and evenness. However, the 16S rRNA based analysis was the most suitable method for classification of nitrifying organisms in the reactors. Analysis based on short *amoA* sequences did not give the necessary resolution for fine-scale classification. *amoA*-based analysis is probably more useful in systems with organic loading and larger microbial diversity, where interfering sequences from heterotrophic organisms may make it difficult to detect nitrifiers by using general 16S rRNA primers. However, *amoA*-based analysis should be based on longer *amoA* sequences and using primers that amplify a longer fragment is recommended. 16S rRNA primers that are more or less specific for groups of nitrifiers are also available (Section 1.5.1), and may be just as useful for investigating complex microbial communities.

FISH has the potential to give information about the distribution of different organisms in microbial communities, free of the biases that can be introduced by PCR (Amann et al. 1995, Hugenholtz 2002). The combination of DGGE and FISH is therefore considered very useful. Methodological and optical limitations were probably the cause of FISH difficulties in this thesis, but the method should be tested further to resolve such problems.

## 4.4 Conclusions

Within the limitations discussed above, it has been shown that:

1. Long-term operation of a nitrifying reactor is possible even with 2/3 seawater, corresponding to a salinity of approximately 23 ‰.

2. The nitrifying culture adapted to high salinity seemed to be more halotolerant than a culture adapted to low salinity

3. DGGE was useful for investigation of the microbial communities in the reactors, but methodological problems with FISH were experienced, and the method should be tested further to resolve those problems.

4. DGGE indicated a lower microbial diversity in the seawater-based reactor compared to the tapwater-based reactor.

5. Different nitrifying species seemed to dominate in the tapwater-based and the seawater-based reactors. Ammonia-oxidizers related to *Nitrosomonas oligotropha* seemed to dominate in the tapwater-based reactor, while ammonia-oxidizers related to *Nitrosomonas oligotropha* and *Nitrosomonas halophila* seemed to dominate in the seawater-based reactor. *Nitrospira*-related nitrite-oxidizers were detected in both reactors.

## 4.5 Future perspectives

The biofilm cultures from this work are available for further research and operation of bench-scale reactors. Reactor operation with 100 % seawater may be more relevant for simulation of aquaculture wastewater treatment plants, but stable operation may then be more difficult. Chen et al. (2003) and Moussa et al. (2006) demonstrated that population shifts in nitrifying cultures exposed to increasing salinity occurred around 10 g $Cl^-$/L, indicating that 2/3 seawater is sufficient for selection of salt-tolerant organisms. Since the concentration of dissolved oxygen is an important factor for nitrification, it can be advantageous to measure the DO in future reactors.

It would be interesting to investigate the microbial communities further by using 16S rRNA primers specific for nitrifiers. Ammonia-oxidizing bacteria have been investigated more than nitrite-oxidizing bacteria, and it would also be interesting to analyze the nitrite-oxidizing communities further by using the *nrxA* gene as a marker gene (Poly et al. 2008). The presence or absence of ammonia-oxidizing *Archaea* could not be established in this thesis, and further research is needed to evaluate their role in the nitrifying reactors. The important role of ammonia-oxidizing *Archaea* have been demonstrated in soil and in the sea (Leininger et al. 2006, Wuchter et al.

2006), but little research have been conducted to evaluate the role of nitrifying *Archaea* in engineered systems. More effort should also be invested into FISH, and the stability of the nitrifying communities during long-term operation should be evaluated.

# Bibliography

Alzerreca, J., Norton, J. & Klotz, M. (1999), 'The amo operon in marine, ammonia-oxidizing gamma-proteobacteria', *FEMS microbiology letters* **180**(1), 21.

Amann, R. & Fuchs, B. (2008), 'Single-cell identification in microbial communities by improved fluorescence in situ hybridization techniques', *Nature Reviews Microbiology* **6**(5), 339.

Amann, R., Krumholz, L. & Stahl, D. (1990), 'Fluorescent-oligonucleotide probing of whole cells for determinative, phylogenetic, and environmental studies in microbiology.', *Journal of Bacteriology* **172**(2), 762.

Amann, R., Ludwig, W. & Schleifer, K. (1995), 'Phylogenetic identification and in situ detection of individual microbial cells without cultivation', *Microbiology and Molecular Biology Reviews* **59**(1), 143.

AnoxKaldnes (n.d), 'AnoxKaldnes™ MBBR ', online, available from: http://www.veoliawaterst.com/mbbr/en/ (downloaded 04-feb 2010).

Barer, M., Gribbon, L., Harwood, C. & Nwoguh, C. (1993), 'The viable but non-culturable hypothesis and medical bacteriology', *Reviews in Medical Microbiology* **4**(4), 183.

Benson, D., Karsch-Mizrachi, I., Lipman, D., Ostell, J. & Wheeler, D. (2008), 'GenBank', *Nucleic Acids Research* **36**(Database issue), D25.

Bergmann, D. & Hooper, A. (1994), 'Sequence of the gene, amoB, for the 43-kDa polypeptide of ammonia monoxygenase of Nitrosomonas europaea', *Biochemical and biophysical research communications* **204**(2), 759.

Bernhard, A., Donn, T., Giblin, A. & Stahl, D. (2005), 'Loss of diversity of ammonia-oxidizing bacteria correlates with increasing salinity in an estuary system', *Environmental Microbiology* **7**(9), 1289.

Bernhard, A., Landry, Z., Blevins, A., de la Torre, J., Giblin, A. & Stahl, D. (2010), 'Abundance of Ammonia-Oxidizing Archaea and Bacteria along an Estuarine Salinity Gradient in Relationship to Potential Nitrification Rates', *Applied and Environmental Microbiology* **76**(4), 1285.

Bock, E. & Wagner, M. (2006), Oxidation of inorganic nitrogen compounds as an energy source, *in* M. Dworkin, S. Falkow, R. E., K. Schleifer & S. E., eds, 'The prokaryotes', Vol. 2, Springer-Verlag, p. 457.

Bollmann, A. & Laanbroek, H. (2002), 'Influence of oxygen partial pressure and salinity on the community composition of ammonia-oxidizing bacteria in the Schelde estuary', *Aquatic Microbial Ecology* **28**(3), 239.

Bray, J. & Curtis, J. (1957), 'An ordination of the upland forest communities of southern Wisconsin', *Ecological Monographs* **27**(4), 325.

Calvó, L. & Garcia-Gil, L. (2004), 'Use of amoB as a new molecular marker for ammonia-oxidizing bacteria', *Journal of microbiological methods* **57**(1), 69.

Campos, J., Mosquera-Corral, A., Sánchez, M., Méndez, R. & Lema, J. (2002), 'Nitrification in saline wastewater with high ammonia concentration in an activated sludge unit', *Water Research* **36**(10), 2555.

Chen, G., Wong, M., Okabe, S. & Watanabe, Y. (2003), 'Dynamic response of nitrifying activated sludge batch culture to increased chloride concentration', *Water research* **37**(13), 3125.

Coci, M., Riechmann, D., Bodelier, P., Stefani, S., Zwart, G. & Laanbroek, H. (2005), 'Effect of salinity on temporal and spatial dynamics of ammonia-oxidising bacteria from intertidal freshwater sediment', *FEMS microbiology ecology* **53**(3), 359.

Colaço, A. B. (2009), Biological water treatment for removal of ammonia from process water in a $CO_2$ capture plant, Master's thesis, Technical University of Lisbon and Norwegian University of Science and Technology.

Cole, J., Chai, B., Marsh, T., Farris, R., Wang, Q., Kulam, S., Chandra, S., McGarrell, D., Schmidt, T., Garrity, G. et al. (2003), 'The Ribosomal Database Project (RDP-II): previewing a new autoaligner that allows regular updates and the new prokaryotic taxonomy', *Nucleic Acids Research* **31**(1), 442.

Collins, T. (2007), 'ImageJ for microscopy', *Biotechniques* **43**(1 suppl), 25.

Coolen, M., Abbas, B., van Bleijswijk, J., Hopmans, E., Kuypers, M., Wakeham, S. & Damsté, J. (2006), 'Putative ammonia-oxidizing Crenarchaeota in suboxic waters of the Black Sea: a basin-wide ecological study using 16S ribosomal and functional genes and membrane lipids', *Environmental Microbiology* **9**(4), 1001.

Cornish-Bowden, A. (1985), 'Nomenclature for incompletely specified bases in nucleic acid sequences: recommendations 1984', *Nucleic Acids Research* **13**(9), 3021.

Daims, H., Brühl, A., Amann, R., Schleifer, K. H. & Wagner, M. (1999), 'The domain-specific probe EUB 338 is insufficient for the detection of all bacteria: Development and evaluation of a more comprehensive probe set', *Systematic and applied microbiology* **22**(3), 434.

Daims, H., Nielsen, J. L., Nielsen, P. H., Schleifer, K. H. & Wagner, M. (2001), 'In situ characterization of Nitrospira-like nitrite-oxidizing bacteria active in wastewater treatment plants', *Applied and Environmental Microbiology* **67**(11), 5273.

Daims, H., Stoecker, K. & Wagner, M. (2005), Fluorescence in situ hybridization for the detection of prokaryotes, *in* A. Osborn & C. Smith, eds, 'Molecular microbial ecology', BIOS Scientific Publ, p. 213.

de Beer, D., Stoodley, P., Roe, F. & Lewandowski, Z. (1994), 'Effects of biofilm structures on oxygen distribution and mass transport', *Biotechnology and bioengineering* **43**(11), 1131.

DeLong, E., Wickham, G. & Pace, N. (1989), 'Phylogenetic stains: ribosomal RNA-based probes for the identification of single cells', *Science* **243**(4896), 1360.

DeSantis, T., Hugenholtz, P., Larsen, N., Rojas, M., Brodie, E., Keller, K., Huber, T., Dalevi, D., Hu, P. & Andersen, G. (2006), 'Greengenes, a chimera-checked 16S rRNA gene database and workbench compatible with ARB', *Applied and Environmental Microbiology* **72**(7), 5069.

Dincer, A. & Kargi, F. (1999), 'Salt inhibition of nitrification and denitrification in saline wastewater', *Environmental Technology* **20**(11), 1147.

*DNeasy® Blood and Tissue Handbook* (2006).

Ebie, Y., Noda, N., Miura, H., Matsumura, M., Tsuneda, S., Hirata, A. & Inamori, Y. (2004), 'Comparative analysis of genetic diversity and expression of amoA in wastewater treatment processes', *Applied microbiology and biotechnology* **64**(5), 740.

Ehrich, S., Behrens, D., Lebedeva, E., Ludwig, W. & Bock, E. (1995), 'A new obligately chemolithoautotrophic, nitrite-oxidizing bacterium, Nitrospira moscoviensis sp. nov. and its phylogenetic relationship', *Archives of Microbiology* **164**(1), 16.

Felske, A. & Osborn, A. (2005), DNA fingerprinting of microbial communities, *in* A. Osborn & C. Smith, eds, 'Molecular microbial ecology', BIOS Scientific Publ, p. 25.

Fiencke, C., Spieck, E. & Bock, E. (2005), Nitrifying Bacteria, *in* D. Werner & W. Newton, eds, 'Nitrogen Fixation in Agriculture, Forestry, Ecology, and the Environment', Vol. 4, Springer Netherlands, p. 255.

Francis, C., Beman, J. & Kuypers, M. (2007), 'New processes and players in the nitrogen cycle: the microbial ecology of anaerobic and archaeal ammonia oxidation', *The ISME Journal* **1**(1), 19.

Francis, C., Roberts, K., Beman, J., Santoro, A. & Oakley, B. (2005), 'Ubiquity and diversity of ammonia-oxidizing archaea in water columns and sediments of the ocean', *Proceedings of the National Academy of Sciences* **102**(41), 14683.

Freitag, T., Chang, L., Clegg, C. & Prosser, J. (2005), 'Influence of inorganic nitrogen management regime on the diversity of nitrite-oxidizing bacteria in agricultural grassland soils', *Applied and Environmental Microbiology* **71**(12), 8323.

Gafan, G. & Spratt, D. (2005), 'Denaturing gradient gel electrophoresis gel expansion (DGGEGE)–an attempt to resolve the limitations of co-migration in the DGGE of complex polymicrobial communities', *FEMS microbiology letters* **253**(2), 303.

Gasteiger, E., Gattiker, A., Hoogland, C., Ivanyi, I., Appel, R. & Bairoch, A. (2003), 'ExPASy: the proteomics server for in-depth protein knowledge and analysis', *Nucleic Acids Research* **31**(13), 3784.

Gieseke, A., Purkhold, U., Wagner, M., Amann, R. & Schramm, A. (2001), 'Community structure and activity dynamics of nitrifying bacteria in a phosphate-removing biofilm', *Applied and environmental microbiology* **67**(3), 1351.

Giovannoni, S., DeLong, E., Olsen, G. & Pace, N. (1988), 'Phylogenetic group-specific oligodeoxynucleotide probes for identification of single microbial cells.', *Journal of Bacteriology* **170**(2), 720.

Graham, D., Knapp, C., Van Vleck, E., Bloor, K., Lane, T. & Graham, C. (2007), 'Experimental demonstration of chaotic instability in biological nitrification', *The ISME Journal* **1**(5), 385.

Granum, E. & Myklestad, S. (2002), 'A photobioreactor with pH control: demonstration by growth of the marine diatom Skeletonema costatum', *Journal of Plankton Research* **24**(6), 557.

Grommen, R., Dauw, L. & Verstraete, W. (2006), 'Elevated salinity selects for a less diverse ammonia-oxidizing population in aquarium biofilters', *FEMS microbiology ecology* **52**(1), 1.

Hanaki, K., Wantawin, C. & Ohgaki, S. (1990), 'Nitrification at low levels of dissolved oxygen with and without organic loading in a suspended-growth reactor', *Water Research* **24**(3), 297.

Haseborg, E., Zamora, T., Fröhlich, J. & Frimmel, F. (2009), 'Nitrifying microorganisms in fixed-bed biofilm reactors fed with different nitrite and ammonia concentrations', *Bioresource Technology* **101**(6), 1701.

Head, I., Hiorns, W., Embley, T., McCarthy, A. & Saunders, J. (1993), 'The phylogeny of autotrophic ammonia-oxidizing bacteria as determined by analysis of 16S ribosomal RNA gene sequences', *Microbiology* **139**(6), 1147.

Hem, L., Rusten, B. & Ødegaard, H. (1994), 'Nitrification in a moving bed biofilm reactor', *Water Research* **28**(6), 1425.

Henze, M., Harremoës, P., Jansen, J. & Arvin, E. (n.d.), *Wastewater Treatment*, 2 edn, Springer-Verlag.

Hollocher, T., Tate, M. & Nicholas, D. (1981), 'Oxidation of ammonia by Nitrosomonas europaea. Definite 18O-tracer evidence that hydroxylamine formation involves a monooxygenase.', *Journal of Biological Chemistry* **256**(21), 10834.

Holmes, A., Costello, A., Lidstrom, M. & Murrell, J. (1995), 'Evidence that participate methane monooxygenase and ammonia monooxygenase may be evolutionarily related', *FEMS Microbiol Lett* **132**, 203.

Holmes, S. (2003), 'Bootstrapping phylogenetic trees: Theory and methods', *Statistical Science* **18**(2), 241.

Hornek, R., Pommerening-Röser, A., Koops, H., Farnleitner, A., Kreuzinger, N., Kirschner, A. & Mach, R. (2006), 'Primers containing universal bases reduce multiple amoA gene specific DGGE band patterns when analysing the diversity of beta-ammonia oxidizers in the environment', *Journal of microbiological methods* **66**(1), 147.

Hoshino, T., Noda, N., Tsuneda, S., Hirata, A. & Inamori, Y. (2001), 'Direct detection by in situ PCR of the amoA gene in biofilm resulting from a nitrogen removal process', *Applied and environmental microbiology* **67**(11), 5261.

Hugenholtz, P. (2002), 'Exploring prokaryotic diversity in the genomic era', *Genome Biol* **3**(2), 1.

Junier, P., Kim, O., Junier, T., Ahn, T., Imhoff, J. & Witzel, K. (2009), 'Community analysis of betaproteobacterial ammonia-oxidizing bacteria using the amoCAB operon', *Applied Microbiology and Biotechnology* **83**(1), 175.

Junier, P., Kim, O., Molina, V., Limburg, P., Junier, T., Imhoff, J. & Witzel, K. (2008), 'Comparative in silico analysis of PCR primers suited for diagnostics and cloning of ammonia monooxygenase genes from ammonia-oxidizing bacteria', *FEMS microbiology ecology* **64**(1), 141.

Juretschko, S., Timmermann, G., Schmid, M., Schleifer, K., Pommerening-Roser, A., Koops, H. & Wagner, M. (1998), 'Combined molecular and conventional analyses of nitrifying bacterium diversity in activated sludge: Nitrosococcus mobilis and Nitrospira-like bacteria as dominant populations', *Applied and environmental microbiology* **64**(8), 3042.

Kim, D. & Kim, S. (2006), 'Effect of nitrite concentration on the distribution and competition of nitrite-oxidizing bacteria in nitratation reactor systems and their kinetic characteristics', *Water research* **40**(5), 887.

Kim, S., Kong, I., Lee, B., Kang, L., Lee, M. & Suh, K. (2000), 'Removal of ammonium-N from a recirculation aquacultural system using an immobilized nitrifier', *Aquacultural Engineering* **21**(3), 139.

Klotz, M., Alzerreca, J. & Norton, J. (1997), 'A gene encoding a membrane protein exists upstream of the amoA/amoB genes in ammonia oxidizing bacteria: a third member of the amo operon?', *FEMS microbiology letters* **150**(1), 65.

Klotz, M. & Norton, J. (1995), 'Sequence of an ammonia monooxygenase subunit A-encoding gene from Nitrosospira sp. NpAV', *Gene* **163**(1), 159.

Könneke, M., Bernhard, A., José, R., Walker, C., Waterbury, J. & Stahl, D. (2005), 'Isolation of an autotrophic ammonia-oxidizing marine archaeon', *Nature* **437**(7058), 543.

Koops, H. & Pommerening-Röser, A. (2005), The Lithoautotrophic Ammonia-Oxidizing Bacteria, 2 edn, Vol. 2, Springer US, p. 141.

Kowalchuk, G., Stephen, J., De Boer, W., Prosser, J., Embley, T. & Woldendorp, J. (1997), 'Analysis of ammonia-oxidizing bacteria of the beta subdivision of the class Proteobacteria in coastal sand dunes by denaturing gradient gel electrophoresis and sequencing of PCR-amplified 16S ribosomal DNA fragments', *Applied and Environmental Microbiology* **63**(4), 1489.

Kristoffersen, M. (2004), Nitrifikasjon for resirkulerte oppdrettsanlegg; salinitetsadaptering, Master's thesis, Norwegian University of Science and Technology.

Leininger, S., Urich, T., Schloter, M., Schwark, L., Qi, J., Nicol, G., Prosser, J., Schuster, S. & Schleper, C. (2006), 'Archaea predominate among ammonia-oxidizing prokaryotes in soils', *Nature* **442**(7104), 806.

Loy, A., Horn, M. & Wagner, M. (2003), 'probeBase: an online resource for rRNA-targeted oligonucleotide probes', *Nucleic acids research* **31**(1), 514.

Loy, A., Maixner, F., Wagner, M. & Horn, M. (2007), 'probeBase–an online resource for rRNA-targeted oligonucleotide probes: new features 2007', *Nucleic Acids Research* **35**(Database issue), D800.

MacDonald, R. & Spokes, J. (1980), 'A selective and diagnostic medium for ammonia oxidising bacteria', *FEMS Microbiol. Lett* **8**, 143.

Madigan, M. & Martinko, J. (2006), *Brock Biology of Microorganisms*, 11 edn, Pearson Education.

Manahan, S. (2005), *Environmental chemistry*, 8 edn, CRC Press.

Marzorati, M., Wittebolle, L., Boon, N., Daffonchio, D. & Verstraete, W. (2008), 'How to get more out of molecular fingerprints: practical tools for microbial ecology', *Environmental Microbiology* **10**(6), 1571.

Massana, R., Murray, A., Preston, C. & DeLong, E. (1997), 'Vertical distribution and phylogenetic characterization of marine planktonic Archaea in the Santa Barbara Channel', *Applied and Environmental Microbiology* **63**(1), 50.

McCaig, A., Embley, T. & Prosser, J. (1994), 'Molecular analysis of enrichment cultures of marine ammonia oxidisers', *FEMS microbiology letters* **120**(3), 363.

McDonald, I. & Murrell, J. (2006), 'The particulate methane monooxygenase gene pmoA and its use as a functional gene probe for methanotrophs', *FEMS microbiology letters* **156**(2), 205.

McTavish, H., Fuchs, J. & Hooper, A. (1993), 'Sequence of the gene coding for ammonia monooxygenase in Nitrosomonas europaea', *Journal of bacteriology* **175**(8), 2436.

Mobarry, B. K., Wagner, M., Urbain, V., Rittmann, B. E. & Stahl, D. A. (1996), 'Phylogenetic probes for analyzing abundance and spatial organization of nitrifying bacteria.', *Applied and Environmental Microbiology* **62**(6), 2156.

Moin, N., Nelson, K., Bush, A. & Bernhard, A. (2009), 'Distribution and Diversity of Archaeal and Bacterial Ammonia Oxidizers in Salt Marsh Sediments', *Applied and environmental microbiology* **75**(23), 7461.

Moter, A. & Göbel, U. (2000), 'Fluorescence in situ hybridization (FISH) for direct visualization of microorganisms', *Journal of Microbiological Methods* **41**(2), 85.

Moussa, M., Sumanasekera, D., Ibrahim, S., Lubberding, H., Hooijmans, C., Gijzen, H. & Van Loosdrecht, M. (2006), 'Long term effects of salt on activity, population structure and floc characteristics in enriched bacterial cultures of nitrifiers', *Water Research* **40**(7), 1377.

Muyzer, G., De Waal, E. & Uitterlinden, A. (1993), 'Profiling of complex microbial populations by denaturing gradient gel electrophoresis analysis of polymerase chain reaction-amplified genes coding for 16S rRNA', *Applied and Environmental Microbiology* **59**(3), 695.

Nicol, G., Leininger, S., Schleper, C. & Prosser, J. (2008), 'The influence of soil pH on the diversity, abundance and transcriptional activity of ammonia oxidizing archaea and bacteria', *Environmental microbiology* **10**(11), 2966.

Nicolaisen, M. & Ramsing, N. (2002), 'Denaturing gradient gel electrophoresis (DGGE) approaches to study the diversity of ammonia-oxidizing bacteria', *Journal of microbiological methods* **50**(2), 189.

Nijhof, M. & Bovendeur, J. (1990), 'Fixed film nitrification characteristics in sea-water recirculation fish culture systems', *Aquaculture* **87**(2), 133.

Norevik, E. (2004), Removal of ammoniuim from "produced water" from offshore operations, Master's thesis, Norwegian University of Science and Technology.

Norland, S. (2004), 'GEL2k gel analysis software. University of Bergen, Norway'.

Norton, J., Alzerreca, J., Suwa, Y. & Klotz, M. (2002), 'Diversity of ammonia monooxygenase operon in autotrophic ammonia-oxidizing bacteria', *Archives of microbiology* **177**(2), 139.

Norton, J., Low, J. & Klotz, M. (1996), 'The gene encoding ammonia monooxygenase subunit A exists in three nearly identical copies in Nitrosospira sp. NpAV', *FEMS microbiology letters* **139**(2), 181.

Østgaard, K., Lee, N. & Welander, T. (1994), Nitrification at low temperatures, *in* 'Institution of Chemical Engineers Symposium Series.', p. 134.

Øvreås, L., Forney, L., Daae, F. & Torsvik, V. (1997), 'Distribution of bacterioplankton in meromictic Lake Sælenvannet, as determined by denaturing gradient gel electrophoresis of PCR-amplified gene fragments coding for 16S rRNA', *Applied and Environmental Microbiology* **63**(9), 3367.

Park, H. & Noguera, D. (2006), 'Characterization of two ammonia-oxidizing bacteria isolated from reactors operated with low dissolved oxygen concentrations', *Journal of applied microbiology* **102**(5), 1401.

Park, H., Wells, G., Bae, H., Criddle, C. & Francis, C. (2006), 'Occurrence of ammonia-oxidizing archaea in wastewater treatment plant bioreactors', *Applied and environmental microbiology* **72**(8), 5643.

Park, S., Park, B. & Rhee, S. (2008), 'Comparative analysis of archaeal 16S rRNA and amoA genes to estimate the abundance and diversity of ammonia-oxidizing archaea in marine sediments', *Extremophiles* **12**(4), 605.

Pedersen, E. B. (2007), Molecular genetics of microbial communities in different nitrifying biofilms, Master's thesis, Norwegian University of Science and Technology.

Peet, R. (1975), 'Relative diversity indices', *Ecology* **56**(2), 496.

Plant Research International (2010), 'Plant research international'. Date retrieved: April 4, 2010.
**URL:** *http://www.pri.wur.nl/UK/research/research+themes/Interaction+ between+plants+pests+and+diseases/Characterization+identification+ and+detection/*

Poly, F., Wertz, S., Brothier, E. & Degrange, V. (2008), 'First exploration of Nitrobacter diversity in soils by a PCR cloning-sequencing approach targeting functional gene nxrA', *FEMS microbiology ecology* **63**(1), 132.

Prosser, J. & Nicol, G. (2008), 'Relative contributions of archaea and bacteria to aerobic ammonia oxidation in the environment', *Environmental Microbiology* **10**(11), 2931.

Purkhold, U., Pommerening-Roser, A., Juretschko, S., Schmid, M., Koops, H. & Wagner, M. (2000), 'Phylogeny of all recognized species of ammonia oxidizers based on comparative 16S rRNA and amoA sequence analysis: implications for molecular diversity surveys', *Applied and Environmental Microbiology* **66**(12), 5368.

Purkhold, U., Wagner, M., Timmermann, G., Pommerening-Roser, A. & Koops, H. (2003), '16S rRNA and amoA-based phylogeny of 12 novel betaproteobacterial ammonia-oxidizing isolates: extension of the dataset and proposal of a new lineage within the nitrosomonads', *International journal of systematic and evolutionary microbiology* **53**(5), 1485.

*QIAquick Spin Handbook* (2008).

Röling, W. & Head, I. (2005), Prokaryotic systematics: PCR and sequence analysis of amplified 16S rRNA genes, *in* A. Osborn & C. Smith, eds, 'Molecular microbial ecology', BIOS Scientific Publ, p. 25.

Rotthauwe, J., Witzel, K. & Liesack, W. (1997), 'The ammonia monooxygenase structural gene amoA as a functional marker: molecular fine-scale analysis of natural ammonia-oxidizing populations', *Applied and Environmental Microbiology* **63**(12), 4704.

Sahan, E. & Muyzer, G. (2008), 'Diversity and spatio-temporal distribution of ammonia-oxidizing Archaea and Bacteria in sediments of the Westerschelde estuary', *FEMS microbiology ecology* **64**(2), 175.

Sayavedra-Soto, L., Hommes, N., Alzerreca, J., Arp, D., Norton, J. & Klotz, M. (1998), 'Transcription of the amoC, amoA and amoB genes in Nitrosomonas europaea and Nitrosospira sp. NpAV', *FEMS microbiology letters* **167**(1), 81.

Schramm, A., De Beer, D., Van Den Heuvel, J., Ottengraf, S. & Amann, R. (1999), 'Microscale distribution of populations and activities of Nitrosospira and Nitrospira spp. along a macroscale gradient in a nitrifying bioreactor: quantification by in situ hybridization and the use of microsensors', *Applied and environmental microbiology* **65**(8), 3690.

Sekiguchi, H., Tomioka, N., Nakahara, T. & Uchiyama, H. (2001), 'A single band does not always represent single bacterial strains in denaturing gradient gel electrophoresis analysis', *Biotechnology Letters* **23**(15), 1205.

Selvik, J., Tjomsland, T. & Eggestad, H. (2007), Teoretiske tilførselsberegninger av nitrogen og fosfor til norske kystområder i 2006, Technical report, Norsk institutt for vannforskning *for* Statens forurensningstiilsyn.

Sinigalliano, C., Kuhn, D. & Jones, R. (1995), 'Amplification of the amoA gene from diverse species of ammonium-oxidizing bacteria and from an indigenous bacterial population from seawater', *Applied and environmental microbiology* **61**(7), 2702.

Sorokin, D., Tourova, T., Schmid, M., Wagner, M., Koops, H., Kuenen, G. & Jetten, M. (2001), 'Isolation and properties of obligately chemolithoautotrophic and extremely alkali-tolerant ammonia-oxidizing bacteria from Mongolian soda lakes', *Archives of microbiology* **176**(3), 170.

Spieck, E. & Bock, E. (2005), The Lithoautotrophic Ammonia-Oxidizing Bacteria, 2 edn, Vol. 2, Springer US, p. 141.

Stackebrandt, E. & Goebel, B. (1994), 'Taxonomic note: a place for DNA-DNA reassociation and 16S rRNA sequence analysis in the present species definition in bacteriology', *International Journal of Systematic and Evolutionary Microbiology* **44**(4), 846.

Stahl, D. (1997), Molecular Approaches for the Measurement of Density, Diversity and Phylogeny, American Society for Microbiology, p. 102.

Staley, J. (2006), 'The bacterial species dilemma and the genomic–phylogenetic species concept', *Philosophical Transactions of the Royal Society B: Biological Sciences* **361**(1475), 1899.

Staley, J. & Konopka, A. (1985), 'Measurement of in situ activities of non-photosynthetic microorganisms in aquatic and terrestrial habitats', *Annual Reviews in Microbiology* **39**(1), 321.

Stephen, J., McCaig, A., Smith, Z., Prosser, J. & Embley, T. (1996), 'Molecular diversity of soil and marine 16S rRNA gene sequences related to beta-subgroup ammonia-oxidizing bacteria', *Applied and Environmental Microbiology* **62**(11), 4147.

Suzuki, I., Dular, U. & Kwok, S. (1974), 'Ammonia or ammonium ion as substrate for oxidation by Nitrosomonas europaea cells and extracts', *Journal of Bacteriology* **120**(1), 556.

Tamura, K., Dudley, J., Nei, M. & Kumar, S. (2007), 'MEGA4: molecular evolutionary genetics analysis (MEGA) software version 4.0', *Molecular biology and evolution* **24**(8), 1596.

Tanaka, H. & Dunn, I. (1982), 'Kinetics of Biofilm Nitrification', *Biotechnology and Bioengineering* **24**(3), 669.

*Taq PCR Handbook* (2008).

Teske, A., Alm, E., Regan, J., Toze, S., Rittmann, B. & Stahl, D. (1994), 'Evolutionary relationships among ammonia-and nitrite-oxidizing bacteria.', *Journal of bacteriology* **176**(21), 6623.

The Climate and Pollution Agency (2009), 'Foreslår strengere regelverk for fiskeoppdrett'. Date of publication: April 9, 2009. Date retrieved: April 22, 2010.
**URL:** *http://www.klif.no/no/Aktuelt/Nyheter/2009/November-2009/Foreslar -strengere-regelverk-for-fiskeoppdrett/*

Tourna, M., Freitag, T., Nicol, G. & Prosser, J. (2008), 'Growth, activity and temperature responses of ammonia-oxidizing archaea and bacteria in soil microcosms', *Environmental Microbiology* **10**(5), 1357.

Treusch, A., Leininger, S., Kletzin, A., Schuster, S., Klenk, H. & Schleper, C. (2005), 'Novel genes for nitrite reductase and Amo-related proteins indicate a role of uncultivated mesophilic crenarchaeota in nitrogen cycling', *Environmental Microbiology* **7**(12), 1985.

Uygur, A. & Kargi, F. (2004), 'Salt inhibition on biological nutrient removal from saline wastewater in a sequencing batch reactor', *Enzyme and Microbial Technology* **34**(3-4), 313.

Venter, J., Remington, K., Heidelberg, J., Halpern, A., Rusch, D., Eisen, J., Wu, D., Paulsen, I., Nelson, K., Nelson, W. et al. (2004), 'Environmental genome shotgun sequencing of the Sargasso Sea', *Science* **304**(5667), 66.

Vogelsang, C., Husby, A. & Østgaard, K. (1997), 'Functional stability of temperature-compensated nitrification in domestic wastewater treatment obtained with PVA-SbQ/alginate gel entrapment', *Water Research* **31**(7), 1659.

Voytek, M. (1996), Relative abundance and species diversity of autotrophic ammonia- oxidizing bacteria in aquatic systems, PhD thesis, University of California.

Voytek, M. & Ward, B. (1995), 'Detection of ammonium-oxidizing bacteria of the beta-subclass of the class Proteobacteria in aquatic samples with the PCR.', *Applied and environmental microbiology* **61**(4), 1444.

Vredenbregt, L., Nielsen, K., Potma, A., Kristensen, G. & Sund, C. (1997), 'Fluid bed biological nitrification and denitrification in high salinity wastewater', *Water Science and Technology* **36**(1), 93.

Wagner, M., Horn, M. & Daims, H. (2003), 'Fluorescence in situ hybridisation for the identification and characterisation of prokaryotes', *Current opinion in Microbiology* **6**(3), 302.

Wagner, M., Loy, A., Nogueira, R., Purkhold, U., Lee, N. & Daims, H. (2002), 'Microbial community composition and function in wastewater treatment plants', *Antonie Van Leeuwenhoek* **81**(1), 665.

Wagner, M., Rath, G., Koops, H. P., Flood, J. & Amann, R. (1996), 'In situ analysis of nitrifying bacteria in sewage treatment plants', *Water Science & Technology* **34**(1), 237.

Watson, S. (1971), 'Taxonomic considerations of the family Nitrobacteraceae Buchanan: requests for opinions', *International Journal of Systematic and Evolutionary Microbiology* **21**(3), 254.

Watson, S. & Waterbury, J. (1971), 'Characteristics of Two Marine Nitrite Oxidizing Bacteria, Nitrospina gracilis nov. ten. nov. sp. and Nitrococcus mobilis nov. ten. nov. sp.', *Archives of Microbiology* **77**(3), 203.

Webster, G., Embley, T. & Prosser, J. (2002), 'Grassland management regimens reduce small-scale heterogeneity and species diversity of {beta}-proteobacterial ammonia oxidizer populations', *Applied and environmental microbiology* **68**(1), 20.

Wertz, S., Poly, F., Le Roux, X. & Degrange, V. (2008), 'Development and application of a PCR-denaturing gradient gel electrophoresis tool to study the diversity of Nitrobacter-like nxrA sequences in soil', *FEMS microbiology ecology* **63**(2), 261.

Wijffels, R. & Tramper, J. (1995), 'Nitrification by immobilized cells', *Enzyme and Microbial Technology* **17**(6), 482.

Wilkinson, L. (2010), 'Systat', *Wiley Interdisciplinary Reviews: Computational Statistics* **2**(2), 256.

Wittebolle, L., Marzorati, M., Clement, L., Balloi, A., Daffonchio, D., Heylen, K., De Vos, P., Verstraete, W. & Boon, N. (2009), 'Initial community evenness favours functionality under selective stress', *Nature* **458**(7238), 623.

Woese, C. (1987), 'Bacterial evolution', *Microbiological reviews* **51**(2), 221.

Wuchter, C., Abbas, B., Coolen, M., Herfort, L., van Bleijswijk, J., Timmers, P., Strous, M., Teira, E., Herndl, G., Middelburg, J. et al. (2006), 'Archaeal nitrification in the ocean', *Proceedings of the National Academy of Sciences* **103**(33), 12317.

Yu, S., Leung, W., Ho, K., Greenfield, P. & Eckenfelder, W. (2002), 'The impact of sea water flushing on biological nitrification-denitrification activated sludge sewage treatment process.', *Water science and technology* **46**(11), 209.

# Appendices

# Appendix A

# Operation of the tapwater-based nitrifying reactor

Table A.1 shows operational changes and activity measurements in the tapwater-based nitrifying reactor. Mass balance refers to the difference between nitrogen into the reactor and nitrogen out of the reactor, $N_{in} - N_{out}$, which should be around 0 mg/mL, assuming that the only nitrogen into the reactor was in the form of $NH_4^+$. The activity refers to the rate of ammonium consumption and nitrite production.

Table A.1: Operation of the tapwater-based nitrifying reactor. The table shows the flowrate, the measured concentrations of ammonium, nitrite and nitrate, and the calculated activities.

| Day | Flow (mL/h) | NH$_4^+$-N (mg/L) in | NH$_4^+$-N (mg/L) out | NO$_2$-N (mg/L) out | NO$_3$-N (mg/L) out | Mass balance | Activity (mg/Lh) NH$_4^+$-N consumed | Activity (mg/Lh) NO$_3$-N formed |
|---|---|---|---|---|---|---|---|---|
| 5 | 34 | 49.2 | 50.7 | 1.2 | 0.5 | -3.2 | -0.1 | 0.0 |
| 8 | 34 | 48.7 | 37.2 | 1.2 | 2.7 | 7.6 | 1.0 | 0.2 |
| 9 | 32 | 47.0 | 19.2 | - | 5.4 |  | 2.2 | 0.4 |
| 10 | 160 | 46.0 | 34.3 | 11.3 | 3.6 | -3.2 | 4.7 | 1.4 |
| 11 | 166 | 45.8 | 17.2 | 29.9 | 6.7 | -8.0 | 11.9 | 2.8 |
| 17 | 78 | 57.4 | 0.5 | 58.5 | 10.0 | -11.6 | 11.1 | 2.0 |
| 18 | 80 | 9.4 | 0.0 | 11.9 | 3.6 | -6.1 | 1.9 | 0.7 |
| 21 | 82 | 9.2 | 0.0 | 7.3 | 3.4 | -1.5 | 1.9 | 0.7 |
| 26 | 80 | 11.8 | 0.0 | 0.0 | 8.9 | 2.8 | 2.4 | 1.8 |
| 28 | 111 | 15.8 | 0.0 | 0.4 | 9.5 | 5.9 | 4.4 | 2.6 |
| 31 | 96 | 15.7 | 0.0 | 1.0 | 17.0 | -2.3 | 3.8 | 4.1 |
| 35 | 102 | 5.9 | 0.0 | 0.6 | 18.5 | -13.2 | 1.5 | 4.7 |
| 38 | 102 | 5.0 | 0.0 | 0.2 | 9.7 | -4.9 | 1.3 | 2.5 |
| 39 | 124 | 20.0 | 1.3 | 0.5 | 17.3 | 0.9 | 5.8 | 5.4 |
| 40 | 105 | 20.0 | 0.2 | 0.6 | 21.8 | -2.6 | 5.2 | 5.7 |
| 41 | 96 | 20.0 | 0.1 | 0.5 | 22.0 | -2.5 | 4.8 | 5.3 |
| 42 | 70 | 20.0 | 0.2 | - | 21.9 |  | 3.5 | 3.8 |
| 45 | 90 | 20.0 | 0.0 | - | 21.7 |  | 4.5 | 4.9 |
| 46 | 60 | 48.9 | 10.9 | - | 22.3 |  | 5.7 | 3.3 |
| 47 | 38 | 48.9 | 1.6 | - | 42.9 |  | 4.5 | 4.1 |
| 49 | 95 | 48.9 | 0.6 | - | 46.4 |  | 11.4 | 11.0 |
| 51 | 102 | 48.9 | 0.5 | - | 47.2 |  | 12.4 | 12.0 |

*Continued on next page*

*Table A.1 continued from previous page*

| Day | Flow (mL/h) | NH$_4^+$-N (mg/L) | | NO$_2$-N out (mg/L) | NO$_3$-N out (mg/L) | Mass balance | Activity (mg/Lh) | |
|---|---|---|---|---|---|---|---|---|
| | | in | out | | | | NH$_4^+$-N consumed | NO$_3$-N formed |
| 53 | 102 | 48.9 | 0.3 | - | 46.3 | | 12.4 | 11.8 |
| 54 | 102 | 48.9 | 0.3 | - | 45.2 | | 12.4 | 11.5 |
| 55 | 114 | 49.9 | 1.1 | - | 46.7 | | 13.9 | 13.3 |
| 56 | 102 | 49.9 | 0.7 | 1.7 | 45.6 | 2.0 | 12.6 | 11.6 |
| 59 | 103 | 49.9 | 0.7 | 7.0 | 42.2 | 0.0 | 12.7 | 10.9 |
| 60 | 112 | 49.9 | 0.7 | 7.2 | 41.7 | 0.3 | 13.8 | 11.7 |
| 61 | 98 | 49.9 | 0.7 | 9.5 | 41.7 | -2.0 | 12.0 | 10.2 |
| 62 | 103 | 49.9 | 1.0 | 9.9 | 40.9 | -1.9 | 12.6 | 10.5 |
| 62 | - | 51.8 | - | - | - | | | |
| 66 | 102 | 51.8 | 0.8 | 4.8 | 47.8 | -1.5 | 13.0 | 12.2 |
| 67 | 101 | 51.8 | 0.6 | 4.5 | 49.1 | -2.3 | 12.9 | 12.4 |
| 68 | 94 | 51.8 | 0.3 | 3.2 | 49.4 | -1.1 | 12.1 | 11.6 |
| 69 | 90 | 51.8 | 2.3 | 3.1 | 47.9 | -1.5 | 11.1 | 10.8 |
| 70 | 90 | 68.7 | 10.5 | 12.3 | 46.7 | -0.8 | 13.1 | 10.5 |
| 72 | 125 | 68.7 | 10.4 | 15.0 | 45.0 | -1.7 | 18.1 | 14.0 |
| 73 | 126 | 56.4 | 11.8 | 3.7 | 42.5 | -1.6 | 14.0 | 13.4 |
| 74 | 132 | 56.4 | 8.4 | 4.5 | 44.4 | -0.9 | 15.8 | 14.7 |
| 75 | 138 | 56.4 | 4.8 | 5.7 | 46.7 | -0.8 | 17.8 | 16.1 |
| 76 | 150 | 56.4 | 0.8 | 1.8 | 55.2 | -1.3 | 20.9 | 20.7 |
| 77 | 150 | 51.3 | 0.9 | 2.1 | 49.3 | -1.0 | 18.9 | 18.5 |

# Appendix B

# Operation of the seawater-based nitrifying reactor

Table B.1 shows all operational changes and activity measurements in the seawater-based nitrifying reactor. Mass balance refers to the difference between nitrogen into the reactor and nitrogen out of the reactor, $N_{in} - N_{out}$, which should be around 0 mg/mL. The activity refers to the rate of ammonium consumption and nitrite production.

Table B.1: Operation of the seawater-based nitrifying reactor. The table shows the measured concentrations of ammonium, nitrite and nitrate, and the calculated activities.

| Day | Flow (mL/h) | NH$_4^+$-N (mg/L) | | NO$_2^-$-N (mg/L) | | NO$_3^-$-N (mg/L) | | Mass balance | Activity (mg/Lh) | |
|-----|-------------|-----|-----|-----|-----|-----|-----|--------------|-----------------|------------|
| | | in | out | in | out | in | out | | NH$_4^+$-N consumed | NO$_3$-N formed |
| 0  | 72  | 42.0 | -    | 0.2 | -    | 3.7 | -    | -     |      |     |
| 1  | 72  | 42.0 | 46.6 | 0.2 | 0.3  | 3.7 | 2.8  | -3.9  | -0.2 | 0.0 |
| 2  | 72  | 42.0 | 42.0 | 0.2 | 3.5  | 3.7 | 6.1  | -5.7  | 0.0  | 0.1 |
| 3  | 0   | 42.0 | -    | 0.2 | -    | 3.7 | -    |       |      |     |
| 5  | 0   | 78.5 | 54.8 | 0.3 | 5.2  | 0.1 | 6.1  | 12.8  |      |     |
| 7  | 0   | 78.5 | 42.0 | 0.3 | 13.9 | 0.1 | 8.0  | 15.0  |      |     |
| 8  | 72  | 78.5 | -    | 0.3 | -    | 0.1 | -    |       |      |     |
| 9  | 114 | 83.7 | 73.4 | 0.3 | 8.5  | 0.7 | 3.9  | -1.1  | 0.8  | 0.3 |
| 10 | 114 | 81.8 | 77.0 | 0.2 | 14.4 | 0.7 | 5.9  | -14.5 | 0.4  | 0.4 |
| 13 | 114 | 73.3 | 4.5  | 0.0 | 26.0 | 1.7 | 12.5 | 32.0  | 5.5  | 0.9 |
| 14 | 114 | 38.3 | 0.0  | 2.0 | 67.0 | 1.6 | 18.0 | -43.1 | 3.1  | 1.3 |
| 16 | 200 | 38.0 | -    | 0.1 | -    | 0.4 | -    |       |      |     |
| 17 | 200 | 0.0  | 0.0  | 0.1 | 1.3  | 0.4 | 1.3  | -2.0  | 0.0  | 0.1 |
| 18 | 200 | 0.0  | -    | 0.1 | -    | 0.4 | -    |       |      |     |
| 20 | 114 | 41.0 | -    | 0.3 | -    | 1.2 | -    |       |      |     |
| 21 | 114 | 41.0 | 0.4  | 0.3 | 46.9 | 1.2 | 9.2  | -14.0 | 3.2  | 0.6 |
| 22 | 200 | 13.0 | 0.0  | 0.0 | 22.1 | 0.0 | 4.5  | -13.7 | 1.8  | 0.6 |
| 23 | 114 | 13.0 | 0.4  | 0.0 | 20.6 | 0.0 | 4.1  | -12.2 | 1.0  | 0.3 |
| 24 | 114 | 18.1 | 0.4  | 0.1 | 18.8 | 0.0 | 4.3  | -5.3  | 1.4  | 0.3 |
| 28 | 114 | 18.0 | 0.0  | 0.0 | 10.8 | 0.0 | 4.7  | 2.5   | 1.4  | 0.4 |
| 29 | 114 | 9.9  | 0.1  | 0.0 | 5.3  | 0.0 | 3.3  | 1.2   | 0.8  | 0.3 |
| 30 | 114 | 9.2  | 0.2  | 0.1 | 3.6  | 0.7 | 7.8  | -1.5  | 0.7  | 0.3 |
| 31 | 114 | 9.2  | 0.3  | 0.1 | 3.2  | 0.7 | 8.3  | -1.8  | 0.7  | 0.6 |
| 32 | 114 | 9.2  | 0.1  | 0.1 | 2.1  | 0.7 | 7.7  | 0.1   | 0.7  | 0.6 |
| 33 | 114 | 9.2  | 5.5  | 0.1 | 1.5  | 0.7 | 3.4  | -0.4  | 0.3  | 0.2 |
| 34 | 114 | 9.2  | 0.2  | 0.1 | 1.8  | 0.7 | 8.2  | -0.2  | 0.7  | 0.6 |

*Continued on next page*

| Day | Flow (mL/h) | NH$_4^+$-N (mg/L) | | NO$_2^-$-N (mg/L) | | NO$_3^-$-N (mg/L) | | Mass balance | Activity (mg/Lh) | |
| | | in | out | in | out | in | out | | NH$_4^+$-N consumed | NO$_3$-N formed |
|---|---|---|---|---|---|---|---|---|---|---|
| 35 | 200 | 9.1 | 0.5 | 0.1 | 2.1 | 0.5 | 7.8 | -0.7 | 1.2 | 1.0 |
| 37 | 200 | 7.7 | 0.3 | 1.5 | 1.0 | 0.7 | 8.4 | 0.2 | 1.0 | 1.1 |
| 38 | 200 | 8.3 | 0.3 | 0.3 | 0.5 | 0.8 | 8.9 | -0.3 | 1.1 | 1.1 |
| 39 | 200 | 14.0 | 1.1 | 0.2 | 0.7 | 1.2 | 13.7 | -0.2 | 1.8 | 1.8 |
| 40 | 200 | 14.0 | 1.1 | 0.2 | 0.5 | 1.2 | 16.1 | -2.2 | 1.8 | 2.1 |
| 41 | 200 | 17.5 | 1.2 | 0.2 | 0.4 | 0.8 | 17.7 | -0.8 | 2.3 | 2.4 |
| 42 | 200 | 17.5 | 1.3 | 0.2 | 0.3 | 0.8 | 18.7 | -1.9 | 2.3 | 2.5 |
| 43 | 0 | 17.5 | 0.2 | 0.2 | 0.2 | 0.8 | 20.6 | -2.4 | | |
| 44 | 200 | 17.5 | 1.7 | 0.2 | 0.3 | 0.8 | 18.1 | -1.6 | 2.2 | 2.4 |
| 45 | 200 | 44.6 | 20.2 | 0.3 | 0.6 | 1.3 | 25.8 | -0.4 | 3.4 | 3.4 |
| 46 | 200 | 44.6 | 16.6 | 0.3 | 0.6 | 1.3 | 31.5 | -2.5 | 3.9 | 4.2 |
| 47 | 200 | 44.6 | 8.6 | 0.3 | 0.9 | 1.3 | 40.9 | -4.2 | 5.0 | 5.5 |
| 48 | 200 | 44.6 | 6.0 | 0.3 | 1.1 | 1.3 | 40.8 | -1.6 | 5.4 | 5.5 |
| 49 | 200 | 90.8 | 36.7 | 0.3 | 8.0 | 1.6 | 53.6 | -5.6 | 7.6 | 7.3 |
| 50 | 200 | 90.8 | 23.9 | 0.3 | 8.5 | 1.6 | 65.8 | -5.5 | 9.4 | 9.0 |
| 51 | 200 | 90.8 | 1.2 | 0.3 | 14.5 | 1.6 | 75.8 | 1.2 | 12.5 | 10.4 |
| 52 | 200 | 90.8 | 4.6 | 0.3 | 16.1 | 1.6 | 81.2 | -9.2 | 12.1 | 11.1 |
| 54 | 200 | 91.7 | 1.6 | 0.1 | 2.6 | 1.0 | 88.7 | -0.1 | 12.6 | 12.3 |
| 55 | 200 | 91.7 | 1.8 | 0.1 | 7.2 | 1.0 | 89.7 | -5.8 | 12.6 | 12.4 |
| 56 | 200 | 91.7 | 1.7 | 0.1 | 2.3 | 1.0 | 90.8 | -2.0 | 12.6 | 12.6 |
| 57 | 200 | 140.0 | 6.5 | 0.3 | 82.0 | 2.4 | 59.7 | -5.5 | 18.7 | 8.0 |
| 58 | 300 | 140.0 | 38.1 | 0.3 | 45.7 | 2.4 | 73.2 | -14.4 | 21.4 | 14.9 |
| 58 | 200 | 140.0 | 35.1 | 0.3 | 46.2 | 2.4 | 45.8 | 15.6 | 14.7 | 6.1 |
| 59 | 200 | 45.6 | 2.2 | 0.4 | 37.5 | 2.3 | 22.6 | -14.1 | 6.1 | 2.8 |
| 60 | 200 | 45.6 | 2.5 | 0.4 | 35.9 | 2.3 | 22.8 | -13.0 | 6.0 | 2.9 |
| 61 | 200 | 8.7 | 0.4 | 0.1 | 0.6 | 0.8 | 10.9 | -2.3 | 1.2 | 1.4 |

*Continued on next page*

Table B.1 continued from previous page

| Day | Flow (mL/h) | $NH_4^+$-N (mg/L) in | out | $NO_2^-$-N (mg/L) in | out | $NO_3^-$-N (mg/L) in | out | Mass balance | Activity (mg/Lh) $NH_4^+$-N consumed | $NO_3$-N formed |
|---|---|---|---|---|---|---|---|---|---|---|
| 62 | 200 | 8.7 | 0.5 | 0.1 | 0.5 | 0.8 | 9.4 | -0.7 | 1.2 | 1.2 |
| 63 | 200 | 22.3 | 1.2 | 0.1 | 1.4 | 0.5 | 20.7 | -0.3 | 3.0 | 2.8 |
| 64 | 200 | 22.3 | 0.0 | 0.1 | 0.1 | 0.5 | 24.6 | -1.8 | 3.1 | 3.4 |
| 65 | 200 | 49.4 | 10.6 | 0.4 | 20.0 | 1.2 | 21.8 | -1.4 | 5.4 | 2.9 |
| 66 | 200 | 21.6 | 0.0 | 0.1 | 0.1 | 0.6 | 25.4 | -3.2 | 3.0 | 3.5 |
| 69 | 200 | 21.6 | 2.4 | 0.1 | 0.4 | 0.6 | 17.7 | 1.8 | 2.7 | 2.4 |
| 70 | 200 | 22.8 | 1.3 | - | 0.5 | - | 17.3 | | 3.0 | |
| 72 | 200 | 22.8 | 1.8 | - | - | - | 18.3 | | 2.9 | |
| 73 | 200 | 22.8 | 1.9 | - | - | - | 15.4 | | 2.9 | |
| 74 | 114 | 46.5 | 9.6 | - | - | 0.6 | 34.2 | | 2.9 | 2.7 |
| 75 | 114 | 46.5 | 9.1 | - | - | 0.6 | 36.9 | | 3.0 | 2.9 |
| 76 | 114 | 46.5 | 2.5 | - | - | 0.6 | 44.1 | | 3.5 | 3.5 |
| 77 | 114 | 46.5 | 1.2 | - | - | 0.6 | 44.4 | | 3.6 | 3.5 |
| 78 | 114 | 46.5 | 1.5 | - | - | 0.6 | 38.6 | | 3.6 | 3.0 |
| 80 | 114 | 46.0 | 0.8 | - | - | 0.6 | 44.4 | | 3.6 | 3.5 |
| 82 | 114 | 46.0 | 0.9 | - | - | 0.6 | 45.2 | | 3.6 | 3.6 |
| 84 | 114 | 46.0 | 0.5 | - | - | 0.6 | 47.5 | | 3.6 | 3.7 |
| 85 | 114 | 46.0 | 0.8 | - | - | 0.6 | 48.2 | | 3.6 | 3.8 |
| 86 | 72 | 94.7 | 2.9 | 0.6 | 10.9 | 1.7 | 71.5 | 11.6 | 4.6 | 3.5 |
| 87 | 72 | 94.7 | - | 0.6 | 8.9 | 1.7 | 81.1 | | | 4.0 |
| 89 | 72 | 94.7 | 1.0 | 0.6 | 19.8 | 1.7 | 77.9 | -1.8 | 4.7 | 3.8 |
| 90 | 72 | 94.7 | 2.1 | 0.6 | 10.0 | 1.7 | 83.1 | 1.8 | 4.7 | 4.1 |
| 91 | 72 | 94.7 | 3.6 | 0.6 | 21.1 | 1.7 | 75.4 | -3.1 | 4.6 | 3.7 |
| 92 | 114 | 93.1 | 8.9 | 0.2 | 27.0 | 1.5 | 62.6 | -3.6 | 6.7 | 4.9 |
| 93 | 114 | 93.1 | 6.9 | 0.2 | 43.3 | 1.5 | 54.7 | -10.0 | 6.9 | 4.2 |
| 94 | 110 | 93.1 | 0.6 | 0.2 | 0.4 | 1.5 | 92.9 | 0.9 | 7.1 | 7.0 |

| Day | Flow (mL/h) | NH$_4^+$-N (mg/L) | | NO$_2^-$-N (mg/L) | | NO$_3^-$-N (mg/L) | | Mass balance | Activity (mg/Lh) | |
| | | in | out | in | out | in | out | | NH$_4^+$-N consumed | NO$_3$-N formed |
| --- | --- | --- | --- | --- | --- | --- | --- | --- | --- | --- |
| 95 | 110 | 93.1 | 0.7 | 0.2 | 0.4 | 1.5 | 93.6 | 0.2 | 7.1 | 7.1 |
| 97 | 110 | 93.1 | 0.8 | 0.2 | 0.5 | 1.5 | 93.2 | 0.4 | 7.1 | 7.1 |
| 99 | 110 | 94.4 | 1.0 | 0.4 | 0.4 | 1.5 | 93.8 | 1.1 | 7.2 | 7.1 |
| 101 | 110 | 94.4 | 0.0 | 0.4 | 0.1 | 1.5 | 94.7 | 1.4 | 7.3 | 7.2 |
| 103 | 130 | 94.4 | 0.9 | 0.4 | 0.6 | 1.5 | 93.1 | 1.7 | 8.5 | 8.3 |
| 104 | 100 | 94.4 | 0.6 | 0.4 | 0.2 | 1.5 | 93.3 | 2.1 | 6.6 | 6.4 |
| 105 | 60 | 94.4 | 0.6 | 0.4 | 0.2 | 1.5 | 91.1 | 4.3 | 3.9 | 3.8 |
| 106 | 130 | 94.4 | 0.7 | 0.4 | 0.4 | 1.5 | 94.1 | 1.0 | 8.5 | 8.4 |
| 107 | 130 | 121.0 | 3.1 | 0.5 | 24.2 | 2.1 | 93.3 | 3.0 | 10.7 | 8.3 |
| 108 | 100 | 121.0 | 0.9 | 0.5 | 0.7 | 2.1 | 113.0 | 9.0 | 8.4 | 7.8 |
| 109 | 100 | 121.0 | 8.6 | 0.5 | 6.0 | 2.1 | 99.8 | 9.2 | 7.9 | 6.8 |
| 110 | 78 | 121.0 | 0.5 | 0.5 | 0.3 | 2.1 | 114.0 | 8.9 | 6.6 | 6.1 |
| 111 | 78 | 121.0 | 0.5 | 0.5 | 0.2 | 2.1 | 113.0 | 9.9 | 6.6 | 6.0 |
| 112 | 100 | 121.0 | 0.9 | 0.5 | 0.3 | 2.1 | 115.0 | 7.4 | 8.4 | 7.9 |
| 114 | 100 | 121.0 | 1.1 | 0.5 | 7.2 | 2.1 | 108.0 | 7.3 | 8.4 | 7.4 |
| 115 | 100 | 110.0 | 1.3 | 1.3 | 5.8 | 2.0 | 111.0 | -4.8 | 7.6 | 7.6 |
| 116 | 100 | 110.0 | 2.5 | 1.3 | 2.1 | 2.0 | 111.0 | -2.3 | 7.5 | 7.6 |
| 118 | 100 | 110.0 | 7.7 | 1.3 | 14.9 | 2.0 | 96.8 | -6.1 | 7.2 | 6.6 |
| 119 | 100 | 110.0 | 18.3 | 1.3 | 20.8 | 2.0 | 80.9 | -6.7 | 6.4 | 5.5 |
| 120 | 80 | 110.0 | 0.6 | 1.3 | 0.5 | 2.0 | 113.0 | -0.8 | 6.1 | 6.2 |
| 121 | 80 | 110.0 | 0.5 | 1.3 | 0.4 | 2.0 | 111.0 | 1.4 | 6.1 | 6.1 |
| 122 | 80 | 110.0 | 0.4 | 1.3 | 0.4 | 2.0 | 113.0 | -0.5 | 6.1 | 6.2 |
| 124 | 80 | 115.0 | 1.2 | 1.6 | 23.8 | 2.2 | 96.2 | -2.4 | 6.4 | 5.3 |
| 125 | 60 | 115.0 | 0.3 | 1.6 | 0.4 | 2.2 | 115.0 | 3.1 | 4.8 | 4.7 |
| 126 | 80 | 115.0 | 0.4 | 1.6 | 0.5 | 2.2 | 112.0 | 5.8 | 6.4 | 6.1 |
| 127 | 80 | 115.0 | 0.3 | 1.6 | 0.6 | 2.2 | 114.0 | 3.9 | 6.4 | 6.3 |

B5

*Table B.1 continued from previous page*

| Day | Flow (mL/h) | NH$_4^+$-N (mg/L) in | out | NO$_2^-$-N (mg/L) in | out | NO$_3^-$-N (mg/L) in | out | Mass balance | Activity (mg/Lh) NH$_4^+$-N consumed | NO$_3$-N formed |
|---|---|---|---|---|---|---|---|---|---|---|
| 128 | 80 | 115.0 | 0.7 | 1.6 | 7.2 | 2.2 | 107.0 | 3.9 | 6.4 | 5.9 |
| 129 | 80 | 115.0 | 0.4 | 1.6 | 0.4 | 2.2 | 113.0 | 5.0 | 6.4 | 6.2 |
| 131 | 80 | 115.0 | 2.1 | 1.6 | 31.2 | 2.2 | 89.5 | -4.1 | 6.3 | 4.9 |
| 132 | 70 | 115.0 | 0.3 | 1.6 | 0.4 | 2.2 | 114.0 | 4.1 | 5.6 | 5.5 |
| 133 | 60 | 115.0 | 0.5 | 1.6 | 11.7 | 2.2 | 103.0 | 3.6 | 4.8 | 4.2 |
| 134 | 60 | 112.0 | 0.5 | 0.3 | 0.4 | 1.8 | 113.0 | 0.2 | 4.7 | 4.7 |
| 135 | 80 | 112.0 | 0.5 | 0.3 | 0.4 | 1.8 | 112.0 | 1.2 | 6.2 | 6.2 |
| 137 | 85 | 112.0 | 0.5 | 0.3 | 0.5 | 1.8 | 114.0 | -0.9 | 6.6 | 6.7 |
| 138 | 85 | 112.0 | 0.7 | 0.3 | 0.8 | 1.8 | 115.0 | -2.4 | 6.6 | 6.7 |

B6

# Appendix C

# Batch culture salinity respons test

Figures C.1, C.2 and C.3 show the concentrations of ammonium, nitrite and nitrate during the batch culture salinity respons test. Measurements were taken over a period of three hours for each seawater percentage. The nitrification activity was calculated for each salinity from the the slopes of linear regression curves based on the plots in Figures C.1, C.2 and C.3.
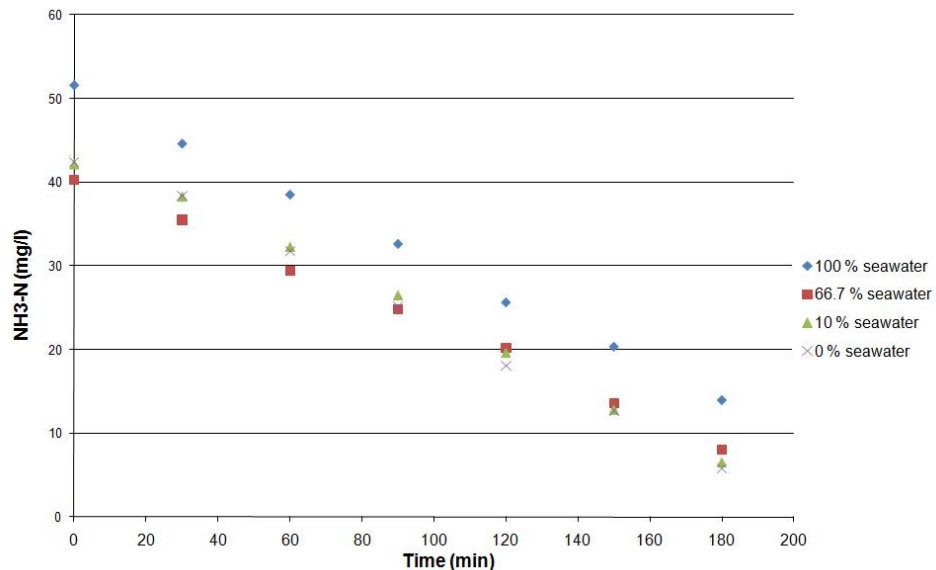


Figure C.1: Concentrations on ammonium measured every 30 minutes for three hours, at different salinities.
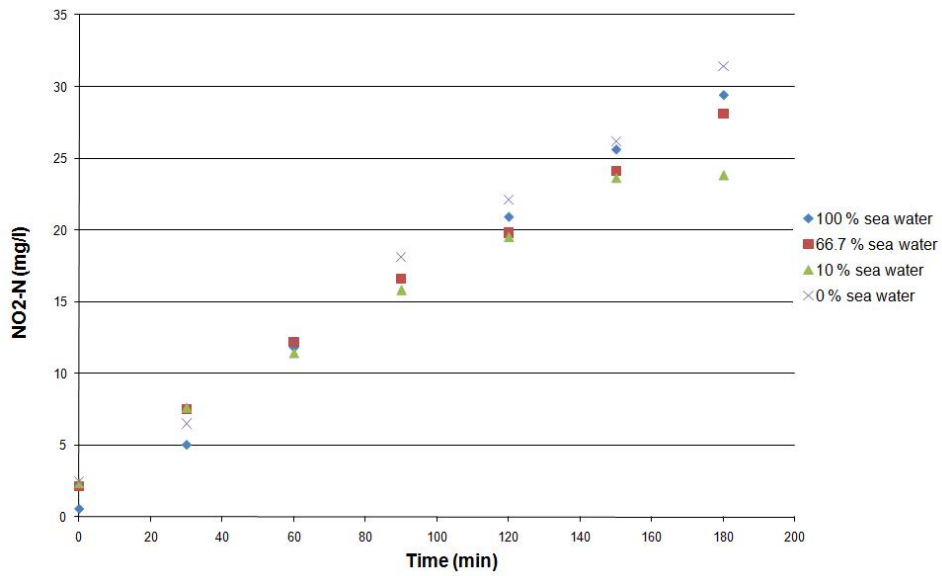
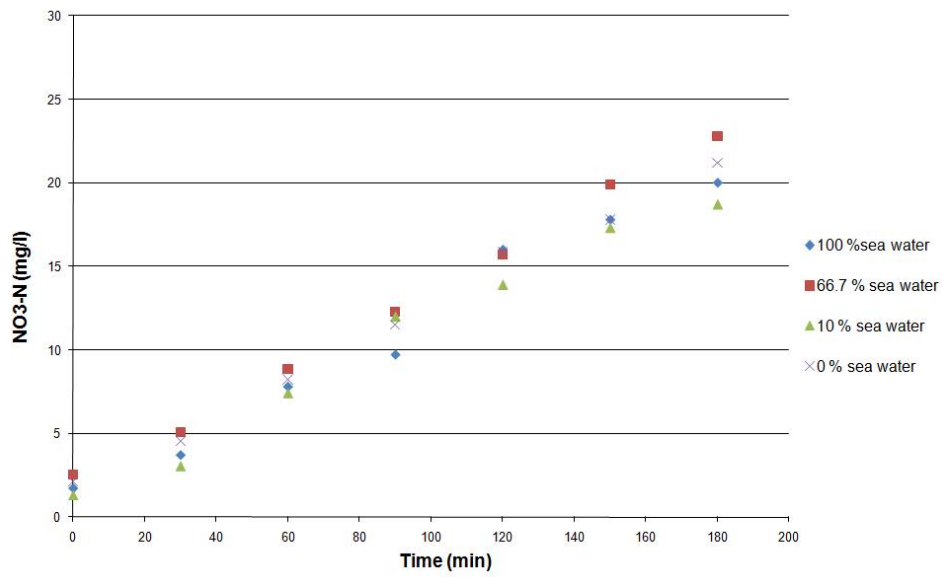Figure C.2: Concentrations on nitrite measured every 30 minutes for three hours, at different salinities.



Figure C.3: Concentrations on nitrate measured every 30 minutes for three hours, at different salinities.

# Appendix D

# Denaturing gradient gel electrophoresis protocol

Acrylamide stock solutions with denaturing percentages of 0 and 80 % were made from a 40 % acrylamide solution (Sigma-Aldrich acrylamide/bis-acrylamide 19:1) that was diluted to 6 % or 8 % with 0.5xTAE buffer (pH 8, composition is specified in section 2.2.3). Urea and deionised formamide (BDH prolabo) were added to the 80 % denaturing stock solution, to concentrations of 7 M and 40 % (v/v), respectively. The formamide was deionised prior to addition to the stock solution by mixing 200 mL of formamide with 7.5 g of Dowex Resin AG® 501-X8 from BioRad in minimum one hour.

To make the appropriate denaturing gradient in the gel, two denaturing acrylamide solutions were made from the denaturing stock solutions of 0 % and 80 %; one solution that had the highest denaturing percentage of the gel, and one solution that had the lowest denaturing percentage of the gel. The correct denaturing percentage was made by adjusting the relative amounts of the 0 % and the 80 % stock solutions. Table D.1 shows the amounts of 0 % and 80 % stock solutions that were mixed to give the wanted denaturing percentage in each solution. To initiate polymerization, 87 $\mu$L of a 10 % APS solution (w/v, sterile filtered and stored as aliquots at -20 °C) and 16 $\mu$L of TEMED (Invitrogen UltraPureTM) were added per 24 mL of the denaturing acrylamide solutions.

The gel was made by using a C.B.S Scientific Co. Gradient Maker, where the acrylamide solution of the highest denaturing percentage was slowly transferred to the gel chamber while being mixed with the acrylamide solution of the lowest denaturing percentage. On top of the denaturing gradient, a 0 % stacking gel was cast. The stacking gel was made from 8 mL of the 0 % stock solution, 40 $\mu$L of the 10 % APS solution and 10 $\mu$L of TEMED. The gel was let to polymerize for at least two hours.

Table D.1: Amounts of 0 % and 80 % denaturing stock solutions mixed to yield acrylamide solutions of specific denaturing percentages.

| Denaturing percentage | 0% stock solution (mL) | 80% stock solution (mL) | Total volume (mL) |
| --- | --- | --- | --- |
| 15 | 19.5 | 4,5 | 24 |
| 25 | 16.5 | 7.5 | 24 |
| 30 | 15 | 9 | 24 |
| 35 | 13.5 | 10.5 | |
| 40 | 12 | 12 | |
| 45 | 10.5 | 13.5 | 24 |
| 50 | 9 | 15 | 24 |
| 55 | 7.5 | 16.5 | 24 |
| 60 | 6 | 18 | 24 |
| 75 | 1.5 | 22.5 | 24 |